
Universitat de Barcelona
Facultat de Química
Departament d'Enginyeria Química

# COUPLED PHOTOCHEMICAL-BIOLOGICAL SYSTEM TO TREAT BIORECALCITRANT WASTEWATERS

Doctoral Thesis directed by Santiago Esplugas Vidal and
Esther Chamarro Aguilera

Jordi Bacardit Peñarroya

Barcelona, Maig de 2007

Programa de Doctorat d'Enginyeria del Medi Ambient i del Producte
Bienni 2003-2005

# *Chapter 3: Photo-Fenton process study. Engineering aspects*

*Biodegradability Enhancement, Interferences, Scaling-up, Mechanistic Models and Optimization*

Different aspects of Photo-Fenton process are presented and discussed in this Chapter. Most of the experiments and studies carried out, aim for the integration of Photo-Fenton and biological processes. Thus, a parameter of importance is the biodegradability, which is assessed by the $BOD_5$/COD ratio. Moreover, engineering aspects such as optimization, scaling-up, mechanistic modelling and process control are discussed.

A first Section, presents a set of results of an Experimental Design and their analysis with a Response Surface Methodology (RSM). By this procedure, the effect caused by different operating conditions, $[H_2O_2]_0$, $[Fe^{2+}]_0$ and temperature, are assessed and mathematically valued, which makes possible to characterize and optimize the process. Another Expeirmental Design is carried out in order to study the influence of NaCl on the process.

Similar operating conditions are later evaluated in a pre-industrial scale installation, which radiation source is the sun. With this scale-up, it is expected to elucidate whether the findings of the laboratory experiments are fulfilled. Moreover, the pilot plant disposes of on-line measure of $H_2O_2$. By analyzing certain aspects of the experiments, it has been observed that an oxidation

indicator (COD) and this on-line parameter ($H_2O_2$), which is the process' main reagent, are closely correlated. A section presents the possibility to use $H_2O_2$ monitoring as a Photo-Fenton control parameter. Moreover, this correlation it is suggested to be an indicator of process Efficiency.

Another study intended for the characterization of the process is the process modelling. The mathematization is based on mechanistic models, which simplify the oxidation of 4-CP and its intermediates in short reaction pathways, in which COD and $BOD_5$ as lump parameters, are considered pseudo-compounds.

All the experiments are performed starting with a solution of 200 $mg.L^{-1}$ of 4-CP as a model compound. The degradation results are not the conclusions of importance of these studies but the methodologies, which attempt to contribute to the industrialization of the coupled process.

# *3.1.- Photo-Fenton study by RSM*

### 3.1.1.- Experimental design

In order to obtain Response Surfaces with high performance, a set of well-defined experiments must be defined. As it is explained in the methods section, a Central Composite Design produces a list of well-designed experiments, with good statistical properties. It is robust and rotatable.

The factors under study in the present section are the effects that the initial concentrations of $Fe^{2+}$ and $H_2O_2$, $[Fe^{2+}]_0$ and $[H_2O_2]_0$ respectively, and temperature can cause on different aspects of Photo-Fenton process. After a bibliographic compilation, for example the works of *Göb et al.* (*1999*) or *Torrades et al.* (*2003*) and some experimental tests, the boundaries of the experimental factors are defined. They are shown in Table 3.1-1.

Table 3.1-1: Operating conditions. Minimum-maximum values for each variable.

| $[H_2O_2]_0$ | $[Fe^{2+}]_0$ | Temp. |
|---|---|---|
| 50-350 $mg.L^{-1}$ | 2-20 $mg.L^{-1}$ | 20-70 |
| 1.47-10.29 mM | 0.036-0.358 mM | ºC |

The upper limit of $[Fe^{2+}]_0$ is fixed taking into account that $Fe^{2+}$ is probably the major cause of undesired reactions of the defined Photo-Fenton mechanism (Section 1.3) if it is present in excess.

As explained above in the methodology concerning and experimental design, the objective is the description of Response Surfaces. The responses to be obtained and observed are 4-CP removal, TOC removal, $BOD_5/COD$ ratio and time. Time is used to develop the operating costs equation, as it is described later. An optimization is attempted by comparing the $BOD_5/COD$ response equation with the costs equation, which is written taking into account the amounts of reagents and the operational costs of the heating jacket and UV lamps. Photon flow is estimated to be 3.61 μEinstein/s by means of an actinometry throughout the experimental phase.

### 3.1.2.- Experimental results

The results of the 17 experiments are shown in Table 3.1-2. A first approach to the experimental results is helpful to describe the main features of the system. In many experiments, total or almost total 4-CP removal is reached. The less efficient experiments regarding the removal achieved are the ones with less $[H_2O_2]_0$. With regard to temperature and $[Fe^{2+}]_0$ it is observed that they are not parameters with a high influence. The replicated experiments, i.e. the three last ones, show a slight deviation.

Table 3.1-2: Tests and results. The three first columns are the experimental conditions of the tests carried out. The other columns are the results obtained from these experiments.

| Nº | $[Fe^{2+}]_0$ (mM) | $[H_2O_2]_0$ (mM) | T (ºC) | 4-CP removal | TOC removal | COD removal | $BOD_5/COD$ ratio | $BOD_5$ (mg $O_2.L^{-1}$) | Time (min) |
|---|---|---|---|---|---|---|---|---|---|
| 1 | 0.082 | 2.76 | 27.3 | 0.710 | 0.002 | 0.183 | 0.068 | 18.5 | 14 |
| 2 | 0.082 | 2.76 | 62.7 | 0.716 | 0.016 | 0.132 | 0.072 | 20.0 | 3.5 |
| 3 | 0.312 | 2.76 | 62.7 | 0.732 | 0.042 | 0.138 | 0.067 | 20.0 | 4 |
| 4 | 0.312 | 2.76 | 27.3 | 0.804 | 0.000 | 0.189 | 0.072 | 20.5 | 6 |
| 5 | 0.082 | 9.00 | 27.3 | 1.000 | 0.170 | 0.463 | 0.174 | 31.5 | 70 |
| 6 | 0.082 | 9.00 | 62.7 | 0.999 | 0.171 | 0.441 | 0.143 | 27.0 | 10 |
| 7 | 0.312 | 9.00 | 62.7 | 1.000 | 0.141 | 0.423 | 0.161 | 32.0 | 5 |
| 8 | 0.312 | 9.00 | 27.3 | 1.000 | 0.117 | 0.480 | 0.139 | 26.0 | 22 |
| 9 | 0.036 | 5.88 | 45.0 | 0.971 | 0.067 | 0.325 | 0.116 | 27.0 | 36 |
| 10 | 0.197 | 1.47 | 45.0 | 0.512 | 0.000 | 0.132 | 0.057 | 18.0 | 5 |
| 11 | 0.197 | 5.88 | 20.0 | 0.990 | 0.049 | 0.291 | 0.098 | 24.0 | 25 |
| 12 | 0.358 | 5.88 | 45.0 | 0.984 | 0.042 | 0.244 | 0.110 | 28.0 | 3 |
| 13 | 0.197 | 10.29 | 45.0 | 1.000 | 0.176 | 0.434 | 0.166 | 33.0 | 17 |
| 14 | 0.197 | 5.88 | 70.0 | 0.967 | 0.071 | 0.328 | 0.137 | 32.0 | 1.5 |
| 15 | 0.197 | 5.88 | 45.0 | 0.981 | 0.070 | 0.321 | 0.116 | 27.5 | 8 |
| 16 | 0.197 | 5.88 | 45.0 | 0.979 | 0.040 | 0.304 | 0.111 | 27.5 | 7 |
| 17 | 0.197 | 5.88 | 45.0 | 0.979 | 0.016 | 0.257 | 0.115 | 30.3 | 7 |

Concerning the TOC removal, the deviation among the replicates is high. The results cannot be taken strictly, but in a qualitative way. The highest TOC removal achieved is around 17.6 %,

when working with the highest $[H_2O_2]_0$. In experiments number 1, 4 and 10 the TOC removal is almost negligible. These results do not correlate to those for the COD removal. The COD removal is higher than the TOC removal. This occurs because the intermediates might be more oxidized as compared with the 4-CP but their structure do not suffer many changes. Some species, such as hydroquinone, quinone, and small amounts of 4-chlorocatechol (see chapter 3.1.4) are identified. All of them are more oxidized than 4-CP but they all have 6 organic carbon atoms in their structure. However, the identification of intermediates is not a matter of concern in the present work, and no further study is done around this subject.

Regarding the $BOD_5$ results, it is remarkable that in all the experiments significant $BOD_5$ values (> 18 in all the cases) are achieved. According to this, the treated product would not be highly toxic or completely inhibitory for the bacterial growth. Concerning the biodegradability ratio, none of the products reach the value of $BOD_5/COD > 0.4$ suggested as biodegradable product by *Metcalf and Eddy* (*1991*). As it has been observed by other authors, for instance *Pulgarin et al.* (*1999*), it is possible that the early intermediates are structurally close to the initial compound, in this case 4-CP, and there is no significant increase in biodegradability.

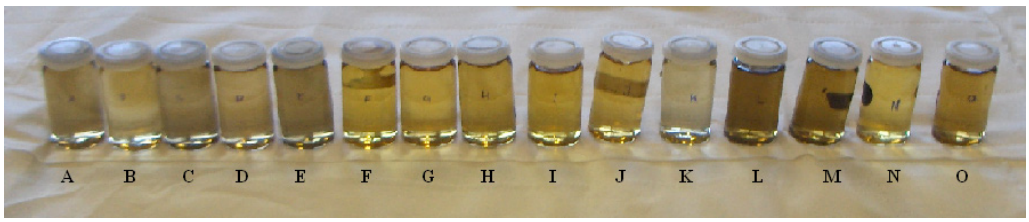


Figure 3.1-1: Photo-Fenton final residues of the different experiments (Experiments 1 to 15 relates to A to O)

### 3.1.3.- Biodegradability Enhancement Study

Although the main purpose of this article is to study the biodegradability enhancement of the wastewater, the 4-CP removal has to be considered, since it is not a biodegradable product ($BOD_5/COD < 0.01$). The degradation of 4-CP to less biorecalcitrant intermediates enhance the biodegradability of the polluted water. Moreover, it is utilized as training for the rest of the study.

As shown in Figure 3.1-2, the initial concentration of hydrogen peroxide has a higher influence than the initial concentration of iron. The increase of 4-CP removal when working with a higher $[Fe^{2+}]_0$ is not very significant. However, the optimum $[H_2O_2]_0$ does not correspond with the highest value. The statistical study shows that there is a maximum around $[H_2O_2]_0 = 7.9$ mM.

This arch-shape behaviour is probably due to an experimental error, since it has been proved that with more $H_2O_2$ than 10.5 mM, the removal of 4-CP is total. However, this fact is not of importance, since the removal rates moves through 0.95-1

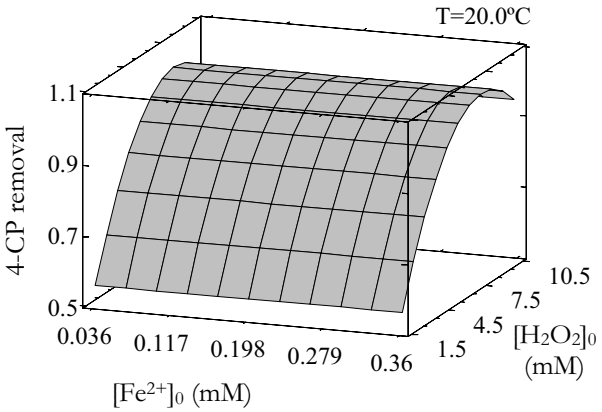


Figure 3.1-2: Surface response for 4-CP removal. Dependence on the $[H_2O_2]_0$ and [Fe(II)]$_0$ is shown. Temperature is fixed at 20ºC. $R^2$=0.983

$$4\text{-}CP\ removal = 0.32(\pm 0.03) + 0.18(\pm 0.01)\cdot[H_2O_2]_0 - 0.01(\pm 0.001)\cdot[H_2O_2]_0^2 \qquad \text{Equation 3.1-1}$$

Equation 3.1-1 is the regression equation that fits the experimental data of 4-CP removal. The equation has only two significant effects, a positive connection with $[H_2O_2]_0$, which means that 4-CP removal increases with this parameter, and a negative squared-effect $[H_2O_2]_0^2$, that is the mathematical description of the plateau that is achieved with the highest $[H_2O_2]_0$. In fact, this is one of the reasons to not use the equation out of the experimentation range, since according to the equation, with higher $[H_2O_2]_0$, the removal would decrease.

As assessed by the statistical tool, the temperature does not increase the degradation rate significantly. A Pareto Chart is shown in Figure 3.1-3. The length of each bar is proportional to the standardised effect, which is the estimated effect divided by its standard error. Any bars, which extend beyond the line correspond to effects that are statistically significant at 95 % of confidence level. As it is shown in the figure, the standardized effects for $[Fe^{2+}]_0$ ("Fe" in the plot) and temperature ("T" in the plot) are below the 95 % of confidence level. The only effects that are statistically significant are $[H_2O_2]_0$ and its interaction ($x^2$), which produces this apparent decrease in 4-CP removal at higher $H_2O_2$ concentrations.

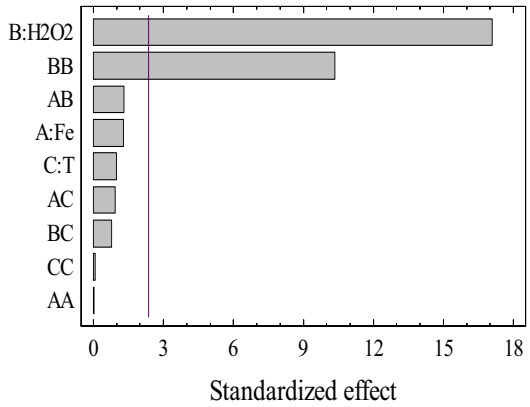


Figure 3.1-3: Standardized Pareto Chart for 4-CP removal.

Figure 3.1-4 shows the response surface of $BOD_5$ obtained from the experiments. As in the 4-CP removal results, the higher the $[H_2O_2]_0$, the higher the $BOD_5$ achieved, but in this case, the maximum value is achieved at the edge. By observing the shape of the response surface, it seems that when increasing the hydrogen peroxide dose, a higher $BOD_5$ would not be achieved. Temperature and $[Fe^{2+}]_0$ do not imply a significant influence on the $BOD_5$ response. The statistical tool proposes a temperature of 62ºC as an optimal condition, but it is only a mathematical optimization. Similar results were obtained for different temperatures. The standardized effect for temperature is below the 95 % of confidence level.

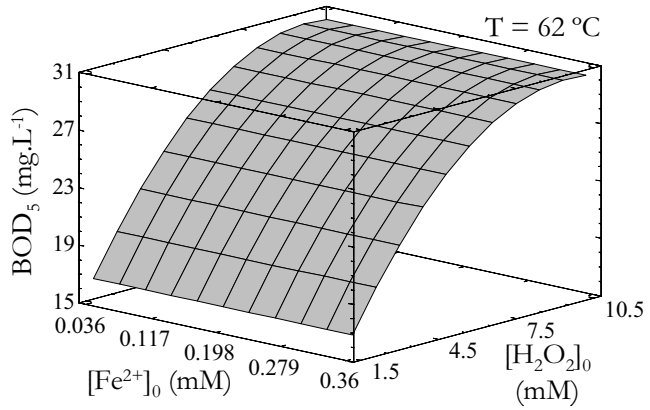


Figure 3.1-4: $BOD_5$ of Ph-F products depending on $[Fe^{2+}]_0$ and $[H_2O_2]_0$, at T = 62 ºC. $R^2$=0.78

$$BOD_5 = 11.18(\pm 2.99) + 3.95(\pm 1.13)\cdot[H_2O_2]_0 - 0.20(\pm 0.09)\cdot[H_2O_2]_0^2 \qquad \text{Equation 3.1-2}$$

The equation that fits the $BOD_5$ experimental data is Equation 3.1-2. The statistically significant variables are the $H_2O_2$ dose, as a positive effect, and its own interaction ($x^2$), which is a negative effect. However, the factor that multiplies the square effect of hydrogen peroxide, it has an order of magnitude 10 times smaller, which means that maximum it "slows down" the biodegradability increase, as it happens with the *4-CP removal* equation.

The effect of $[H_2O_2]_0$ and $[Fe^{2+}]_0$ on the biodegradability is shown in Figure 3.1-5. The highest the $[H_2O_2]_0$, the highest the $BOD_5/COD$ ratio, but $[Fe^{2+}]_0$ and temperature do not imply a significant effect on the response, as observed by the statistical software. Any $[Fe^{2+}]_0$ and Temperature used would attain a similar $BOD_5/COD$ result.

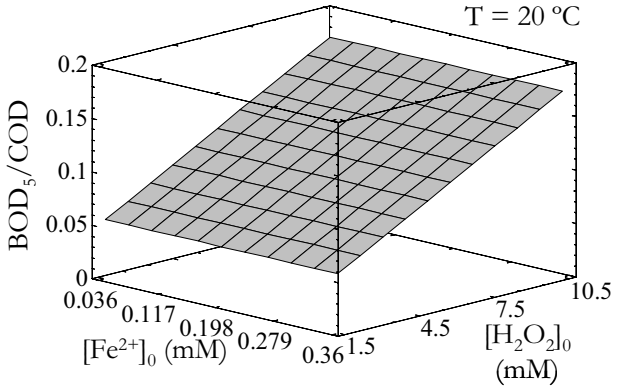


Figure 3.1-5: $BOD_5/COD$ versus $[Fe^{2+}]_0$ and $[H_2O_2]_0$. Temperature fixed at 20ºC. $R^2$=0.882.

$$BOD_5/COD = 0.036(\pm 0.006) + 0.013(\pm 0.001)[H_2O_2]_0 \qquad \text{Equation 3.1-3}$$

In this case, any of the $BOD_5/COD$ results did not reach a value higher than 0.4. However, this is not a significant problem since it is well known (*Moreno and Buitron, 2004*), it is possible to feed a bioreactor with a wastewater which biodegradability ratio is lower than 0.4. In these cases, the biofilter start-up might be longer.

The regression equation (Equation 3.1-3) for $BOD_5/COD$ results correlates with the flat surface response fitted. Only $[H_2O_2]_0$ affects the estimation.

When comparing 4-CP removal, $BOD_5$ and $BOD_5/COD$ results, the main parameter is $[H_2O_2]_0$. Both the temperature and $[Fe^{2+}]_0$ do not demonstrate a significant effect on the results.

According to the $BOD_5$/COD results, it is advisable to carry out more experiments using higher $[H_2O_2]_0$, since the maximum value was achieved with the maximum $H_2O_2$ dose. However, the flat behaviour of the $BOD_5$ response at the highest $H_2O_2$ doses could mean that a maximum $BOD_5$ is achieved. This correlates with the TOC and COD removal results. Higher peroxide doses would entail higher oxidation and mineralization, and therefore, fewer amounts of substances able to be oxidized by biological activity (i.e. $BOD_5$).

After being treated by Ph-F, all the effluents might be fed into a biological reactor, since none of them shows toxic or significant inhibitory effects on $BOD_5$ analysis. In all the experiments, a $BOD_5$ over 18 mg $O_2.L^{-1}$ is achieved.

### 3.1.4.- By-products of 4-chlorophenol degradation

The treatment of 4-chlorophenol solutions by photo-Fenton leads to different intermediates. A literature review has been done. Some of the intermediates match the HPLC results obtained.

The first mechanism involves the attack of hydroxyl radicals to benzene rings by substitution reactions. It is also possible that occurs the formation of p-chloro-phenoxy radical that, in turn, reacts with 4-CP giving rise to the formation of bigger molecules, such as the ones labelled under "Polymerization" in Figure 3.1-6. The process continues with the further oxidation to aliphatic intermediates, such as carboxylic acids and finally occurs the mineralization up to $CO_2$.

Concerning the biodegradability, it stands out that some of the species in the first group of by-products (substitution) are equal or even more toxic than 4-chlorophenol. The HPLC analysis of the samples identified some of these compounds, but small amount of them. This results correlates to the fact that all the obtained effluents have significant value of $BOD_5$ but not a high value. The toxic intermediates, in this low concentration do not produce an inhibitory effect.

### 3.1.5.- Optimization. Operating costs calculation

The statistical tool proposes a strong dependency with the $H_2O_2$, but no dependency concerning the other factors. In this case, the lowest value for $[Fe^{2+}]_0$ and Temperature are proposed, which are 2 $mg.L^{-1}$ (0.036 mM) and 20ºC for the $[Fe^{2+}]_0$ and Temperature respectively. However, these operating conditions entail long operating time, and consequently high operating costs could be expectable. Thus, an optimization is suggested.

For the evaluation of the optimal operating conditions, a comparison between the biodegradability results with the operating costs is proposed. For this purpose, Equation 3.1-4 is

suggested. The equation is established taking into consideration the amounts of the reagents and the energy costs, i.e. those related to time.

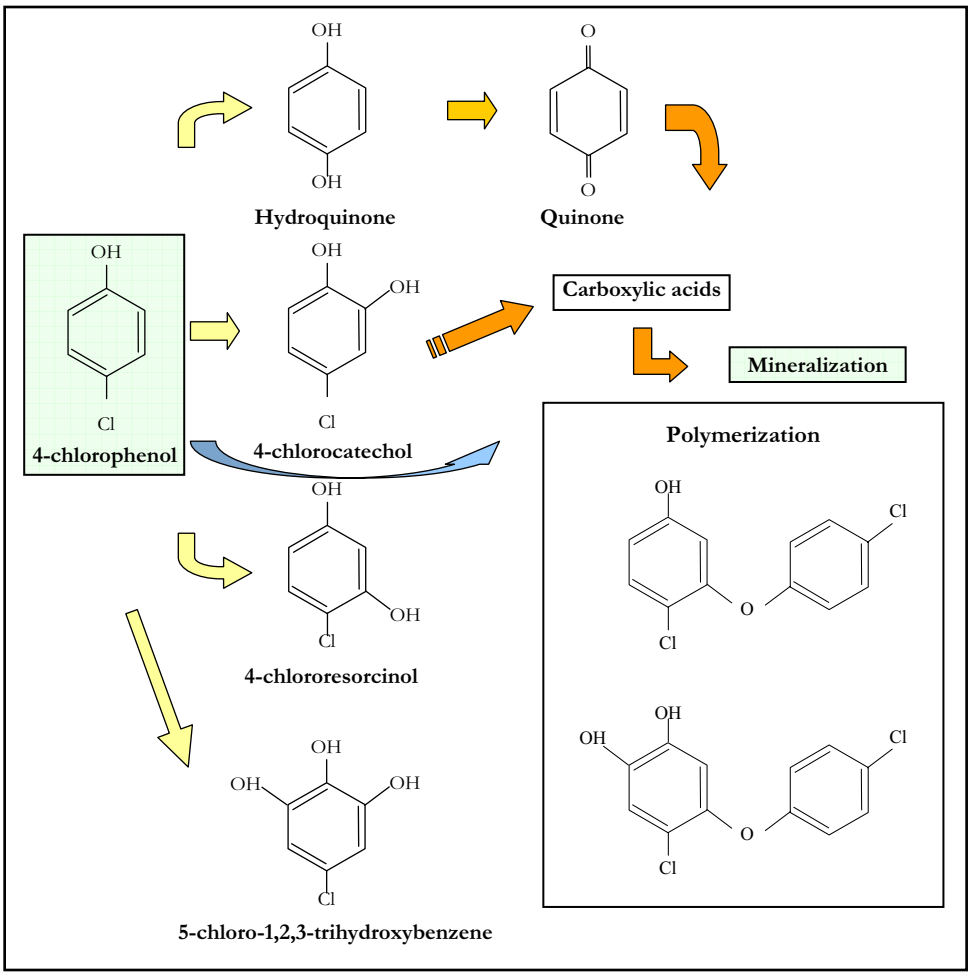


Figure 3.1-6: Some of the by-products of 4-chlorophenol degradation. Adapted from *Raja et al* (*2005*).

$$Costs = C_{H_2O_2} \cdot A + C_{Fe^{2+}} \cdot B + \left(C_{heating} + C_{UV}\right) \cdot time \qquad \text{Equation 3.1-4}$$

Where $C_{H2O2}$ and $C_{Fe2+}$ are the reagents costs, and $A$ and $B$ their amounts; $C_{heating}$ and $C_{UV}$ are the costs of the heating and the UV systems per time; and time, represents the period of time needed to consume all the hydrogen peroxide.

In these calculation the energy cost is 0,083 €/kWh, and the reagents costs are 17.95 €/kg for $FeSO_4 \cdot 7H_2O$ as the source of $Fe^{2+}$ and 7.814 €/L for $H_2O_2$ 30% p/v. When calculating the heating costs the operating temperature must be taken into consideration. The UV costs are calculated considering that 3 lamps of 8 W each (24 W altogether) are used.

To carry out the optimization is necessary to fix some operating condition. Since the aim of this work is to enhance the biodegradability, the optimization is done fixing the highest $[H_2O_2]_0$ value, because the highest biodegradability is achieved when working at this operating conditions (Figure 3.1-7).

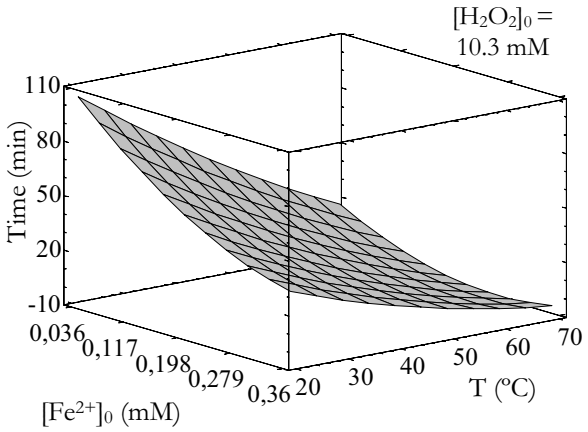


Figure 3.1-7: Experiment time versus $[Fe^{2+}]_0$ and temperature. $[H_2O_2]_0$ fixed at 10.29. $R^2$=0.934

$$Time = 23.7 - 289.0 \cdot [Fe^{2+}]_0 + 12.3 \cdot [H_2O_2]_0 - 0.3 \cdot T + 411.4 \cdot [Fe^{2+}]_0^2 - 15.8 \cdot [Fe^{2+}]_0 \cdot [H_2O_2]_0 + 3.2 \cdot [Fe^{2+}]_0 \cdot T - 0.1 \cdot [H_2O_2]_0 \cdot T$$

Equation 3.1-5

One of the possibilities that allow the statistical tool is the Effect Plot (Figure 3.1-8), which shows the response as a function of each experimental factor. In each line, the variable of interest varies from its lowest level to its highest level, while all the other factors remain constant at their central values. Regarding Time response, it can be observed that all the variables in this case are significant. In an opposite way than in the previous results, $[Fe^{2+}]_0$ and temperature entail high influence on the experiment time.

The influence of iron in this case is not negligible. Iron acts in the mechanism as the catalyst of the reaction. The total absence of iron would involve a negligible degradation rate, but in the

presence of iron, the hydroxyl radical production begins. An explanation for this behaviour would be that the amount of hydroxyl radical (or oxidizing agent) produced depends on the hydrogen peroxide, as the reagent in the mechanism, but the iron concentration affects the rate at which they are produced, since it acts as a catalyst of the reaction. Regarding the influence of the temperature, the higher the temperature is, the faster the reaction becomes.

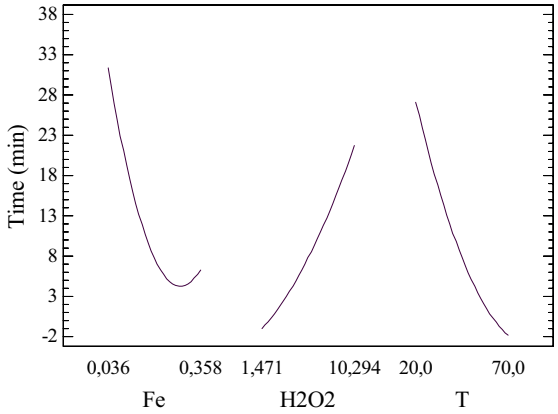


Figure 3.1-8: Main Effect plot for Time

In this case, regression equation (Equation 3.1-5) is affected by many parameters, if compared with the previous ones. This means that not only the reagents doses but also the temperature, and other interactions, affect significantly the results. If the equation is analyzed, it can be noticed that $[Fe^{2+}]_0$, temperature and the interactions of $[H_2O_2]_0$ with temperature and $[Fe^{2+}]_0$ reduce time, but $[H_2O_2]_0$ produces an increase of time. Iron (as a catalyst) and temperature (because affects the kinetics) obviously reduce time, as seen before in the surface response analysis. The higher the $[H_2O_2]_0$, the longer the reaction, because it lasts more to consume the whole amount of reagent.

A response surface adjustment of operating costs is plotted in Figure 3.1-9. In this case, $H_2O_2$ is fixed at its maximal value, since it produces the highest biodegradability. As shown in the figure, the effect of $[Fe^{2+}]_0$ seems to be stronger than the temperature effect. The statistical software only assesses the $[Fe^{2+}]_0$ (apart from $[H_2O_2]_0$) statistically significant at a 95.0% confidence level.

Observing the temperature effect, the operating costs are reduced when increasing the temperature, but the difference is not high. It would be possible to take advantage of temperature, but if it does not bring any additional cost. For example, it would be fine when the wastewater is received at a high temperature, but it is not necessary to heat the wastewater

produced at lower temperatures. When operating at high temperatures, it has to be taken into consideration recovering energy.

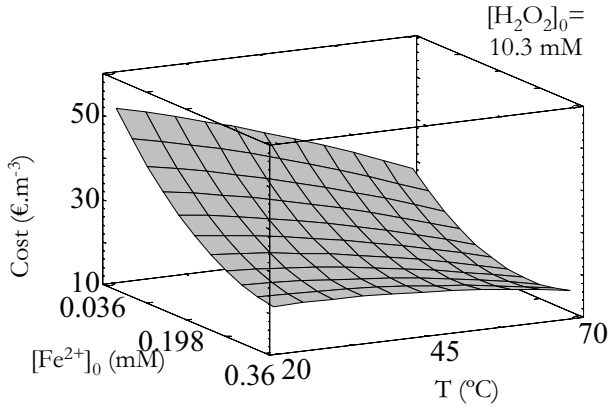


Figure 3.1-9: Operating Costs versus $[Fe^{2+}]_0$ and temperature. $[H_2O_2]_0$ fixed at 10.29 mM. $R^2$=0.92

One more aspect to point out about the temperature is that if a further biological treatment is expected, to work at a higher temperature than 40 ºC is not desirable, since can result in the death of the microorganisms, as observed by *Rivas et al.* (*2003a*).

## *3.2.- Characterization of Photo-Fenton products*

The present Section aims for the characterization of the Photo-Fenton products obtained in Laboratory experiments. A list of parameters is presented in order to describe the properties of a determined Ph-F product.

As the objective is the integration of the photochemical process and a biological SBBR treatment, the listed parameters are related to concepts such as organic content, biodegradability and toxicity.

A set of 6 experiments is compared. These experiments are named concerning the doses of $H_2O_2$ applied in the Ph-F treatment, which range from 50 to 500 mg.L$^{-1}$. The range of $H_2O_2$ is broader than in the Experimental Design, since more readily biodegradable Ph-F products are likely to be required for the SBBR study. In all these experiment, operating temperature is fixed and controlled at 27 ºC and the dose of $Fe^{2+}$ is 10 mg.L$^{-1}$. As seen above (Section 3.1.3) there is no significant influence of iron and temperature on the degradation obtained by Ph-F.

Furthermore, by this iron concentration of 10 mg.L$^{-1}$, the experiments do not last too much (around 50 minutes in the longest case), and it obeys the legislation limit for industrial wastewater discharge to public treatment network in the Barcelona (Spain) Metropolitan Area, which is precisely 10 mg.L$^{-1}$ (*EM, 2004*).

### 3.2.1.- Organic content and biodegradability

The first information for the characterization concerns to chemical and biochemical oxygen demands. Actually, it is a direct measure of organic matter, since inorganic sources of oxygen demand (sulphides, nitrites, etc.) are not present in the solution. Results are summarized in Figure 3.2-1 and Figure 3.2-2. On the left, the figure shows the COD and $BOD_5$ reached depending on the initial concentrations of $H_2O_2$ tested. On the right figure, the ratio $BOD_5/COD$ is shown, together with the Average Oxidation State (AOS).

AOS is an indicator of the oxidation degree of complex solutions and may give information on the probability of being degraded by biological means. AOS is a ratio between TOC and COD in molar units, and is calculated as follows.

$$AOS = 4 \cdot \frac{TOC - COD}{TOC}$$ Equation 3.2-1

In the figures, the results labelled as "0 mg.L$^{-1}$" of $H_2O_2$, indicate the properties of the initial solution (200 mg.L$^{-1}$ of 4-CP).

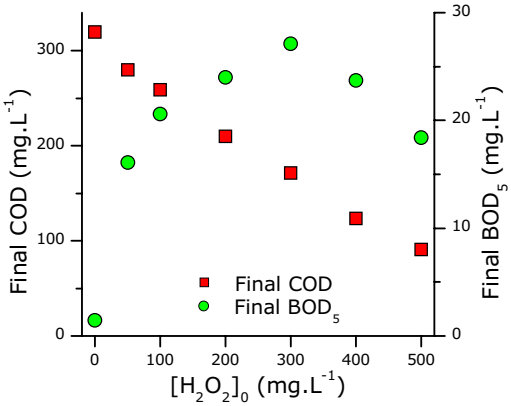


Figure 3.2-1: Summary of COD and $BOD_5$ results. $Fe^{2+}$ = 10 mg.L$^{-1}$; T = 27 ºC.

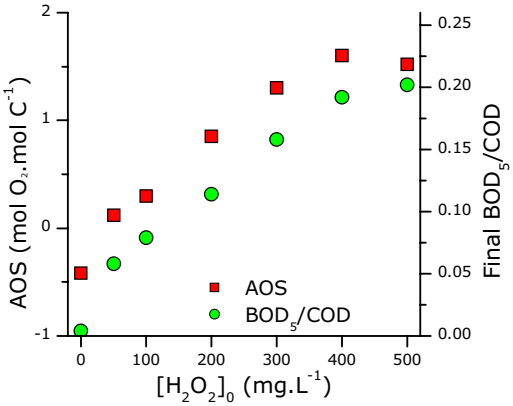


Figure 3.2-2: Summary of Biodegradability and AOS results. $Fe^{2+}$ = 10 mg.L$^{-1}$; T = 27 ºC.

Regarding COD results, as the dose of $H_2O_2$ increases, the product's COD decrease linearly. On the other hand, $BOD_5$ values increase up to a certain dose of $H_2O_2$ (300 $mg.L^{-1}$), and from then on, decrease. Their ratio ($BOD_5/COD$) which uses to mean the biodegradability, increase significantly in the beginning and the enhancement becomes more slightly with the highest $H_2O_2$ doses. It can be emphasized that for $BOD_5$ and $BOD_5/COD$ results, between 50 and 350 $mg.L^{-1}$ of $H_2O_2$, which are the boundary conditions of the previous experimental design, very similar tendencies than in that case are observed. Concerning $BOD_5$, a hard increase with low $H_2O_2$ doses takes place and thereafter it tends towards a plateau. In relation to $BOD_5/COD$, a linear increase over this experimental region (50-350 $mg.L^{-1}$ of $H_2O_2$) is observed.

According to these results, it would be suitable to feed the biological reactor with the Ph-F product obtained with 300 $mg.L^{-1}$ of $H_2O_2$. By these operating conditions, mineralization is low, which means that there remains a considerable organic load for the biological reactor and most of the oxidation serves for increasing the biodegradability. AOS does not provide any conclusive information. AOS profile is practically identical than the biodegradability. It corroborates the $BOD_5/COD$ results, but it does not contribute with new arguments for the identification of biodegradable Ph-F products.

The decrease of $BOD_5$ when the highest $H_2O_2$ doses are applied does not mean that these products are less biodegradable. It is, in fact, a consequence of mineralization of organic matter, which can be observed in Figure 3.2-3. According to the results, with $H_2O_2$ amounts up to 300 $mg.L^{-1}$, mineralization achieved rounds only 10 %. From then on, mineralization increase significantly.

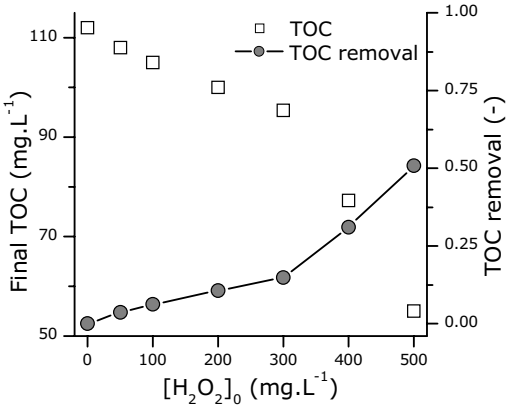


Figure 3.2-3: Ph-F products TOC content and removal. $Fe^{2+}$ = 10 $mg.L^{-1}$; T = 27 ºC.

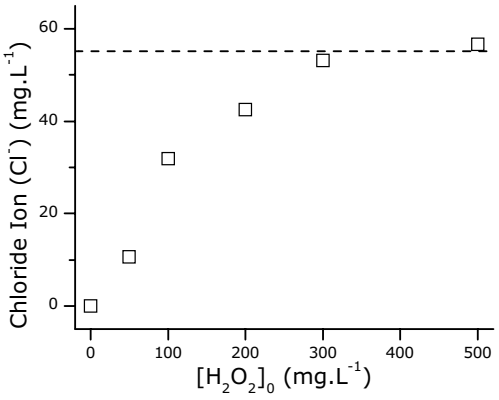


Figure 3.2-4: Release of chloride ion depending on the $H_2O_2$ dose in Laboratory Ph-F treatment; $[Fe^{2+}]_0$ = 10 $mg.L^{-1}$; T = 27 ºC.

Chloride Ion in solution has been also analyzed. As there is no chloride in the solution prior to the Ph-F treatment, all chloride detected has been released due to the treatment. By comparision with the stoichiometric amount, it is likely to know the chloride that is still part of organic compounds, i.e. the chlorinated compounds that may remain in the mixture. Consequently, it is an indicator of the product's toxicity, since chlorinated compounds are ususally toxic. Figure 3.2-4 shows the values of chloride ion in solution depending on the dose of $H_2O_2$ applied in Photo-Fenton experiments. The dashed line indicates the stoichiometric chloride ion that may release 200 mg.L$^{-1}$ of 4-CP.

### 3.2.2.- Acute Toxicity of Photo-Fenton products

A standardized parameter to assess the acute toxicity of a solution is the $EC_{50}$ measured by Microtox. $EC_{50}$ is defined as the median effective concentration, and is a calculated toxicity value representing the sample concentration (%) estimated to cause 50 % response by the exposed test organisms. In this case, the organisms are marine bioluminescent bacteria, and the response is the light emitted by these bacteria, measured at 490 nm of wavelength.

As explained in the analytical methods section (Section 2.3.5), the effect is measured after a determined time. In this case, the effects are observed after 15 minutes of contact between a sample and the bacteria. An additional assessment of toxicity is the Toxicity Unit (TU), which is calculated by Equation 3.2-2.

$$TU = \frac{100}{EC_{50}} \qquad \text{Equation 3.2-2}$$

Figure 3.2-5 and Figure 3.2-6 show the results obtained by the Microtox test. The former is a representation of the $EC_{50}$ at 15 minutes, and the latter is the TU concerning the dose of $H_2O_2$.

It can be observed clearly, that toxicity is significantly high for Ph-F products obtained with $H_2O_2$ doses lower than 300 mg.L$^{-1}$. That is to say that a small fraction of sample is enough to cause at least 50 % of effect on the tested bacteria. In fact, the value of toxicity for the 50 mg.L$^{-1}$ experiment has been obtained by a strong extrapolation after dilution of the initial sample, which means that the $EC_{50}$ could be even lower (or the TU even higher). On the other hand, the products obtained with doses up to 400 mg.L$^{-1}$ present no toxicity. In fact, these results are really linked to chloride ion values; in so far as there remain less chlorinated compounds, toxicity decreases.

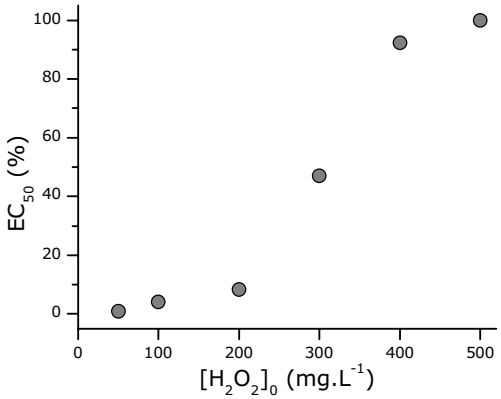


Figure 3.2-5: Microtox Results. Median Effective Concentration – 50 % response – 15 min test. Laboratory Ph-F. $[Fe^{2+}]_0$ = 10 mg.$L^{-1}$; T = 27 ºC.

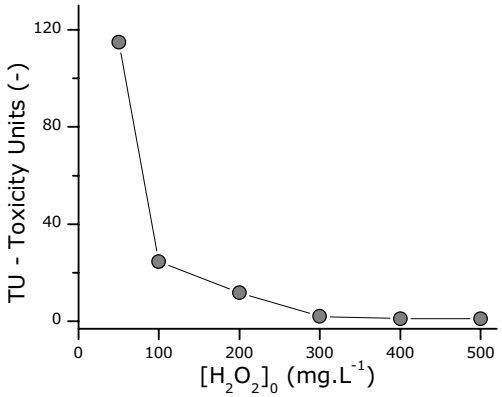


Figure 3.2-6: Microtox Results. Toxicity Units. Laboratory Ph-F. $[Fe^{2+}]_0$ = 10 mg.$L^{-1}$; T = 27 ºC

According to the results, Photo-Fenton treatment demonstrates to be a good technology to decrease toxicity of solutions polluted by toxic aromatic compounds.

## *3.3.- Scaling-up of the Photo-Fenton process*

One of the main engineering aspects of the study of a process is the scaling-up. In this stage, a process is tested at a so-called pre-industrial scale, in order to prove whether the laboratory considerations are fulfilled, and efficiencies decrease or increase.

In this case, the experiments were carried out at the facilities of "Plataforma Solar de Almería", in the province of Almería, Spain. The reactor has a capacity of 82 L and consists of amongst other, a solar panel, which means that the irradiation source is not artificial, but the sun.

As stated in the introduction, solar spectrum is wider than a simple UVA spectrum. In this case, there is emission in the visible spectrum. There are many possible interactions between visible radiation and diverse compounds and complexes likely to be present during a Ph-F reaction. As these interactions are very difficult to be controlled, and contribution of UVA is supposed to be of more importance, visible light is obviated.

Another aspect is that radiation may fluctuate over an experiment and may be different from an experiment to another. It is not a fixed variable. Thus, in order to compare experiments the normalized 30 W time ($t_{30W}$) is used. It has been explained in the methods section (2.1.2).

### 3.3.1.- Experimental Design

In order to study the scale-up of the photo-Fenton process and compare the results with the ones obtained by the laboratory reactor, an experimental design is planned. The operating conditions are chosen taking into account the best results in the laboratory experiments. As a model wastewater to be treated, a solution of 200 $mg.L^{-1}$ of 4-chlorophenol is going to be used as well.

Thus, the lowest hydrogen peroxide doses are excluded of this study, since their products do not entail a significant improve of biodegradability and the doses that produce better biodegradable products (in the laboratory) are chosen for this study ($[H_2O_2]_0$ = 300, 400 and 500 $mg.L^{-1}$). As it is shown in Table 3.3-1, only iron and hydrogen peroxide doses are modified this time, while temperature is fixed at 27 ºC and pH at 2.8.

Table 3.3-1: Experimental Design. Operating conditions of the experiments carried out with the solar reactor. $[4\text{-CP}]_0$ = 200 $mg.L^{-1}$.

| Exp. | $[4\text{-CP}]_0$ ($mg.L^{-1}$) | $[Fe^{2+}]_0$ ($mg.L^{-1}$) | $[H_2O_2]_0$ ($mg.L^{-1}$) | codification | | Temperature (ºC) | Initial pH |
|---|---|---|---|---|---|---|---|
| | | | | $Fe^{2+}$ | $H_2O_2$ | | |
| 1 | 200 | 10 | 500 | 0 | + | 27 | 2.8 |
| 2 | 200 | 10 | 400 | 0 | 0 | 27 | 2.8 |
| 3 | 200 | 10 | 300 | 0 | - | 27 | 2.8 |
| 4 | 200 | 2 | 300 | - | - | 27 | 2.8 |
| 5 | 200 | 20 | 300 | + | - | 27 | 2.8 |
| 6 | 200 | 20 | 500 | + | + | 27 | 2.8 |
| 7 | 200 | 2 | 500 | - | + | 27 | 2.8 |

The first aim is the evaluation of biodegradability enhancement produced by the Up-scaled Solar-Photo-Fenton process.

The second aim is the evaluation of the efficiency, which is estimated by comparing the $H_2O_2$ consumed with the COD abated. To this end, three different iron doses are tested, different enough to observe an improvement or worsening of the process, if exist. These results are not shown in the current section, but in Section 3.4.

As seen previously, iron dose plays a significant role on the degradation kinetics and so does temperature. However, temperature is fixed at near ambient conditions (27 ºC). Economically it is preferable to allow temperature to fluctuate free. However, this might cause interferences on the effects prompted by an excess or lack of iron. In order to avoid these interferences, and to study with accuracy the process, temperature is fixed.

### 3.3.2.- Experimental results

Results of TOC and COD removal as well as final COD and $BOD_5$ values are presented in Table 3.3-2 and depicted in Figure 3.3-1 and Figure 3.3-2.

Table 3.3-2: Main degradation results of the experiments in the PSA

| Exp. | $[Fe^{2+}]_0$ (mg.L$^{-1}$) | $[H_2O_2]_0$ (mg.L$^{-1}$) | TOC removal | COD removal | Final COD (mg.L$^{-1}$) | Final $BOD_5$ (mg.L$^{-1}$) | Q (kJ.L$^{-1}$) |
|---|---|---|---|---|---|---|---|
| 1 | 10 | 500 | 0.60 | 0.77 | 75.8 | 14.5 | 4.44 |
| 2 | 10 | 400 | 0.38 | 0.67 | 122.0 | 25.5 | 3.1 |
| 3 | 10 | 300 | 0.22 | 0.47 | 176.2 | 25.5 | 2.76 |
| 4 | 2 | 300 | 0.31 | 0.56 | 146.6 | 35.5 | 7.57 |
| 5 | 20 | 300 | 0.22 | 0.51 | 175.8 | 23.5 | 1.24 |
| 6 | 20 | 500 | 0.59 | 0.76 | 80.3 | 14.5 | 1.93 |
| 7 | 2 | 500 | 0.67 | 0.82 | 59.9 | 15.5 | 8.38 |

Interestingly, the results of the experiments carried out with the same amount of $H_2O_2$ but with 10 or 20 mg.L-1 of $Fe^{2+}$ are practically identical. Experiments carried out with the lowest amount of iron, entail around 8 % more degradation. As seen in the introduction, $Fe^{2+}$ is an accelerator of the so-called scavenging reactions. Moreover, all the coloured compounds and iron complexes absorb in the visible spectrum. There is an experiment, number 4, that stands out from the rest. Its performance is around 10 % better in degradation properties, and $BOD_5$ is much over the average.

Q is the accumulated energy over an experiment related to the UVA spectrum. Obviously, as long is the experiment, more energy has arrived to the system, and this happens with the experiments with the lowest amount of $Fe^{2+}$ applied.

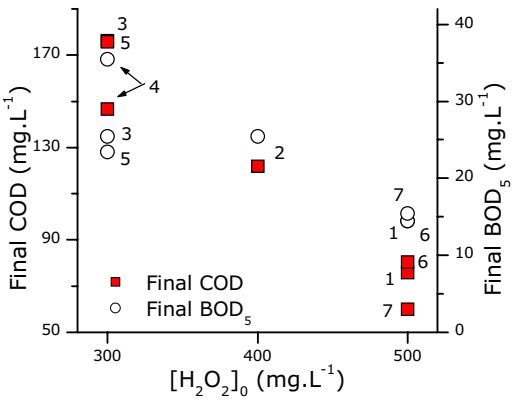


Figure 3.3-1: Final COD and $BOD_5$ values for scaled-up experiments.

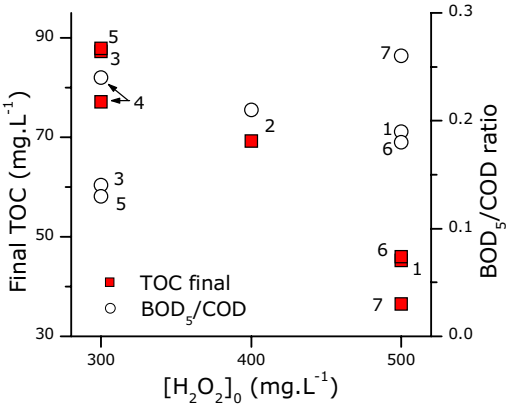


Figure 3.3-2: Final TOC and biodegradability results for scaled-up experiments.

In the figures, the values concerning the experiments carried out with 10 or 20 $mg.L^{-1}$ of iron are practically superposed, whereas the values for the experiments with 2 $mg.L^{-1}$ are better in any case (more degradation or higher biodegradability).

### 3.3.3.- Data collected over the Experiments

Within these experiments, TOC and $H_2O_2$ concentrations are monitored over time. The device disposes of on-line H2O2 measurement. However, as it does not show a good performance, $H_2O_2$ titrimetric analysis is carried out. Data of two different experiments are presented in Figure 3.3-3 and Figure 3.3-4. The values of $H_2O_2$ are going to be used in Section 3.5 for modelling the process by mechanistic models.

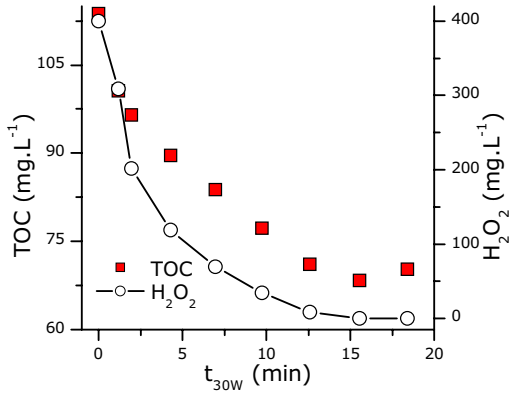


Figure 3.3-3: Exp. 2. $[H_2O_2]_0$ = 400 $mg.L^{-1}$; $[Fe^{2+}]_0$ = 10 $mg.L^{-1}$

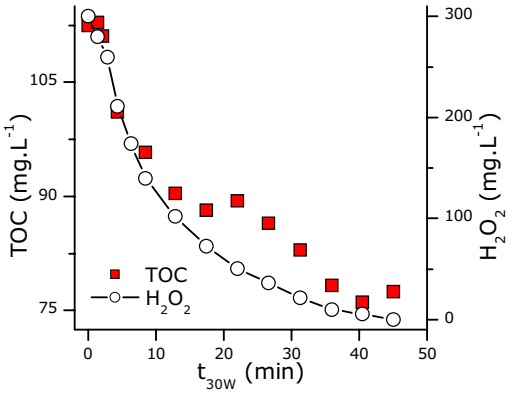


Figure 3.3-4: Exp. 4. $[H_2O_2]_0$ = 300 $mg.L^{-1}$; $[Fe^{2+}]_0$ = 2 $mg.L^{-1}$

### 3.3.4.- Comparison with laboratory results

Figure 3.3-5 and Figure 3.3-6 show a comparison of up-scaled experiments with laboratory experiments. No major differences can be observed. Regarding degradation and biodegradability results there are no differences. Consequently, similar relations between results and $H_2O_2$ can be written for both laboratory and up-scaled experiments.

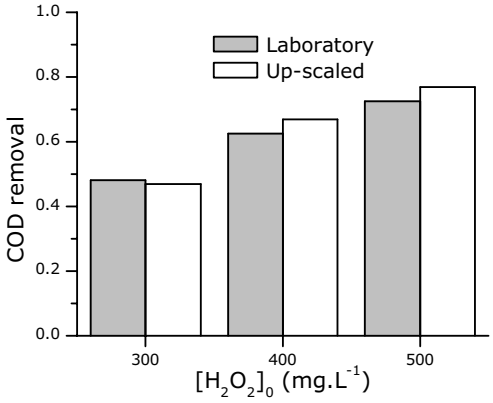


Figure 3.3-5: Comparison of COD removal

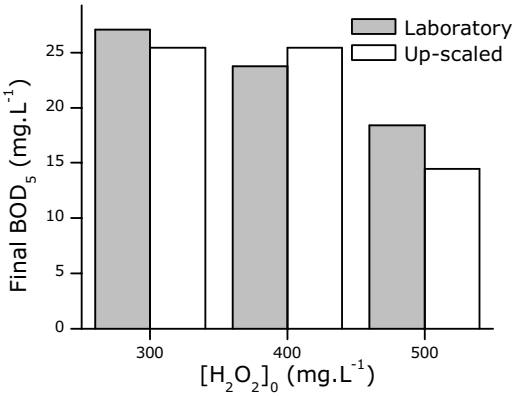


Figure 3.3-6: Comparison of Final $BOD_5$

### 3.3.5.- The Addition Experiment

Another experiment is carried out. It is called "Addition experiment" because in this case, $H_2O_2$ is added in doses of 50 mg.L$^{-1}$. When the first dose of $H_2O_2$ is totally consumed, 50 mg.L$^{-1}$ more are added. This is repeated until 550 mg.L$^{-1}$ have been consumed. Figure 3.3-7 compares the results of the individual with the present addition experiment. The results are practically superposed. These results are going to be very useful in the studies presented in sections 3.4 and 3.5.

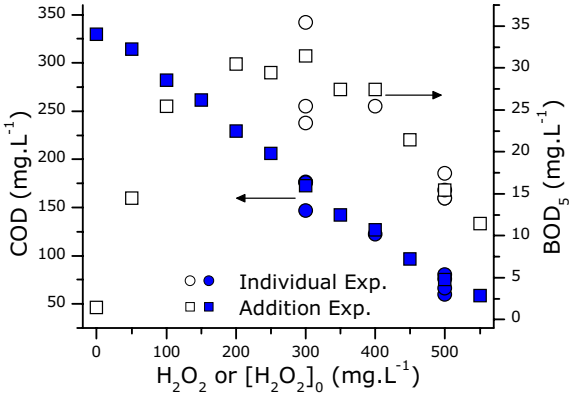


Figure 3.3-7: Comparison of Addition and Individual Experiments carried out in the pre-industrial scale installation. Solid figures: COD; white figures: $BOD_5$

## 3.4.- Simple Models for the control of Photo-Fenton by monitoring $H_2O_2$

Different responses can be observed in order to control Photo-Fenton efficiency. The most common are the abatement rate of single species, the analysis of Total Organic or Dissolved Organic Carbon (TOC and DOC respectively) and Chemical Oxygen Demand (COD), which usually is the most required for the legislation.

In the last years, different methods have been evaluated in order to describe the behavior of different responses of Fenton and Photo-Fenton processes under diverse operating conditions. Several studies have discussed and modeled the abatement of numerous single pollutants (*Paterlini and Nogueira, 2005*), real wastewater (*Torrades et al., 2003*), degradation of TOC and COD, process kinetics (*Chu et al., 2005*), and also the integration with biological treatment (*Rivas et al., 2003b*). Some recent studies, deal with the identification and modeling of Ph-F process control parameters. Specifically, *Gernjak et al.* (*2006*), present models for predicting DOC degradation over time and also regarding the amount of hydrogen peroxide consumed. Furthermore, *Alvarez et al.* (*2007*) contribute with a successful attempt to model hydrogen peroxide control in solar Ph-F systems.

In this section, it is attempted to describe a mathematical model that correlates the amount of COD degraded depending on the supply of $H_2O_2$. For this purpose, COD is considered a pseudo-compound and it is supposed to behave as a sole substance. COD describes the average oxidation degree of the mixture substances in the way of mineralization to $CO_2$. COD is used as a target parameter instead of TOC, because the first is more sensitive to process oxidation capacity and is a direct measurement of oxidation efficiency. COD is a sum parameter of all species able to be oxidized during the process. As there are no inorganic species in these experiments, COD is a direct measure of organic matter.

If a pattern of COD degraded depending on operating conditions can be defined, it may be possible to estimate the amount of reagent ($H_2O_2$) needed to obtain a certain degree of degradation. By means of this model and with the appropriate supervision of the process, such as monitoring the $H_2O_2$ consumed during the process, it could be possible to control the COD degraded, and in consequence, the Photo-Fenton process.

The experimental part consists of UV-laboratory and solar-up-scaled Photo-Fenton oxidation on 200 $mg.L^{-1}$ 4-chlorophenol (4-CP) solutions under various operating conditions and strategies. In

a first stage, an experimental design is carried out in order to elucidate the importance of operating factors ($H_2O_2$ dose, $Fe^{2+}$ and temperature). In next stages, only $H_2O_2$ is modified, and similar experiments are carried out in laboratory and solar up-scaled devices. In all of them, hydrogen peroxide is supplied at the beginning of the experiment. Finally, a different strategy in the supply of $H_2O_2$ is tested. The reagent is dosed over the experiment in small amounts in order to evaluate if there is a difference of degradation achieved with the other strategy.

### 3.4.1.- Observing the laboratory experiments

Influence of temperature, iron and hydrogen peroxide

The results that are observed in this Section are shown in Table 3.1-2 (Section 3.1.2) and are the result of an Experimental Design in which $H_2O_2$ and $Fe^{2+}$ initial doses and Temperature are analyzed at 5 levels. Table 3.4-1 shows the experimental design and the results concerning COD, which are the COD removal, the amount of COD removed and the Efficiency.

Table 3.4-1: Experimental design of experiments carried out in the laboratory scale reactor.

| Exp. | $[Fe^{2+}]_0$ (mg.L$^{-1}$) | $[H_2O_2]_0$ (mg.L$^{-1}$) | T (ºC) | COD removal (±0.08) | COD removed (mg.L$^{-1}$) (±7.1) | Efficiency (±0.04) |
|---|---|---|---|---|---|---|
| 1 | 4.6 | 93.9 | 27.3 | 0.183 | 60.5 | 0.68 |
| 2 | 4.6 | 93.9 | 62.7 | 0.132 | 43.7 | 0.49 |
| 3 | 17.4 | 93.9 | 62.7 | 0.138 | 45.6 | 0.52 |
| 4 | 17.4 | 93.9 | 27.3 | 0.189 | 62.3 | 0.71 |
| 5 | 4.6 | 306.1 | 27.3 | 0.463 | 152.7 | 0.53 |
| 6 | 4.6 | 306.1 | 62.7 | 0.441 | 145.6 | 0.51 |
| 7 | 17.4 | 306.1 | 62.7 | 0.423 | 139.5 | 0.48 |
| 8 | 17.4 | 306.1 | 27.3 | 0.480 | 158.4 | 0.55 |
| 9 | 2 | 200 | 45 | 0.325 | 107.1 | 0.57 |
| 10 | 11 | 50 | 45 | 0.132 | 43.7 | 0.93 |
| 11 | 11 | 200 | 20 | 0.291 | 96.0 | 0.51 |
| 12 | 20 | 200 | 45 | 0.244 | 80.6 | 0.43 |
| 13 | 11 | 350 | 45 | 0.434 | 143.1 | 0.43 |
| 14 | 11 | 200 | 70 | 0.328 | 108.4 | 0.58 |
| 15 | 11 | 200 | 45 | 0.321 | 105.9 | 0.56 |
| 16 | 11 | 200 | 45 | 0.304 | 100.2 | 0.53 |
| 17 | 11 | 200 | 45 | 0.257 | 103.0 | 0.55 |

Confidence intervals calculated at 95 % of probability.

In order to compare experiments and try to find a pattern that describes the Photo-Fenton process a concept is introduced. The COD removed in each experiment is divided by the supply of oxygen given by the dose of $H_2O_2$, considering this reagent as the sole source of oxygen able to oxidize. Consequently, results are normalized from 0 (no oxidation) to 1 (maximum possible

oxidation). The result of this operation is named "Efficiency" of Photo-Fenton process and is estimated according to the following ratio:

$$Efficiency = \frac{COD_{removed}}{[H_2O_2]_0 \ as \ O_2} \qquad \text{Equation 3.4-1}$$

where hydrogen peroxide initial concentration is expressed in mg $O_2.L^{-1}$.

For example, 350 $mg.L^{-1}$ of $H_2O_2$ supply 329.4 $mg.L^{-1}$ of $O_2$ able to oxidize organic matter (or any species able to be oxidized). A low value of efficiency does not mean that the process in itself is inefficient, since hydrogen peroxide without a catalyst or supply of energy cannot carry out the same oxidation that hydroxyl radicals do (Refer to Table 1.2-1: Standard oxidation potentials).

The response surface of COD removed depending on $[H_2O_2]_0$ and $[Fe^{2+}]_0$ is shown in Figure 3.4-1. As is a mathematical representation that only takes into account the statistically significant parameters, the surface is a plane without any curvature depending on $[Fe^{2+}]_0$. Furthermore, the regression equation, which has been fitted to the experimental data (Equation 3.4-2), expresses that the relation between COD removed and the supply of $H_2O_2$ is linear.

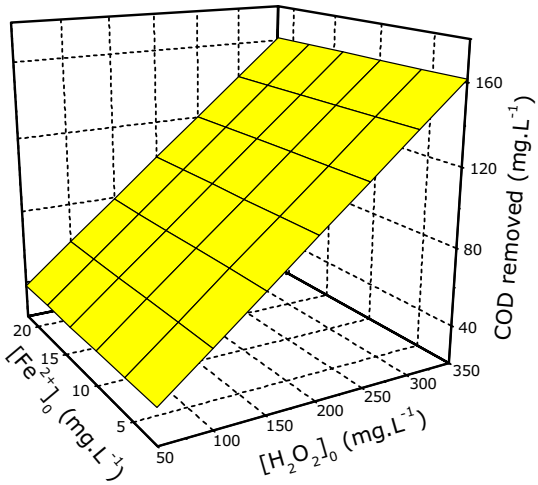


Figure 3.4-1: COD removed Response Surface depending on $Fe^{2+}$ and $H_2O_2$ initial concentrations.

$$COD_{removed} = 17.3\ (\pm 13.0) + 0.41\ (\pm 0.06) \cdot [H_2O_2]_0$$

Equation 3.4-2: COD removed Response Equation.
Valid Range $[H_2O_2]_0$ = 50 – 350 $mg.L^{-1}$. Confidence interval: 95 %

Observing the Efficiency estimations in Table 3.4-1, it is seen that in most of the experiments, the estimated value is similar, and round 0.5, that means that around 50 % of oxygen supplied by

$H_2O_2$ is used to oxidize organic matter. With preciseness, the mean value is 0.56 ±0.06 (confidence interval stated at 95 %).

As the equation that describes COD removed is a polynomial function, it has poor physical-chemical sense. It is possible to describe mathematically the same results with also a linear regression, but in this case, forcing the equation to cross the "0" intersection. This has more chemical sense compared to the polynomial equation, since oxidation cannot take place without hydrogen peroxide (Equation 3.4-3). Another option is a multiplicative equation, which means that the effect of $H_2O_2$ on removed COD is not linear, i.e. changes with concentration (Equation 3.4-4).

$$COD_{removed} = 0.48(\pm 0.03)\cdot[H_2O_2]_0 \qquad \text{Equation 3.4-3}$$

$$COD_{removed} = 1.44(\pm 1.11)\cdot[H_2O_2]_0^{0.80(\pm 0.14)} \qquad \text{Equation 3.4-4}$$

By means of Equation 3.4-3, values of COD removed by Photo-Fenton depending on the $H_2O_2$ initial concentrations can be estimated. Undoubtedly, the estimations of COD removed with low concentrations of $H_2O_2$ by this equation have more error than by the previous equation, because of the suppression of the interception parameter.

As by Equation 3.4-3 the efficiency is considered to be constant for all $H_2O_2$ doses it is also possible to calculate the efficiency, which in this case is 0.52 (±0.06). The value is lower than in the previous estimation, since is estimated from a model in which the extreme values are omitted. This equation does not explain these particular cases.

A specific observation of all experiments in Table 3.4-1 is carried out in order to obtain some considerations to improve the process characterization. The amount of COD removed by different $[H_2O_2]_0$ and different conditions of Temperature and iron concentration are shown in Figure 3.4-2. Each experiment is a square-mark in the plot. The line shows the theoretical stoichiometric oxidation with hydrogen peroxide, in which two moles of $H_2O_2$ release one mole of oxygen ($O_2$) able to oxidize. Most of the results slightly overcome the stoichiometry. Moreover, it seems that the results follow a similar pattern.

As experiments that are carried out with very different initial concentrations of $H_2O_2$ are compared (from 50 to 350 $mg.L^{-1}$) in the same Figure, it is not possible to observe clearly the differences that exist among them. For example, the result of the experiment performed with 50

mg.L$^{-1}$ of $[H_2O_2]_0$, is slightly above the line, like some of the experiments carried out with 300 mg.L$^{-1}$ of $[H_2O_2]_0$. However, the first case is much efficient, since 50 mg.L$^{-1}$ of $H_2O_2$ mean 47 mg.L$^{-1}$ of oxygen supplied, that abate 43 mg.L$^{-1}$ of COD.

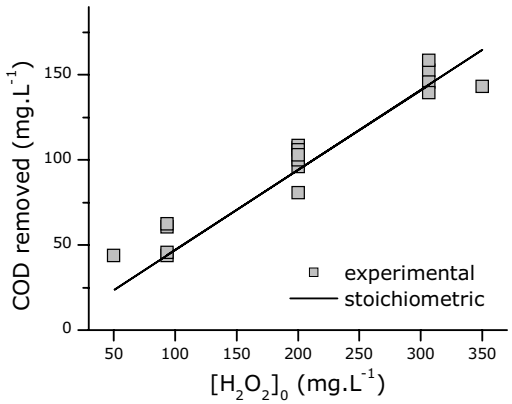


Figure 3.4-2: COD removed vs. hydrogen peroxide initial concentration.

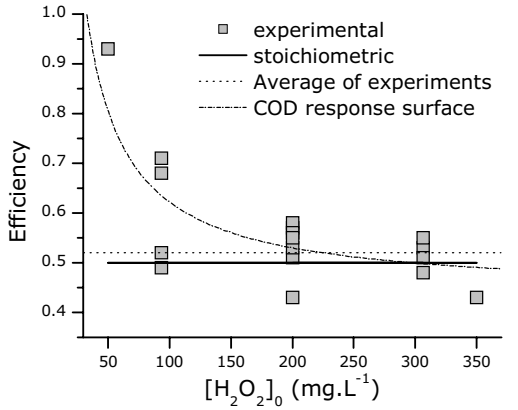


Figure 3.4-3: Efficiency regarding hydrogen peroxide initial concentration.

Experiments with different $Fe^{2+}$ concentrations and at different temperatures.

When observing the representation of efficiency estimations as it is defined by Equation 3.4-1 (Figure 3.4-3) it can be pointed out that most of the experiments round 50-60 % of Efficiency. However, some experiments stand out clearly from the majority, not only above but also below average. Two tendencies are observed from the efficiency estimations. The former, can be explained by Equation 3.4-3, in which the efficiency is constant and does not change with $H_2O_2$ dose. The latter is an asymptotic tendency, described by Equation 3.4-2 and Equation 3.4-4, where the efficiency is higher with low $H_2O_2$ dose and tends to be constant after a certain value.

The most efficient experiments are logically the ones carried out with less hydrogen peroxide. At the beginning of the experiment, there is a higher amount of organic carbon, which is more readily oxidizable. On the other hand, there are values below average and below the line as well, which means that are experiments even less efficient than the oxidation with hydrogen peroxide. In these cases, it is not possible to state that $[H_2O_2]_0$ is the only reason of these results, since it occurs with medium and high concentrations of $H_2O_2$.

If the experiments are observed in more detail, some more considerations can be obtained in order to isolate the operating conditions that cannot be explained by the mathematical models. Figure 3.4-4 and Figure 3.4-5 show the same results as Figure 3.4-3 but in this occasion temperature (left) and iron dose (right) of every experiment are distinguished.

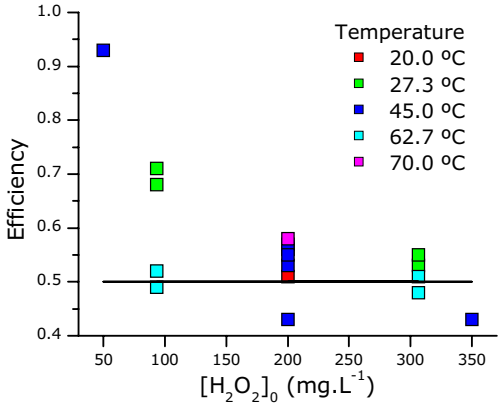


Figure 3.4-4: Efficiency regarding hydrogen peroxide initial concentration. Detail of operating temperatures.

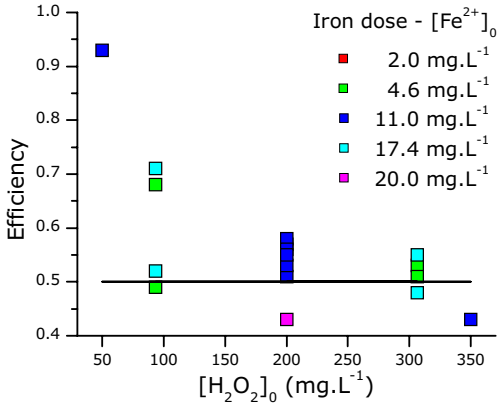


Figure 3.4-5: Efficiency regarding hydrogen peroxide initial concentration. Detail of iron doses.

Experiments with different $Fe^{2+}$ concentrations and at different temperatures.

As it is well-known, in Photo-Fenton process different parameters such as high concentrations of $H_2O_2$ (excess of reagent), iron (catalyst) or operating at high temperatures (higher kinetic constants), accelerate the undesirable reactions that instead of improving the production of hydroxyl radicals increase the $H_2O_2$ abatement with no further organic matter oxidation.

One of these effects can be observed in the Figure on the left (Figure 3.4-4). The difference among the experiments done with ≈100 $mg.L^{-1}$ of $[H_2O_2]_0$ seems significant. Green squares mark the experiments carried out at 27.3 ºC and their result is 20 % above light-blue squares, which mark experiments carried out at 62.7 ºC. The tendency is repeated in the experiments with ≈ 300 $mg.L^{-1}$ of $[H_2O_2]_0$ but in this case the differences are not significant enough to state categorically that there occur the same cases. It might be that in this case the influence of a considerable $H_2O_2$ dose covers other effects.

Although the statistical treatment of results, as seen above, do not find any significant difference among experiments with the same $H_2O_2$ and carried out at different temperatures or with different iron doses, it seem that combining particular operating conditions produce some synergies that cannot be mathematically modelled. Therefore, it is suggested to avoid these conditions in further experiments.

Different models to fit COD degraded

In a second set of experiments, temperature is fixed at 27 ºC and all the experiments are performed with 10 mg.L$^{-1}$ of $[Fe^{2+}]_0$. In this case, 6 experiments are carried out, each of them with a different initial dose of $H_2O_2$. Results of COD removed of each experiment are shown in Figure 3.4-6 to Figure 3.4-8. In each Figure, a mathematical function is suggested in order to fit the experimental results. The mathematical functions are described as follows.

$$COD_{removed} = 30.61(\pm 9.34) + 0.43(\pm 0.03)\cdot[H_2O_2]_0 \quad \text{Equation 3.4-5}$$

$$COD_{removed} = 0.51(\pm 0.06)\cdot[H_2O_2]_0 \quad \text{Equation 3.4-6}$$

$$COD_{removed} = 2.45(\pm 1.11)\cdot[H_2O_2]_0^{0.74(\pm 0.08)} \quad \text{Equation 3.4-7}$$

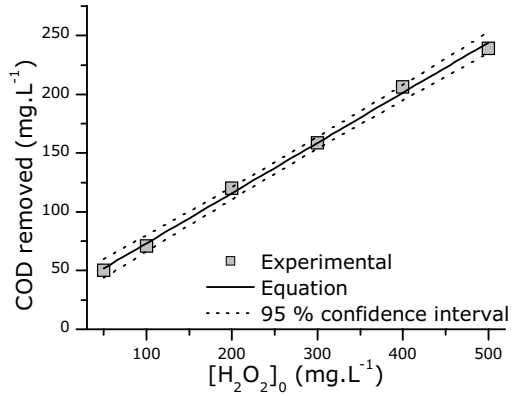


Figure 3.4-6: COD removed vs. $[H_2O_2]_0$. $[Fe^{2+}]_0$ = 10 mg.L$^{-1}$; T = 27 ºC. Line plots Equation 3.4-5. *$R^2$ = 0.997*.

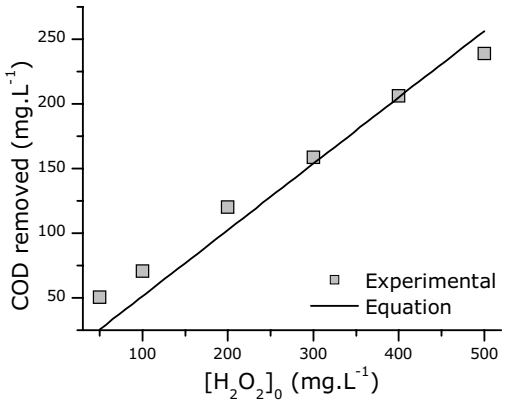


Figure 3.4-7: COD removed vs. $[H_2O_2]_0$. $[Fe^{2+}]_0$ = 10 mg.L$^{-1}$; T = 27 ºC. Line plots Equation 3.4-6. *$R^2$ = 0.94*

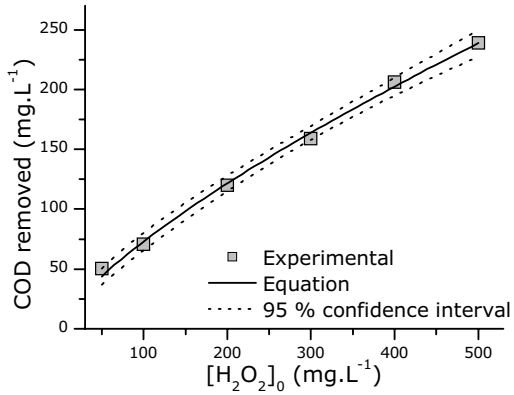


Figure 3.4-8: COD removed vs. $[H_2O_2]_0$. $[Fe^{2+}]_0$ = 10 mg.L$^{-1}$; T = 27 ºC. Line plots Equation 3.4-7. *$R^2$ = 0.997*

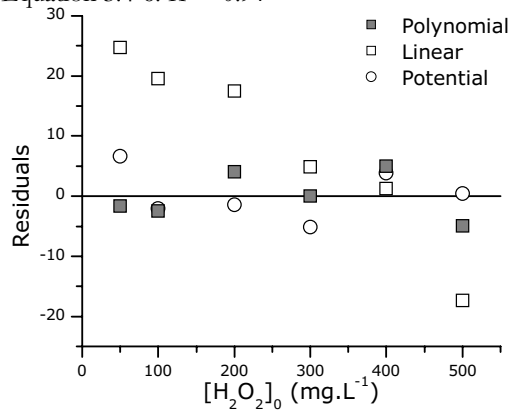


Figure 3.4-9: Residuals Plot for Equation 3.4-5 (Polynomial), Equation 3.4-6 (linear) and Equation 3.4-7 (multiplicative).

Equation 3.4-5 is a polynomial function, similar to Equation 3.4-2 (which expresses the surface response). The second function, Equation 3.4-6, is a linear regression without interception parameter. Finally, Equation 3.4-7 is a potential function, which in general usually is more probable to depict curve responses and has more physical-chemical sense.

Figure 3.4-9 shows the distribution of residuals between experimental and predicted values by polynomial, linear and multiplicative models. As shown in the figure, residuals of linear model are not homogenously distributed, which means that the model is not suitable for predicting the degraded COD depending on the initial hydrogen peroxide dose. Furthermore, the values are much higher than the residuals of polynomial and multiplicative models, which values are homogenously distributed. As shown in Figure 3.4-7, it is not possible to depict the confidence interval at 95 % due to the error that accumulate the equation.

Therefore, the linear model as described by Equation 3.4-6 is discarded. Between the polynomial and the potential function as described in Equation 3.4-5 and Equation 3.4-7 respectively, there are no adjustment differences. However, Equation 3.4-7 is more plausible, since polynomial functions tend to have poor extrapolation qualities, and potential equations are probably more closely related to physical-chemical behaviour of the system.

Another reason to discard the linear equation to describe COD abated is that this function supposes the efficiency to be equal in all experiments. As shown in Figure 3.4-10, the efficiency of $H_2O_2$ in the abatement of COD is higher with low doses of $H_2O_2$ and decreases up to a plateau, around 54 % (0.54±0.07).

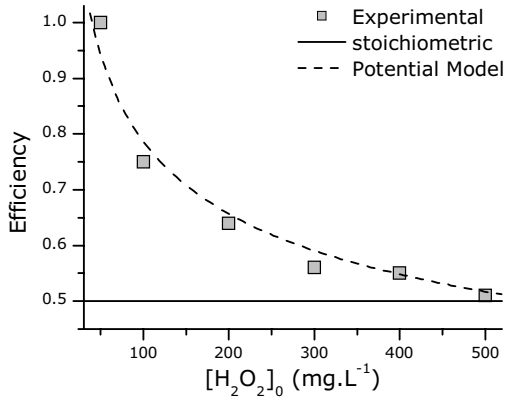


Figure 3.4-10: Efficiency of $H_2O_2$ on COD removed. $[Fe^{2+}]_0$ = 10 mg.L$^{-1}$; T = 27 ºC.

### 3.4.2.- Evaluation of the up-scaled experiments

Addition of $H_2O_2$ at the beginning

As explained above, only $[H_2O_2]_0$ and $[Fe^{2+}]_0$ are modified in this case. However, low iron experiments are obviated, since they do not fit well and present a more complex case. Temperature is fixed at 27 ºC and controlled during each experiment. The present Experimental Design is shown in Table 3.3-1 and evaluated in Section 3.3.1. In this case, low $H_2O_2$ doses are not employed, because the main objective of the experimental design is to study the possible connection with a biological treatment, and as it has been observed in the laboratory studies high doses of reagent are necessary in order to achieve a suitable biodegradability degree.

Results of COD removed ($mg.L^{-1}$) and Efficiency estimations depending on hydrogen peroxide initial doses are shown in Figure 3.4-11 and Figure 3.4-12 respectively. By an overview of these results, it can be pointed out that in all the experiments the COD removed and the Efficiency achieved is above the stoichiometry. According to the results, there is in average no increase or decrease of efficiency regarding the $H_2O_2$ dose. Actually, the efficiency achieved in experiments with 300, 400 and 500 $mg.L^{-1}$ of $H_2O_2$ initial concentration is around 55 % in all experiments, except for two.

One experiment, number 4, which is performed with 300 $mg.L^{-1}$ of $[H_2O_2]_0$, seems to be significantly more efficient than the average. As shown in Figure 3.4-14, this experiment is carried out with 2 $mg.L^{-1}$ of $[Fe^{2+}]_0$.

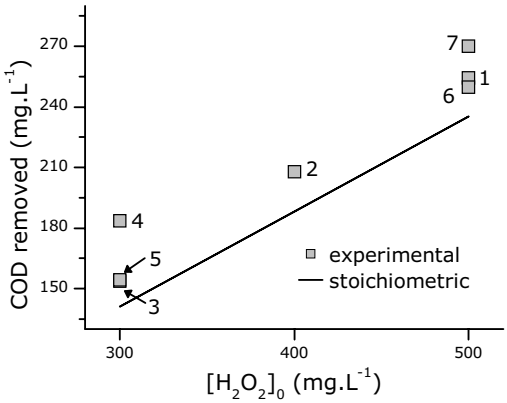


Figure 3.4-11: Comparison of COD removed vs. $H_2O_2$ dose in the solar reactor. Numbers correspond to experiment number in Table 3.3-1.

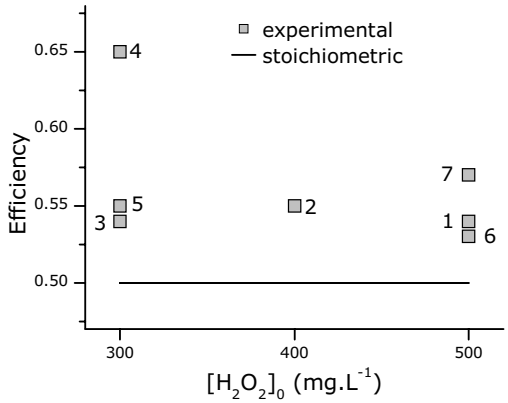


Figure 3.4-12: Efficiency regarding hydrogen peroxide initial concentration. Numbers correspond to experiment number in Table 3.3-1.

The second one is number 7, which is carried out with 500 mg.L$^{-1}$ of $[H_2O_2]_0$. This experiment attains and efficiency slightly above the other experiments performed with the same dosage of $H_2O_2$. Interestingly, this experiment is also carried out with 2 mg.L$^{-1}$ of $[Fe^{2+}]_0$, like experiment 2. As these experiments entail a more complex case, are going to be obviated for model purposes.

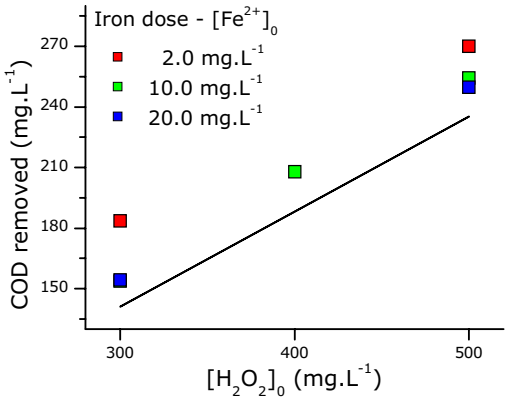


Figure 3.4-13: Comparison of COD removed vs. $H_2O_2$ dose in the solar reactor. Detail of iron doses.

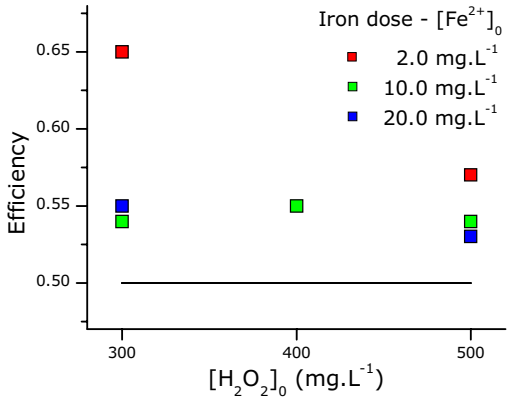


Figure 3.4-14: Efficiency regarding hydrogen peroxide initial concentration.

In Figure 3.4-15, the line plots Equation 3.4-7, which is found to be the function that best fits the laboratory results. As shown in the figure, the estimation is not far from the experimental results. However, in order to obtain a better estimation, other functions, such as a polynomial (Equation 3.4-8) or a linear equation (Equation 3.4-9) are again suggested, as it is done in the previous section for the laboratory results.

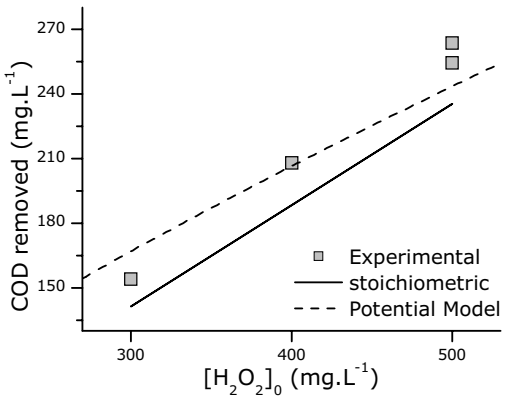


Figure 3.4-15: COD removed vs. $[H_2O_2]_0$. $[Fe^{2+}]_0$ = 10 mg.L$^{-1}$; T = 27 ºC. Dashed Line plots Equation 3.4-7 (Solar Photo-Fenton)

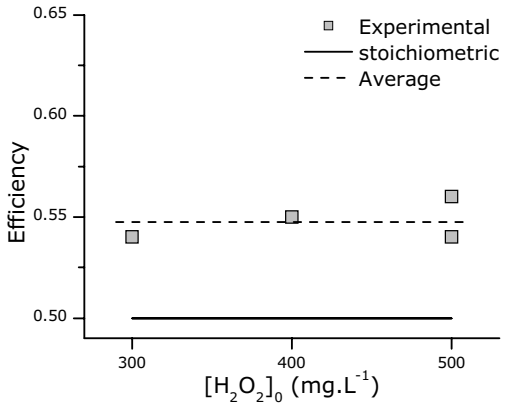


Figure 3.4-16: Efficiency of $H_2O_2$ on COD removed. $[Fe^{2+}]_0$ = 10 mg.L$^{-1}$; T = 27 ºC. (Solar Photo-Fenton)

$$COD_{removed} = -2.94\,(\pm 54.34) + 0.52\,(\pm 0.13)\cdot[H_2O_2]_0 \qquad \text{Equation 3.4-8}$$

$$COD_{removed} = 0.518\,(\pm 0.015)\cdot[H_2O_2]_0 \qquad \text{Equation 3.4-9}$$

Both equations are quite similar. It is curious that the independent term of the polynomial equation, Equation 3.4-8, is near "0". This means that forcing the interception to be "0" as it is done in the other function (Equation 3.4-9) does not accumulate much error. Figure 3.4-17 and Figure 3.4-18 show the experimental COD removed together with two suggested models, the polynomial and the linear, respectively. As in this case the experimental set consists of few experiments, confidence intervals at 95 % of probability are higher. Nevertheless, the regression coefficients in both cases are high enough to be acceptable.

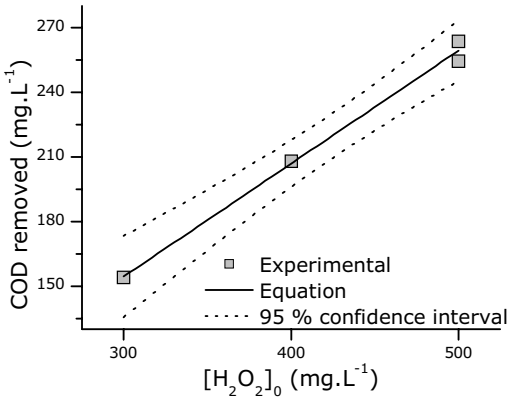


Figure 3.4-17: COD removed vs. $[H_2O_2]_0$. $[Fe^{2+}]_0$ = 10 mg.L$^{-1}$; T = 27 ºC. Line plots Equation 3.4-8. $R^2$ = 0.994

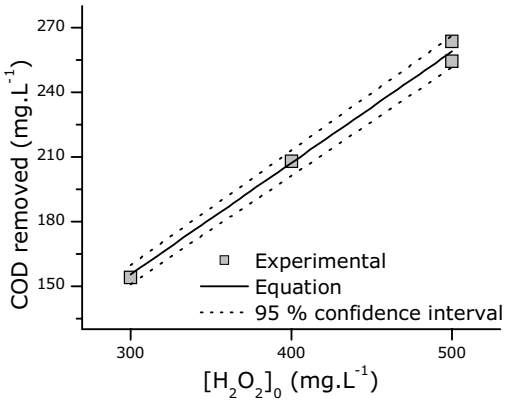


Figure 3.4-18: COD removed vs. $[H_2O_2]_0$. $[Fe^{2+}]_0$ = 10 mg.L$^{-1}$; T = 27 ºC. Line plots Equation 3.4-9. $R^2$ = 0.994

Interestingly, the equation that best fits the results is a linear equation, which is discarded for the description of laboratory results. Furthermore, accepting the linear equation, as described by Equation 3.4-9, means that at least within the range between 300 and 500 mg.L$^{-1}$ of $[H_2O_2]_0$ efficiency is constant against $H_2O_2$. In fact, this behaviour is also described by the potential equation, since within the same range of hydrogen peroxide, estimates of Efficiency calculated by the function tend to depict a plateau. The estimated efficiency is in this case 0.55(±0.015).

Experiment of Addition

The last set of experiments is an attempt to elucidate if dosing $H_2O_2$ in multiple doses produces an improvement of degradation. According to the laboratory results (Figure 3.4-10) the efficiency of oxidation when supplying low amounts of $H_2O_2$ is higher. Consequently, it might be possible that supplying $H_2O_2$ in multiple small doses instead of one dose at the beginning can improve the

oxidation efficiency. The experiment is called "Addition Experiment" and it is shown above in Section 3.3.5. According to the results presented in that section, there are no major differences between the common experiments and the current "addition experiment".

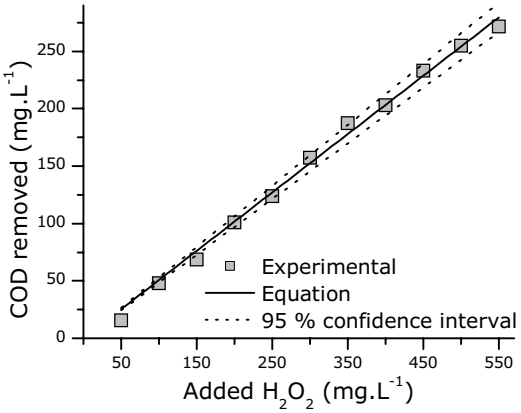


Figure 3.4-19: Addition Experiment. $[4\text{-CP}]_0$ = 200 $mg.L^{-1}$; $[Fe^{2+}]_0$ = 10 $mg.L^{-1}$; T = 27 ºC. $R^2$ = 0.995

COD removed through the Addition Experiment is shown in Figure 3.4-19. Results of COD removed depict surprisingly a straight line, which crosses by extrapolation the "0" intersection. Thus, the efficiency throughout the process is a constant, i.e. does not increase or decrease in dependence of supplied $H_2O_2$. Furthermore, experimental results are fitted with a high regression coefficient, by the same linear equation that describes the batch experiments (Equation 3.4-9). In this case, the average of efficiencies is 0.53(±0.10), really close to the efficiencies estimated in the laboratory and the solar batch experiments.

Table 3.4-2: Review of results. Efficiency of oxidation depending on $H_2O_2$.

| **Experiments** | **Range of $H_2O_2$ ($mg.L^{-1}$)** | **Efficiency of oxidation** |
|---|---|---|
| Laboratory Experimental Design | 50-350 | 0.56 (±0.06) |
| Laboratory | 50-500 | 0.54 (±0.07) |
| Solar up-scaled | 300-500 | 0.55 (±0.02) |
| Solar up-scaled (addition exp.) | 50-550 | 0.53 (±0.10) |

Table 3.4-2 is a review of results of Efficiency. As shown in the Table, the efficiencies estimated for different operating methods and different strategies are really similar. These results can be taken as a stoichiometry between COD and $H_2O_2$ supplied for the oxidation of 4-CP solution by Photo-Fenton. As 4-CP is abated fast, and the remaining COD consist of a mixture of by-products, these efficiency estimations are likely to be extrapolatable for a wide range of species

and wastewaters containing organic compounds. Finally, it has to be remarked that this results are valid between COD values of 330 $mg.L^{-1}$ (initial) up to 60 $mg.L^{-1}$ (the lowest COD attained), i.e. 80 % of COD degradation.

### 3.4.3.- Conclusions

According to the results, it is possible to define a pattern that describes the amount of COD degraded depending on the dose of $H_2O_2$ supplied. There is a ratio of COD degraded per amount of $H_2O_2$ consumed that fits a wide range of operating conditions. The ratio is estimated to be 0.51 (mg $0_2$/mg $H_2O_2$) which can be considered as a stoichiometry of Photo-Fenton process in the current conditions. It has to be taken into account that *a priori* the following considerations are only strictly extrapolatable to Photo-Fenton of single-ring halogenated aromatics and their oxidation by-products. Although the correlations are likely to be different in other cases, the suggested models are probably suitable for a wide range of wastewaters.

Regarding the less efficient results, certain conditions may increase the pollutant degradation rate but at the same time also produce that undesirable reactions are of importance. For example, operating at high temperatures does not improve the mineralization, and in certain cases, its consequences cannot be predicted or fitted in a simple model. Hence, it is suggested to operate at room temperature. In this way, results are more comparable among them and it might be easier to characterize and model the process. Concerning the outstanding results, it is remarkable that only occur when a low dosage of $H_2O_2$ is used, and only in the laboratory-scaled experiments. This result cannot be extrapolated at useful operating conditions since it is undeniable that certain levels of oxidation must be carried out, in order to reach different objectives; for example a final removal, biodegradability enhancement or the abatement of a certain pollutant among other objectives. Consequently, noticeable amounts of reagent, i.e. $H_2O_2$, must be used. There is, nevertheless, a region that cannot be explained mathematically with the same function for both laboratory and scaled-up experimental results. Although in both cases the estimated oxidation efficiency with high doses of $H_2O_2$ is apparently equal, this phenomenon cannot be extrapolated when a low amount of $H_2O_2$ is used. Interestingly, in the laboratory experiments, the efficiency is shown to be higher than in the solar up-scaled experiments. Furthermore, it has been observed that in solar pre-industrial tests, supplying the same amount of $H_2O_2$ in low doses instead of at the beginning of an experiment does not produce any significant change or improvement.

By means of a precise analysis of $H_2O_2$ consumed, analytically or by a probe, it might be possible to estimate the amount of COD degraded, and in consequence, it might be possible to control Photo-Fenton process.

# 3.5.- Mechanistic Models for the Oxidation by Photo-Fenton

In order to elucidate and describe engineering aspects of the oxidation by Photo-Fenton, mathematical modelling is a good resort. ***Mechanistic models*** are suggested to describe the process. By means of these models, which are desirable to be as simple as possible, it might be possible to ***predict*** the evolution of different *families* of organic matter, and consequently predict the biodegradability enhancement. Unlike polynomial equations, which can be obtained by a surface response methodology like in Section 3.1.3, mechanistic models attempt to have physical-chemical sense.

Once the model is fulfilled, it is possible to optimize the resources to consume in order to obtain a certain result, e.g. to obtain an appropriate product to feed a biological reactor.

### 3.5.1.- Considerations on Mechanistic models

Some previous works have presented different Lumped kinetics and mechanistic models (*Esplugas et al., 2004; Garcia-Molina et al., 2006; Li et al., 1991; Verenich and Kallas, 2002; Verenich et al., 2003; Verenich et al., 2004; Verenich et al., 2005*). However, most of them deal with wet oxidation or ozonation, in which oxidizing agents can be considered constant during the process. Only in one work (*Verenich et al., 2003*), it is suggested to include the concentration of oxidizing agent, $O_2$ in that case, and to study the reaction order.

The model that is presented in this work suggests that organic matter can be grouped in different ***sum parameters*** or ***Lumps***, which are used as pseudo-species. Each of them is supposed to behave in the same manner in front of Photo-Fenton oxidation.

The model distinguishes the following parameters:

- Concentration of Non-biodegradable organic matter: [(COD-$BOD_5$)]
- Concentration of biodegradable organic matter [$BOD_5$]
- Concentration of organic matter [COD] = [(COD-$BOD_5$)] + [$BOD_5$]
- Concentration of End-products

The last group, the "End-products", is not determined by analysis. It can be estimated by the difference between $[COD]_0$ – [COD], where $[COD]_0$ is the initial concentration of organic matter. Figure 3.5-1 shows the routes of oxidation reactions that are suggested to happen.

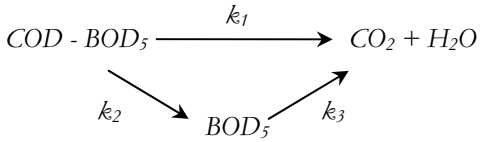


Figure 3.5-1: Mechanistic model according to *Verenich and Kallas* (*2002*).

The following constraints and conditions are established:

- Pseudo-First kinetic order concerning the concentration of organic matter
- Concentration of oxidizing agents is constant and included in the pseudo-kinetic constants.

The oxidation process for such a reaction network can been described by the following system of Ordinary Differential Equations (ODEs):

$$-\frac{d[(COD-BOD_5)]}{dt}=(k_1+k_2)\cdot[(COD-BOD_5)] \qquad \text{Equation 3.5-1}$$

$$-\frac{d[BOD_5]}{dt}=-k_2\cdot[(COD-BOD_5)]+k_3\cdot[BOD_5] \qquad \text{Equation 3.5-2}$$

By analytical integration of these ODEs, equations that predict the concentration of each group at a certain moment of the process are obtained. It is also suggested that it is likely to obtain equations that predict the concentration of these different lumps concerning the reagent dose. In this case, instead of being kinetic equations, they can be named Stoichiometric-mechanistic equations.

### 3.5.2.- Stoichiometric-mechanistic model

As seen above in Section 3.1.5, in Photo-Fenton systems the duration of the process can be described as a function of the initial reagent doses ($[H_2O_2]_0$ and $[Fe^{2+}]_0$) and temperature. Nevertheless, according to the equations regarding degradation (COD, TOC or BOD) only $[H_2O_2]_0$ significantly affects the result. Consequently, it is likely to write differential equations that express the mechanics of *COD-BOD5* and *BOD5* but instead of being a pseudo-kinetic model, i.e. a description over time, is a pseudo-stoichiometric model, which expresses the evolution of these parameters regarding the doses of $H_2O_2$ applied in Photo-Fenton.

According to the mechanistic model suggested by *Verenich and Kallas* (*2002*) (shown in Figure 3.5-1), Photo-Fenton oxidation of non-biodegradable substances, biodegradable species and

"End Products" is linked in a 3 pathways mechanism. The oxidation over time of these lumped parameters can be described as seen above by differential equations. By substitution of time differential parameter for $H_2O_2$ term in Equation 3.5-1 and Equation 3.5-2, the following differential equations are obtained:

$$-\frac{d[(COD-BOD_5)]}{d[H_2O_2]_0}=(k_1+k_2)\cdot[(COD-BOD_5)] \qquad \text{Equation 3.5-3}$$

$$-\frac{d[BOD_5]}{d[H_2O_2]_0}=-k_2\cdot[(COD-BOD_5)]+k_3\cdot[BOD_5] \qquad \text{Equation 3.5-4}$$

As temperature and iron do not affect significantly COD and BOD results, as seen above, it is not necessary to include them in the functions. Then a possible source of overestimation of the model is avoided, since the model has only 3 parameters to be iterated.

In this case, *k*'s (L.mg$^{-1}$) are pseudo-stoichiometric constants, which link hydrogen peroxide dose with a group parameter: (COD-$BOD_5$) and $BOD_5$. Consequently, express the removal that can produce 1 mg.L$^{-1}$ of $H_2O_2$.

By analytical integration of these differential equations, the following expressions are obtained:

$$[(COD-BOD_5)]=[(COD-BOD_5)]_0\cdot e^{-(k_1+k_2)\cdot[H_2O_2]_0} \qquad \text{Equation 3.5-5}$$

$$[BOD_5]=[BOD_5]_0\cdot e^{-k_3\cdot[H_2O_2]_0}+ \\ +\frac{k_2\cdot[(COD-BOD_5)]_0}{k_1+k_2-k_3}\cdot\left(e^{-k_3\cdot[H_2O_2]_0}-e^{-(k_1+k_2)\cdot[H_2O_2]_0}\right) \qquad \text{Equation 3.5-6}$$

Later, by combination of both equations, the expression describing the stoichiometry of $H_2O_2$ over COD is obtained.

$$[COD]=[BOD_5]_0\cdot e^{-k_3\cdot[H_2O_2]_0}+ \\ +[(COD-BOD_5)]_0\cdot\left(\frac{k_2}{k_1+k_2-k_3}e^{-k_3\cdot[H_2O_2]_0}+\frac{k_1-k_3}{k_1+k_2-k_3}e^{-(k_1+k_2)\cdot[H_2O_2]_0}\right) \qquad \text{Equation 3.5-7}$$

In order to determine the constants' values, a simulation by minimizing the difference among experimental and model values must be carried out. As the order of magnitude of COD and $BOD_5$ has a difference of a factor of around 10, simulation by minimization of the sum of

squared-mean values is not likely to be the best option, since it might base the minimization on COD equation and obviate $BOD_5$ values. On the other hand, a sum of individual errors is proposed to be better, since each error is normalized, and the order of magnitude is not likely to interfere with the minimization. Equation 3.5-8 and Equation 3.5-9 show the parameters to be minimized by iteration.

$$Individual\ \ error(\%) = Abs\left[\frac{Experimental - Model}{Experimental}\right]\cdot 100 \qquad \text{Equation 3.5-8}$$

$$Sum\ of\ errors = \sum Individual\ \ error \qquad \text{Equation 3.5-9}$$

Laboratory and pre-industrial scale experiments are used to fit Equation 3.5-6 and Equation 3.5-7. Experimental values and fitted equations are shown in Figure 3.5-2 and Figure 3.5-3, and the constants' values, determined by iteration are shown in Table 3.5-1.

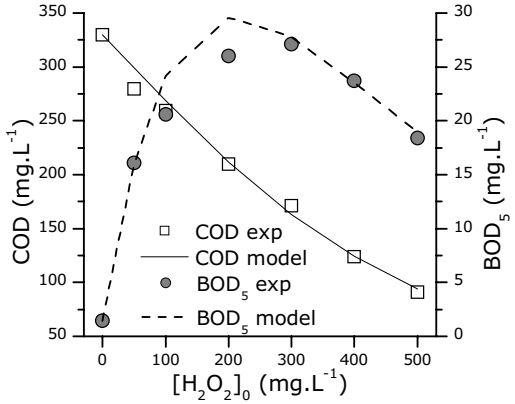


Figure 3.5-2: Laboratory - $[Fe^{2+}]_0$ = 10 mg.L$^{-1}$; T = 27 ºC. $R^2$ = 0.996.

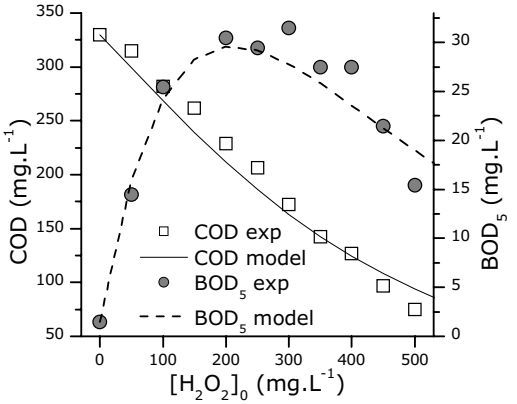


Figure 3.5-3: Pre-industrial scale - $[Fe^{2+}]_0$ = 10 mg.L$^{-1}$; T = 27 ºC. $R^2$ = 0.987

As shown in Figure 3.5-2, the model seems to predict with a certain precision the laboratory experimental values of both COD and $BOD_5$. On the other hand, in the case of pre-industrial scale experiments (Figure 3.5-3) the model deviates slightly from experimental values but shows a good trend.

Table 3.5-1: Stoichiometric parameters determined by simulation using Excel and Origin Lab software.

| Stoichiometric constant | Value | Error |
|---|---|---|
| $k_1$ | $1.79 \cdot 10^{-3}$ | $\pm\ 2.20 \cdot 10^{-4}$ |
| $k_2$ | $1.17 \cdot 10^{-3}$ | $\pm\ 2.04 \cdot 10^{-4}$ |
| $k_3$ | $6.94 \cdot 10^{-3}$ | $\pm\ 1.10 \cdot 10^{-3}$ |

Another method to compare both fittings is by determination of the average individual error, estimated by Equation 3.5-10.

$$Average\ \ error(\%) = \frac{\sum individual\ \ error}{number\ \ of\ \ experiments} \qquad \text{Equation 3.5-10}$$

Average error of the model fitting Laboratory experiments is estimated to be 4.15 %, whereas in pre-industrial scale experiments the average is 11.5 %, which is significantly higher.

The model has good prediction capabilities and according to the results, fits quite well the experimental values, with an average of 11.5 % of error in the worst case. Any attempt to describe a more complicated model, with one or two steps more, needs more and more varied experimental data, in order to fix more constraints and not produce an overestimation. For example some works (*Esplugas et al., 2004; Verenich and Kallas, 2002; Verenich et al., 2003*) suggest an alternative, which is differentiate between readily and slow BOD. Thus, it is taken into account the different nature that might have BOD, with the corresponding behaviour in front of oxidation.

In fact, in the experimentation with the biological reactor (commented later), often it occurs that biochemical degradation attained in a biological reactor is much higher than the value of $BOD_5$ estimated by the standard method.

With this modification, the model would describe that the oxidation of non-biodegradable compounds (COD-BOD) would lead to slowly biodegradable matter, which can be identified as $BOD_{21}$ for example. This group later would go to readily biodegradable substrate, which is the common $BOD_5$, and their further oxidation finally would release $CO_2$.

Another fact that must be taken into account is the possibility that a fraction of a wastewater present recalcitrant properties to oxidation (*Foussard et al., 1989*). In this case, the differential equations should be rewritten (*Verenich et al., 2005*) in order to insert in the equation the quantities of organic compounds that cannot be oxidized. Equation 3.5-3 is rewritten as follows:

$$-\frac{d[(COD - BOD_5)]}{d[H_2O_2]_0} = (k_1 + k_2)\cdot[(COD - BOD_5) - (COD - BOD_5)_r] \qquad \text{Equation 3.5-11}$$

Where $(COD\text{-}BOD_5)_r$ is the concentration of non-biodegradable compounds that cannot be oxidized, i.e. are recalcitrant to Photo-Fenton oxidation.

Obviously, as more complicated the model becomes, it can mathematically fit more experimental results, and probably lose its physical-chemical sense.

### 3.5.3.- Pseudo-Kinetic Model

As it has been introduced above (Section 3.5.1) by a Pseudo-kinetic model like the suggested one it is possible to write equations that predict concentration of different sum parameters (lumps) over time, i.e. the reaction kinetics. As it is well known, several parameters may affect reaction kinetics, such as Temperature or concentration of substances that may act as a catalyst. Furthermore, reaction order is a common reason of discussion when it is attempted to model a system with a reaction that simplifies a complex mechanism.

However, in a first approach to the pseudo-kinetic model, similar considerations that have set previous authors when modelling other AOPs are used. These Kinetic Lumps were initially thought to model AOPs such as wet oxidation and ozonation. In these processes oxidizing agents are supplied or generated continuously and concentration of $HO^{\bullet}$ during the process is supposed to be constant or the concentration of oxygen in the liquid phase is assumed to be in excess and, therefore, the reaction order with respect to oxygen is set to "zero".

Thus, ODEs as expressed by Equation 3.5-1 and Equation 3.5-2 are used to describe the routes mathematically. The following boundary conditions are established to solve the ODEs:

At time $t = 0$, $[(COD\text{-}BOD_5)] = [(COD\text{-}BOD_5)]_0$

$[BOD_5] = [BOD_5]_0$

Where $[(COD\text{-}BOD_5)]_0$ and $[BOD_5]_0$ are respectively the initial concentration of refractory and biodegradable compounds. By solving the differential equations, the following analytical solution is found.

$$\left[(COD - BOD_5)\right] = \left[(COD - BOD_5)\right]_0 \cdot e^{-(k_1+k_2)t} \qquad \text{Equation 3.5-12}$$

$$\left[BOD_5\right] = \left[BOD_5\right]_0 \cdot e^{-k_3 \cdot t} + \frac{k_2\left[(COD - BOD_5)\right]_0}{k_1 + k_2 - k_3} \cdot \left(e^{-k_3 t} - e^{-(k_1+k_2)t}\right) \qquad \text{Equation 3.5-13}$$

By combination of these two equations, COD concentration can be expressed as follows:

$$[COD] = [BOD_5]_0 \cdot e^{-k_3 \cdot t} + [(COD - BOD_5)]_0 \cdot \left( \frac{k_2}{k_1 + k_2 - k_3} e^{-k_3 \cdot t} + \frac{k_1 - k_3}{k_1 + k_2 - k_3} e^{-(k_1 + k_2)t} \right)$$

Equation 3.5-14

It can be pointed out that there is no term describing hydrogen peroxide decomposition. Thus, according to the characteristics of Photo-Fenton in batch operation, it is expected that the deviation of the model increases as the process goes forward, since at the end of the reaction, the low concentration of $HO^{\bullet}$ is likely to be the limiting parameter.

Two experiments are commented, both carried out in PSA facilities with the pre-industrial scale solar reactor (Section 2.1.2). In the equation, instead of using the irradiation time, the normalized 30 W time ($t_{30W}$) is used. Thus, fluctuations of radiation that might happen during an experiment can be obviated. Both experiments are carried out with a supply of 500 mg.L$^{-1}$ of $[H_2O_2]_0$. One experiment is carried out with 10 mg.L$^{-1}$ of $Fe^{2+}$ (Figure 3.5-4) while the other is carried with 2 mg.L$^{-1}$ (Figure 3.5-5). Intermediate points are estimated from hydrogen peroxide concentration by equations of the Stoichiometric model (Equation 3.5-5 to Equation 3.5-7).

Table 3.5-2 shows the values of the kinetic constants obtained by iteration and minimization of the difference between experimental and calculated values.

Table 3.5-2: Kinetic constants calculated by minimization of Equation 3.5-9.

| **Kinetic constant** | **Value $[Fe^{2+}]_0$ = 10 mg.L$^{-1}$** | **Value $[Fe^{2+}]_0$ = 2 mg.L$^{-1}$** |
|---|---|---|
| $k_1$ | 0.097 | 0.024 |
| $k_2$ | 0.044 | 0.019 |
| $k_3$ | 0.241 | 0.109 |

Obviously, kinetic constants' values for experiment with 10 mg.L$^{-1}$ of $Fe^{2+}$ are higher. The experiment is faster. Furthermore, they follow similar tendencies; $k_3 > k_1 > k_2$ for both experiments. This means that the route of oxidation of biodegradable compounds is assessed to be the fastest, and on the other hand, oxidation of non-biodegradable compound to biodegradable is evaluated to be the slowest route.

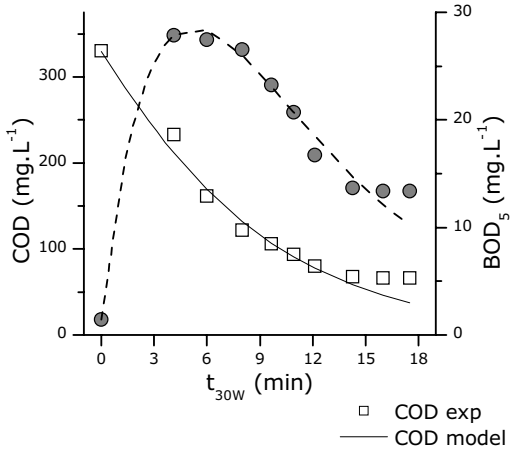


Figure 3.5-4: Photo-Fenton reaction in PSA. $[4\text{-CP}]_0$ = 200 mg.L$^{-1}$; $[H_2O_2]_0$ = 500 mg.L$^{-1}$; $[Fe^{2+}]_0$ = 10 mg.L$^{-1}$; T = 27 ºC

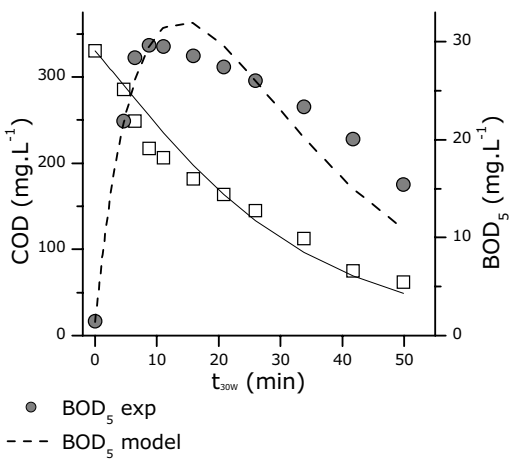


Figure 3.5-5: Photo-Fenton reaction in PSA. $[4\text{-CP}]_0$ = 200 mg.L$^{-1}$; $[H_2O_2]_0$ = 500 mg.L$^{-1}$; $[Fe^{2+}]_0$ = 2 mg.L$^{-1}$; T = 27 ºC

As it is insinuated above, the lines, which depict the fitted model, deviate from the experimental values at the latest points of the experiment. Probably, the model should be rewritten. However, the model shows good prediction capacities, and it seems to indicate a good beginning to elucidate a better mechanistic model.

### 3.5.4.- Suggestions to improve the pseudo-kinetic model

In this point, it is very useful all the study presented in Sections 3.1.2 to 3.1.5 with the Experimental Design and the Response Surface Methodology. By that study, it is possible to know how Photo-Fenton process is affected by iron, hydrogen peroxide and Temperature, which can be probably the most important operation variables of this process. According to those results, it is known that the duration of the process is significantly affected by iron and temperature if the same amount of $H_2O_2$ is considered.

**Taking into account $H_2O_2$ concentration**

In order to solve the lack of precision, a term considering oxidizing agent concentration in the ODEs should be included. However, this force to carry out some suppositions; HO$^{\bullet}$ production is "*simply*" function of $H_2O_2$, iron, temperature and irradiation, and there is no significant influence of certain substances on the production of HO$^{\bullet}$. The last point is in fact a source of error, since it has been demonstrated that the presence of some aromatic oxidation intermediates may affect hydroxyl radicals production (*Chen and Pignatello, 1997*).

By accepting the suppositions, $H_2O_2$ concentration can be included in the differential equations as representative of hydroxyl radicals, since the other parameters are thought to be constant and are included in the *k*'s. Furthermore, the system becomes even more complicated, since a reaction order must be calculated. The simplest option in this case is considering pseudo-first kinetics order concerning $H_2O_2$ concentration. For example, Equation 3.5-1 becomes Equation 3.5-15.

$$-\frac{d[(COD-BOD_5)]}{dt}=(k_1+k_2)\cdot[(COD-BOD_5)]\cdot[H_2O_2] \qquad \text{Equation 3.5-15}$$

However, as shown by Figure 3.5-4 and Figure 3.5-5, the deviation occurs only at the end of the process, when $H_2O_2$ concentration is low. An alternative instead of including the $H_2O_2$ term, which entail that other suppositions must be carried out, is including a term to "tell" to the model that $H_2O_2$ is being finished. With the influence of hydrogen peroxide in the kinetics occurs an analogous situation than in biological reactions explained by Monod kinetics.

In these systems, substrate is considered in excess, and consequently non-limiting except when concentration is below a certain point. From this point on, the mathematical term that indicates the influence of substrate, instead of being ≈1, is lower, and is a limiting parameter in the kinetics. This function is usually named "Switch Function". The importance of such function increases when the concentration of $H_2O_2$ approaches the $K_{H2O2}$ value, which can be defined as the $H_2O_2$ exhaustion constant.

In Photo-Fenton, it is suggested that from a certain point on, concentration of $H_2O_2$ starts to be limiting since it is low. Thus, the differential equation explaining the abatement of non-biodegradable compounds can be written as follows:

$$-\frac{d[(COD-BOD_5)]}{dt}=(k_1+k_2)\cdot[(COD-BOD_5)]\cdot\frac{[H_2O_2]}{K_{H_2O_2}+[H_2O_2]} \qquad \text{Equation 3.5-16}$$

It has been observed that the reaction rate decrease significantly when $[H_2O_2]$ is lower than 25 $mg.L^{-1}$. Thus, $K_{H2O2}$ should be 12.5 $mg.L^{-1}$, since it is the half of the "saturation".

Obviously, to integrate the ODEs containing the $H_2O_2$ concentration term, a function describing the evolution of $[H_2O_2]$ over time must be written, since $H_2O_2$ is not constant. As in all these models, the simplest case is suggested, which is a first-kinetic order. Iron concentration (ferrous

and ferric species) in solution over the entire process is considered constant and the effect of light radiation is included in the "30 W time", which is a normalized time. The result is Equation 3.5-17.

$$[H_2O_2]_t = [H_2O_2]_0 \cdot e^{-k_{H_2O_2} \cdot [Fe^{2+}]_0 \cdot t_{30W}}$$ Equation 3.5-17

Figure 3.5-6 to Figure 3.5-9 show the experimental and simulated values of hydrogen peroxide concentration in different experiments carried out with the pre-industrial scale device at the PSA. By minimization of individual errors, the constant is determined to be 0.042. With this value, the model shows good prediction properties for experiments carried out with 300 mg.L$^{-1}$ of $[H_2O_2]_0$ but the simulation for experiments performed with 500 mg.L$^{-1}$ is not acceptable.

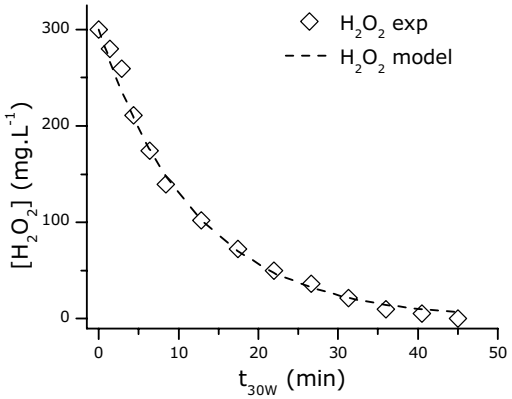


Figure 3.5-6: Hydrogen peroxide concentration over time in pre-industrial scale experiments. $[Fe^{2+}]_0$ = 2 mg.L$^{-1}$; $[H_2O_2]_0$ = 300 mg.L$^{-1}$.

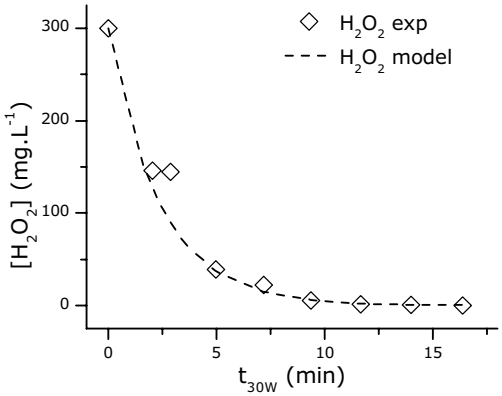


Figure 3.5-7: Hydrogen peroxide concentration over time in pre-industrial scale experiments. $[Fe^{2+}]_0$ = 10 mg.L$^{-1}$; $[H_2O_2]_0$ = 300 mg.L$^{-1}$.

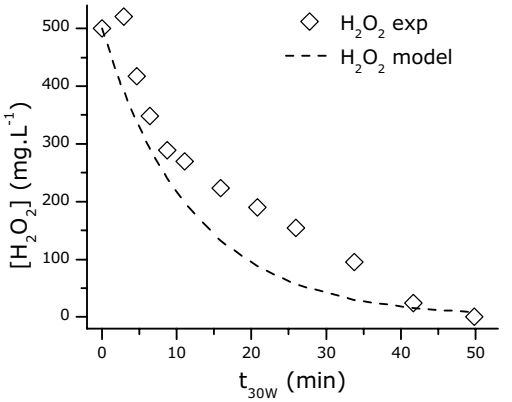


Figure 3.5-8: Hydrogen peroxide concentration over time in pre-industrial scale experiments. $[Fe^{2+}]_0$ = 2 mg.L$^{-1}$; $[H_2O_2]_0$ = 500 mg.L$^{-1}$.

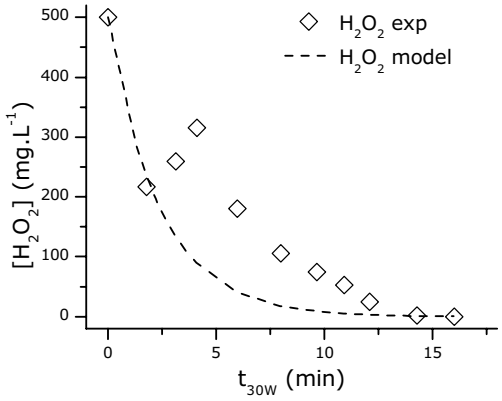


Figure 3.5-9: Hydrogen peroxide concentration over time in pre-industrial scale experiments. $[Fe^{2+}]_0$ = 10 mg.L$^{-1}$; $[H_2O_2]_0$ = 500 mg.L$^{-1}$.

It is not possible to fit all the experiments with this equation. Probably, $H_2O_2$ decomposition reaction does not follows first-kinetic order.

As it is not possible to write an appropriate equation for $H_2O_2$ decomposition, an alternative instead of obtaining integrated equations is the determination of the constants' values, simulation, and modelling by numerical integration of the ODEs by Runge-Kutta or Euler methods (*Aubanell et al., 1991*).

**Iron as a catalyst**

As iron affects significantly the kinetics of the process, as seen in Section 3.1.5, should be included in the ODEs. In the mathematical representation of catalytic reactions, catalyst concentration divides the reaction rate term. Thus, it is considered that the catalyst improves proportionally the reaction rate.

$$-\frac{d[(COD-BOD_5)]}{dt\cdot[Fe]_0}=[\ldots] \qquad \text{Equation 3.5-18}$$

$$-\frac{d[BOD_5]}{dt\cdot[Fe]_0}=[\ldots] \qquad \text{Equation 3.5-19}$$

According to this ODEs when $[Fe]_0$ is 0, the reaction rate is also 0, and on the other hand, when the catalyst concentration is high, the reaction rate is also high.

**Adding a light influence parameter**

A parameter including the influence of light must be also included, since in affects significantly the reaction rate. A good option is using a parameter that normalizes different types of experiments, with different light sources, or does not change depending on weather conditions (artificial source or solar, summer or winter day …). The normalized 30 W time ($t_{30W}$) as explained in Section 2.1.2 seems a good option. Thus, fluctuations of radiation that might happen during an experiment can be obviated.

### 3.5.5.- Complete Model. Solving by Euler iteration method

Following the previous suggestions, the ODEs as described by Equation 3.5-1 and Equation 3.5-2 are modified, and the following equations are obtained:

$$-\frac{d[(COD-BOD_5)]}{dt_{30W}\cdot[Fe]_0}=(k_1+k_2)\cdot[(COD-BOD_5)]\cdot\frac{[H_2O_2]}{K_{H_2O_2}+[H_2O_2]}$$ Equation 3.5-20

$$-\frac{d[BOD_5]}{dt_{30W}\cdot[Fe]_0}=-k_2\cdot[(COD-BOD_5)]\cdot\frac{[H_2O_2]}{K_{H_2O_2}+[H_2O_2]}+k_3\cdot[BOD_5]\cdot\frac{[H_2O_2]}{K_{H_2O_2}+[H_2O_2]}$$ Equation 3.5-21

To solve these ODEs, the following boundary conditions are applied:

At time $t = 0$, $[(COD\text{-}BOD_5)] = [(COD\text{-}BOD_5)]_0$

$[BOD_5] = [BOD_5]_0$

$[H_2O_2] = [H_2O_2]_0$

$K_{H2O2}$ is fixed at 12.5 mg.L$^{-1}$ since it has been observed that the decrease in the reaction rate occurs when $[H_2O_2] < 25$ mg.L$^{-1}$.

As said above, it is not possible to solve the ODEs analytically. In this case, the iterative solving method named Euler is applied. This method considers small timed intervals, in which the reaction rate and concentrations are supposed to be constant. By fitting $H_2O_2$ experimental values, a polynomial function is obtained, which allow estimating $H_2O_2$ concentration for each time interval. Thus, it is possible to calculate the concentration of the next timed interval. Iteration is carried out until calculated concentrations fit experimental values with the lowest error. Figure 3.5-10 and Figure 3.5-11 show the results. Table 3.5-3 shows the values of the kinetic constants obtained by iteration. Refer to Figure 3.5-1 to identify the reaction routes.

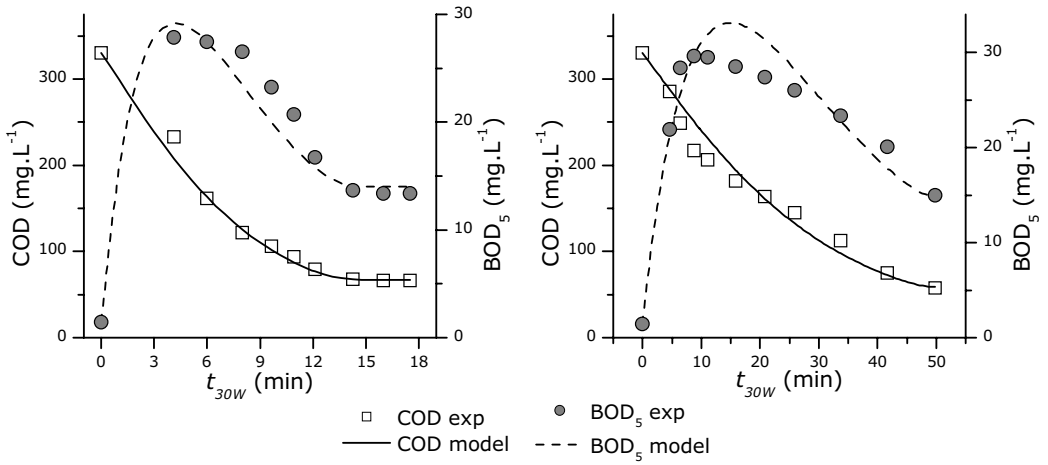


Figure 3.5-10: Photo-Fenton reaction in PSA. $[4\text{-CP}]_0$ = 200 mg.L$^{-1}$; $[H_2O_2]_0$ = 500 mg.L$^{-1}$; $[Fe^{2+}]_0$ = 10 mg.L$^{-1}$; T = 27 ºC. Complete Model.

Figure 3.5-11: Photo-Fenton reaction in PSA. $[4\text{-CP}]_0$ = 200 mg.L$^{-1}$; $[H_2O_2]_0$ = 500 mg.L$^{-1}$; $[Fe^{2+}]_0$ = 2 mg.L$^{-1}$; T = 27 ºC. Complete Model.

Table 3.5-3: Kinetic constants calculated by minimization of Equation 3.5-9.

| Kinetic constant | Value $[Fe^{2+}]_0$ = 10 mg.L$^{-1}$ | Value $[Fe^{2+}]_0$ = 2 mg.L$^{-1}$ |
|---|---|---|
| $k_1$ | 0.0095 | 0.0139 |
| $k_2$ | 0.0052 | 0.0091 |
| $k_3$ | 0.0329 | 0.0468 |

The model shows good prediction properties for both experiments. Probably, the worst fitting properties correspond to $BOD_5$. In these cases, unlike in the simple kinetic model (Section 3.5.3) the reaction rate slows down when $H_2O_2$ starts to be limiting, due to the "Switch Function", and oxidation stops properly when $H_2O_2$ is totally consumed. The pseudo-kinetic constants values have similar order of magnitude for both experiments.

However, there are still significant differences. Two sources of error are more likely to be the most important; first, $BOD_5$ values may have important error since they are estimated by the consumed $H_2O_2$. The second is that the model considers the effect of iron as directly proportional, and probably the increase or decrease of reaction rate is not as linear as expected. In fact, observing the equations obtained by Response Surface Methodology (Section 3.1.5) the decrease of time is not proportional to the increase of iron in the same order. Mathematically, if iron acts as a pure catalyst, 5 times of iron dose, should lead to a process 5 times faster. Nevertheless, the model is suggested to be a good work basis for future developments.

A following step of study might be to fit experimental values of different wastewater sources and different model compounds, in order to know if it is possible to group wastewaters according to their behaviour in front of Photo-Fenton oxidation, that is to say that by the same pseudo-kinetic constants, it is possible to fit their oxidation profiles.

# 3.6.- Effect of Salinity on Photo-Fenton process

The existence or presence of diverse hydrocarbons and persistent pollutants in seawater or saline wastewater due to different industrial activities is considerable. Photo-Fenton process is suggested as a possible treatment but the effect of salinity must be explored. An experimental design is carried out in order to elucidate the influence of NaCl on the efficiency of the process. According to the results, the global TOC removal is not influenced by the presence of chloride, but the process becomes much slower, even more than 10 times in some of the operating conditions. If solar irradiation is possible, Photo-Fenton seems a good option to treat polluted water with high salinity.

### 3.6.1.- Introduction

It has been reported that the presence of inorganic ions, such as chloride or sulphate may decrease the efficiency of oxidations processes based on the hydroxyl radical $HO^{\bullet}$ (*Lipczynskakochany et al., 1995*). In this sense, *De Laat et al.*(*2004*) point out that, inorganic anions, such as $Cl^-$, $SO_4^{2-}$, $H_2PO_4^-/HPO_4^{2-}$ and so on, may produce significant effects on the overall reaction rates in the Fenton process. Anions can capture hydroxyl radicals producing less reactive (than hydroxyl radicals) anion radicals that may react with hydrogen peroxide.

The interaction of chloride on the Fenton mechanism may be due to the complexation of $Fe^{2+}/Fe^{3+}$ with $Cl^-$ (Reaction 3.6-1 to Reaction 3.6-4) or the scavenging of hydroxyl radicals (Reaction 3.6-5) (*De Laat et al., 2004; Lu et al., 2005*) which may further generate chloride radicals $Cl^{\bullet}$, which are less reactive than hydroxyl.

$$Fe^{2+} + Cl^- \leftrightarrow FeCl^+ \qquad \text{Reaction 3.6-1}$$

$$FeCl^+ + Cl^- \leftrightarrow FeCl_2^0 \qquad \text{Reaction 3.6-2}$$

$$Fe^{3+} + Cl^- \leftrightarrow FeCl^{2+} \qquad \text{Reaction 3.6-3}$$

$$Fe^{3+} + 2Cl^- \leftrightarrow FeCl_2^+ \qquad \text{Reaction 3.6-4}$$

$$Cl^- + HO^{\bullet} \rightarrow [ClOH]^{\bullet -} \qquad \text{Reaction 3.6-5}$$

As indicated by *Sima and Makanova* (*1997*) $Fe^{3+}$ forms complexes, which undergo thermal or photochemical reduction to $Fe^{2+}$. In the presence of chloride, $Fe^{3+}$ forms complexes with unidentate ligands which by absorption of photons drive to complexed or non-complexed $Fe^{2+}$ species, furthermore generating chloride radicals or organic radicals, if organic compounds are present (Reaction 3.6-6 and Reaction 3.6-7).

$$^{*}Fe_{aq}^{3+} \cdot Cl^{-} \rightarrow Fe_{aq}^{2+} + Cl^{\bullet}$$ Reaction 3.6-6

$$^{*}FeCl_3 + RH \rightarrow FeCl_2 + HCl + R^{\bullet}$$ Reaction 3.6-7

where the species indicated as *Fe are photoexcited species.

Most of the studies of saline wastewater treatment have been carried out with the Fenton process, i.e. without light irradiation. Few works have studied the effects on Photo-Fenton treatment. For example, *Maciel et al.* (*2004*) showed that the abatement of Phenol and TOC removal in the Fenton process in moderately saline media were improved when using the Photo-Fenton. However, in the highest NaCl concentration tested, the TOC removal achieved was moderate.

A high content of inorganic salts, especially sodium chloride, has been shown in different kind of wastewaters, such as waters generated during the manufacture of pesticides, herbicides, pharmaceuticals and dyes (*Rivas et al., 2003a*). Processes like oil and gas recovery or crystallisation also generate wastewater containing high concentration of salts (*Maciel et al., 2004*). Saline wastewater or soil contaminated with hydrocarbons can be found as well in petroleum-based industry sites (*Moraes et al., 2004*), due to petroleum spills in the sea or over coastal areas or due to accidents during transportation (*Ferguson et al., 2004; Millioli et al., 2003*).

The aim of the present work is to study the effect of NaCl salts in the Photo-Fenton process. Chemical or photochemical oxidation processes, such as AOPs, seem to be appropriate to reduce the contaminant load in saline effluents. An experimental design is performed in order to elucidate the interactive influences of $H_2O_2$ and $Fe^{2+}$ (Fenton's reagents) initial concentrations ($[H_2O_2]_0$, $[Fe^{2+}]_0$ respectively) with the inorganic salt concentration ([NaCl]).

### 3.6.2.- Experimental Design

A solution of 200 mg.L$^{-1}$ of 4-chlorophenol (4-CP) as a model compound and with different concentrations of NaCl is treated with different initial concentrations of $H_2O_2$ and $Fe^{2+}$. The concentrations of salt and Fenton's reagents range from mild conditions ($[H_2O_2]_0$ = 50 mg.L$^{-1}$; $[Fe^{2+}]_0$ = 2 mg.L$^{-1}$; [NaCl] = 3000 mg.L$^{-1}$) to highly concentrated ($[H_2O_2]_0$ = 1000 mg.L$^{-1}$; $[Fe^{2+}]_0$ = 35 mg.L$^{-1}$; [NaCl] = 50000 mg.L$^{-1}$). The Central Composite Design (CCD) generates an experimental design of 19 experiments, with 5 replicates of the centre point, which are random placed (Table 3.6-1). Statistical treatment of data is performed by Statgraphics Plus 4.1 software.
Photon flow is estimated to be in average 9.15 μEinstein/s throughout this experimental phase by means of an actinometry.

Table 3.6-1: Central Composite Design. List of experiments carried out and TOC removal results in the study of the effect of salinity.

| Experiment number | $[H_2O_2]_0$ (mg.L$^{-1}$) | $[Fe^{2+}]_0$ (mg.L$^{-1}$) | [NaCl] (mg.L$^{-1}$) | TOC removal (± 0.021) |
|---|---|---|---|---|
| 1 | 524.5 | 18.5 | 26500 | 0.61 |
| 2 | 524.5 | 18.5 | 26500 | 0.65 |
| 3 | 524.5 | 35.0 | 26500 | 0.75 |
| 4 | 242.0 | 28.3 | 12527 | 0.21 |
| 5 | 807.0 | 28.3 | 12527 | 0.67 |
| 6 | 242.0 | 8.7 | 12527 | 0.11 |
| 7 | 524.5 | 18.5 | 26500 | 0.61 |
| 8 | 50.0 | 18.5 | 26500 | 0.06 |
| 9 | 524.5 | 18.5 | 26500 | 0.61 |
| 10 | 1000 | 18.5 | 26500 | 0.80 |
| 11 | 524.5 | 18.5 | 26500 | 0.65 |
| 12 | 242.0 | 8.7 | 40473 | 0.23 |
| 13 | 807.0 | 28.3 | 40473 | 0.82 |
| 14 | 524.5 | 2.0 | 26500 | 0.75 |
| 15 | 807.0 | 8.7 | 40473 | 0.78 |
| 16 | 524.5 | 18.5 | 3000 | 0.62 |
| 17 | 807.0 | 8.7 | 12527 | 0.74 |
| 18 | 242.0 | 28.3 | 40473 | 0.13 |
| 19 | 524.5 | 18.5 | 50000 | 0.61 |

### 3.6.3.- Results and discussion

#### 3.6.3.1.- Effect on 4-CP and TOC abatements

The effect of salinity on 4-CP removal rate is shown in Figure 3.6-1. The presence of chloride slow down the removal rate but the final removal obtained is the same. This fact is observed in all experiments with the same amount of reagents but different concentration of NaCl. In a more detailed approach, the pseudo-first-order kinetic constants can be taken into account. 4-CP degradation rate in the early minutes of experiment can be simplified as shows Equation 3.6-1.
In a more detailed approach, the pseudo-first-order kinetic constants can be taken into account.

The 4-CP degradation rate may be simplified, in the early minutes of experiment, as described in the following expression.

$$-\frac{d[4-CP]}{dt} = k_{obs} \cdot [4-CP] \qquad \text{Equation 3.6-1}$$

The constant $k_{obs}$ is the previously mentioned pseudo kinetic constant and is calculated by linear regression with a confidence coefficient of 95 %. This constant gathers the effects of Fenton's reagent and the irradiation.

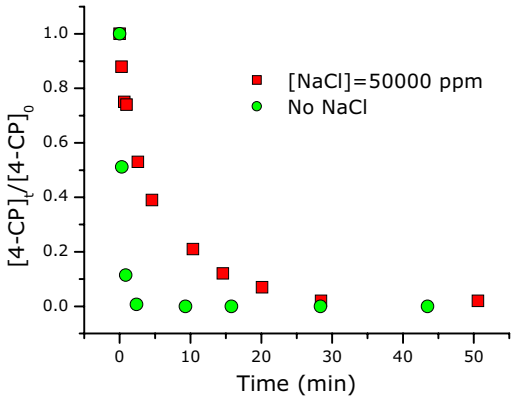


Figure 3.6-1: Normalized 4-CP evolution through two experiments. $[H_2O_2]_0$ = 524.5 mg.L$^{-1}$; $[Fe^{2+}]_0$ = 18.5 mg.L$^{-1}$.

Experiments with the same initial concentrations of $H_2O_2$ and $Fe^{2+}$ (524.5 mg.L$^{-1}$ and 18.5 mg.L$^{-1}$ respectively) and different concentration of NaCl are examined. Results and the confidence intervals are shown in Table 3.6-2. The experiments with lower concentration of NaCl prove faster kinetics, which means that the production rate of hydroxyl radicals is faster. It can be pointed out that $k_{obs}$ with 3000 mg.L$^{-1}$ of NaCl in the solution has the same order of magnitude than the experiment without NaCl, which means that at this NaCl concentration the process is not significantly affected. On the other hand, $k_{obs}$ is drastically lower for the experiment with 26500 mg.L$^{-1}$ of NaCl and even less with 50000 mg.L$^{-1}$, which means that with this NaCl concentrations, the process kinetics is strongly affected.

Table 3.6-2: Observed pseudo-first-order kinetic constants for 4-chlorophenol removal

| **Experiment number** | **[NaCl] (mg.L$^{-1}$)** | **$k_{obs}$ (min$^{-1}$)** |
|---|---|---|
| 1 | 26500 | 1.07 ± 0.18 |
| 16 | 3000 | 2.98 ± 0.08 |
| 19 | 50000 | 0.45 ± 0.02 |
| No NaCl | 0 | 2.60 ± 0.19 |

In Figure 3.6-2 and Figure 3.6-3, the evolution of TOC under different conditions is shown. It is remarkable that with higher $[H_2O_2]_0$, TOC removal achieved is higher. On the other hand, with different $[Fe^{2+}]_0$ the same TOC conversion is achieved, but the removal rate is higher with higher $[Fe^{2+}]_0$.

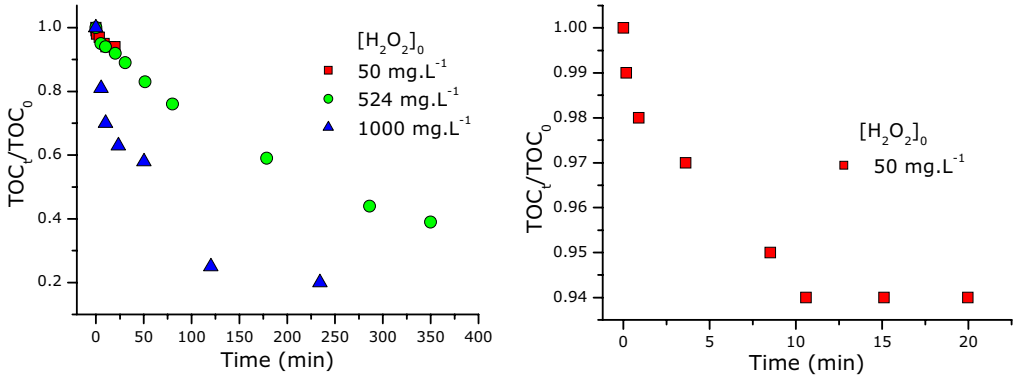


Figure 3.6-2: TOC evolution in the presence of NaCl. Effect of $[H_2O_2]_0$. $[Fe^{2+}]_0$ = 18.5 mg.L$^{-1}$; [NaCl] = 26500 mg.L$^{-1}$. On the right: Extension of experiment at $[H_2O_2]_0$ = 50 mg.L$^{-1}$

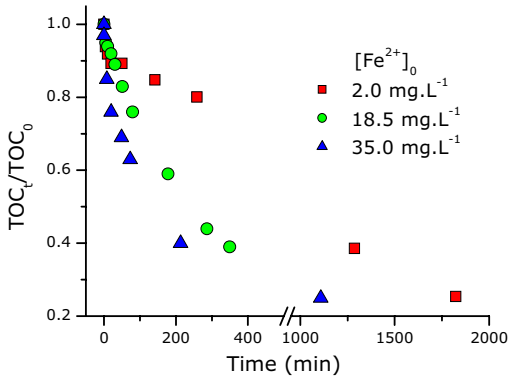


Figure 3.6-3: TOC evolution in the presence of NaCl. Effect of $[Fe^{2+}]_0$. $[H_2O_2]_0$ = 524.5 mg.L$^{-1}$; [NaCl] = 26500 mg.L$^{-1}$.

In Figure 3.6-4, the progress of TOC in the course of two experiments is shown. One is carried out with the highest amount of NaCl tested, and the other with the same reagents concentration but without salt. As shown in the Figure, the TOC removal is around 60% in both experiments, and even higher in the presence of NaCl. This fact is due to the low participation of the Fenton's scavenging reactions, which are mainly induced by iron. The difference of time for the complete depletion of $H_2O_2$ is significant.

Interestingly, TOC conversion achieved with 18.5 mg.L$^{-1}$ of $Fe^{2+}$ seems to be lower than with 2 and 35 mg.L$^{-1}$ of $Fe^{2+}$ (compare Figure 3.6-3 and Figure 3.6-4). In the experiment with less iron, it is provable that quinones might enhance the reduction of $Fe^{3+}$ to $Fe^{2+}$, which uses to occur at low iron concentrations. In addition, a considerable number of scavenging reactions, mostly

participated by iron, are not promoted. It has not been found any convincing explanation for the high conversion with 35 ppm of $Fe^{2+}$. However, the difference is not assessed to be statistically significant, since in the rest of experiments carried out with 524.5 ppm of $[H_2O_2]_0$, conversion ranges from 61 to 65 % (refer to Table 3.6-1).

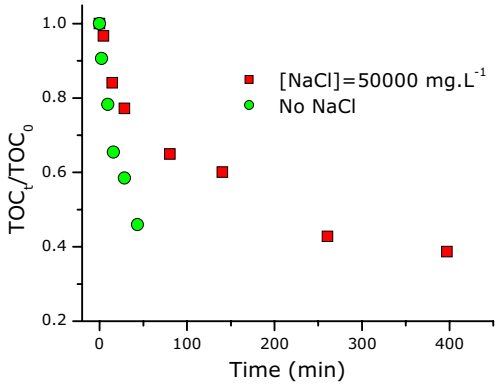


Figure 3.6-4: Normalized TOC evolution through two experiments. $[H_2O_2]_0$ = 524.5 mg.L$^{-1}$; $[Fe^{2+}]_0$ = 18.5 mg.L$^{-1}$.

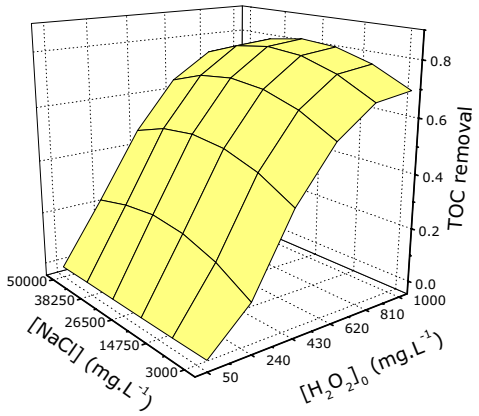


Figure 3.6-5: Response Surface representing TOC removal by Ph-F in the presence of NaCl. $[Fe^{2+}]_0$ = 18.5 mg.L$^{-1}$.

In Figure 3.6-5, a response surface representing TOC removal in the presence of NaCl is shown. According to the results and as shown in Figure 3.6-5, TOC removal is only affected by $H_2O_2$ loading. It can be emphasized, that neither the presence of NaCl nor $Fe^{2+}$ concentration, produce a significant influence on TOC removal. It should be pointed out that in most of the works concerning (non photo-enhanced) Fenton process, TOC removal was significantly affected by the presence of chloride in concentrations of NaCl higher than 2500 mg.L$^{-1}$ (*Maciel et al., 2004*). The response surface can be mathematically described as a quadratic function with the effect of each variable and their interactions. If only the statistically significant variables are taken into account, the function is simplified as described by Equation 3.6-2. In this case, only $[H_2O_2]_0$ is affecting TOC removal response, as said above.

$$\text{TOC removal} = -0.20\ (\pm\ 0.08) + 2.21 \cdot 10^{-3}\ (\pm\ 3.1 \cdot 10^{-4}) \cdot [H_2O_2]_0 - 1.23 \cdot 10^{-6}\ (\pm\ 2.8 \cdot 10^{-7}) \cdot [H_2O_2]_0^2$$

Equation 3.6-2

According to the results, the presence of chloride does not affect the mineralization of organic compounds. Therefore, it seems that the presence of chloride does not affect the amount of oxidizing agents produced, but it affects the rate in which they are produced. This fact agrees with the formation of photoactive iron complexes stated in the introduction. The generation of

$Fe^{3+}$-Cl complexes (Reaction 3.6-1 to Reaction 3.6-4) slows down the reduction of $Fe^{3+}$ to $Fe^{2+}$ (Reaction 3.6-6 and Reaction 3.6-7) which is necessary for the continuity of Photo-Fenton mechanism. Consequently, the oxidation of organic matter is slower. Another event that might contribute to the reduction of $Fe^{3+}$, hence to the continuity of the process, is the generation of quinones, as intermediates of aromatics degradation. However, their presence over the process might be short, since quinones are the earliest by-products. In most of experiments, a high dose of $H_2O_2$ is used and high levels of mineralization are achieved.

### 3.6.3.2.- Effect on the duration of the experiment

If the effect on process duration is taken into account, it should be emphasized that the influence of NaCl might severely affect the economy of the process. As seen above (Section 3.1.5), a strong influence of the duration of the process on the operating costs has been described. Figure 3.6-6 shows the Time difference for total depletion of $H_2O_2$ between experiments at $[H_2O_2]_0$ = 524.5 $mg.L^{-1}$ of the current experimental design and experiments with the same operating conditions but without NaCl. The dependence is represented in front of the molar ratio $Cl^-/Fe^{2+}$. As shown in the figure, when the ratio is higher, i.e. when the concentration of salt is high and/or the concentration of $Fe^{2+}$ is low, the difference increase significantly. The dashed line indicates a qualitative tendency. This fact reaffirms the importance of the influence of chloride on the iron mechanism and minimizes the possible scavenging of hydroxyl radicals by chloride.

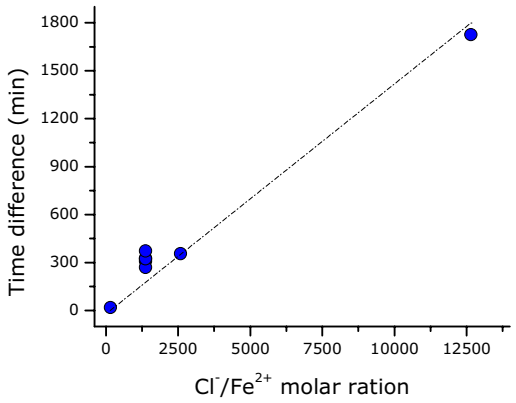


Figure 3.6-6: Time difference depending on the $Cl^-/Fe^{2+}$ molar ratio in experiments with $[H_2O_2]_0$ = 524.5 $mg.L^{-1}$.

In some experiments (not shown) is has been observed that the presence of anion phosphate ($PO_4^{3-}$) stops almost completely the process and affect severely TOC removal, like in Fenton process. Some authors (*Oller et al., 2006*) have dealt with this problem too. The formation of iron-

phosphate complexes is described as a method in wastewater treatment to precipitate and separate phosphate. Up to now, this problem has been solved by the addition of more iron sulphate to carry out Photo-Fenton. This effect could be investigated in more detail in order to find another solution.

#### 3.6.3.3.- The possible connection with biological treatment

There is now significant interest in the physiological capabilities and uses of bacteria that thrive in extreme conditions of pH, temperature, salinity or pressure (*Ventosa and Nieto, 1995*). It has been demonstrated that it is possible to treat biologically phenol in high salt solutions (*Peyton et al., 2002*). Consequently, it might be possible to combine Photo-Fenton and a special biological treatment to treat wastewater polluted with biorecalcitrant compounds.

### 3.6.4.- Conclusions

The presence of chloride slows down the process, but according to our results, do not affect the overall TOC removal. Thus, the anion seems to affect strongly the iron mechanism, due to the generation of iron-chloride complexes, but does not produce scavenging of hydroxyl radicals. In the photochemically enhanced Fenton process, unlike Fenton process, the generated iron-chloride complexes, which are photoactive (*Sima and Makanova, 1997*), take part in the process but in a slower rate. As during Photo-Fenton degradation of 4-CP quinones are generated as intermediates, these conclusions must be a priori restricted to wastewaters containing aromatic compounds, due to the influence of quinones on $Fe^{3+}$ reduction. More research with non-aromatic species should be done in order to know if these conclusions might be extrapolated as a feature of Photo-Fenton process.

Mineralization of organic matter (TOC removal) can be described as a function of $H_2O_2$ loading as a sole parameter, which means that $Fe^{2+}$ and NaCl do not affect on the overall degradation.

The experimental design has shown to be a suitable tool to study the overall effect of chloride on the TOC removal. In order to model the behaviour of the system it is necessary to perform detailed analysis on the $H_2O_2$ degradation kinetics, and the $Fe^{2+}/Fe^{3+}$ remaining in the solution. Although mineralization is not affected by salinity, the process is very slow and it would be economically unacceptable if an artificial radiation source is used. Solar photo-Fenton is severely advisable.

## *3.7.- Conclusions*

Diverse aspects of Photo-Fenton process have been studied and analyzed in this Chapter. The most relevant conclusions are point-by-point presented.

A Response Surface Methodology (RSM) has been used in order to describe the effects that different process's variables produce. It has been observed, that all degradation results are connected to $H_2O_2$. On the other hand, iron and temperature only affect the kinetics of the process, and this can entail strong influences on the operating costs.

According to the characterization of Ph-F products, biodegradability results seems to be connected with the dose of $H_2O_2$, but at the highest doses, the increase in biodegradability is small. It seems low sensitive, since the values do not differ much. Microtox analysis seems to be quite sensitive to Ph-F product characteristics. It can be, probably, a good indicator of integration possibilities.

Similar experiments have been carried out in a solar pre-industrial scale reactor. Parallel results are achieved, and the efficiency of the process is comparable.

Chemical Oxygen Demand (COD) of a Ph-F product appears to be directly connected with $H_2O_2$, and this relation can be described by simple mathematical equations. Thus, $H_2O_2$ monitoring may be a possible control parameter for this process.
A modelling of the process has been attempted by means of Mechanistic Models. According to the results, these models fit fairly well the experimental values, and can be a good base for future investigation around this field.

Finally, the effect that salinity can have on the process has been studied. It seems that the presence of NaCl does not influence the degradation possibilities of Photo-Fenton.

# *Chapter 4: Integration of Photo-Fenton and Biological treatments*

In the present chapter, Photo-Fenton and Biological processes are finally combined. The biological reactor is a ***SBBR***, which means Sequencing Batch Biofilter Reactor, i.e. an attached-growth biological reactor that operates in batches. In a first stage, a preliminary study is carried out, which serves for getting used to the reactor operation, for solving problems and for ascertaining the importance of different phenomena, such as adsorption or stripping.

The second step is a ***Start-up*** of the SBBR. In this phase, the bioreactor is fed with a Photo-Fenton product (named ***Feed***) which is assumed to be, at least, partially biodegradable, and different batches are repeated until a steady state is observed. Each batch is named ***Cycle***, and the duration of this cycle, is the Cycle Time, or the Hydraulic Retention Time, ***HRT***.

Finally, an optimization of the ***coupled system*** is endeavoured, in order to obtain the highest degradation with the shortest time. The objective is to achieve more than 90 % of TOC abatement by the combined process in 8 hours of HRT in the biological reactor. For this purpose, the amount of $H_2O_2$ consumed in the Photo-Fenton process is varied and the SBBR is forced to operate in short HRT.

# 4.1.-Introduction

Due to the high costs of AOPs, a commonly suggested economically viable option is the combination of an AOP and a biological treatment. In this case the chemical step is used to enhance the biodegradability of the wastewater, so that it can be treated by biological means (*Sarria et al., 2003*).

As stated in the intial introduction, Sequencing Batch Reactors (SBR), present some advantages for biodegrading problematic compounds, since the operation in sequences force the population to be selected and adapted (*Buitron et al., 2004*). Among SBR, the Sequencing Batch Biofilter Reactors (SBBR) -or biofilm- with fixed biomass, can be mentioned. In these systems, an improved bioreactor activity is achieved by means of a high biomass concentration (*Grady, 1990*). In the present study, the biological reactor is a biofilm supported on volcanic stones, on which porous surface the bacteria can be easily attached. Biofiltration is a technology based on the biological oxidation of pollutants using micro-organisms which are immobilized forming biofilms or biolayers around solid particles, such as any porous structure (*Zarook and Shaikh, 1997*). Synthetic and as well natural materials can be used. Among the former ones, polymer shaped for example as Rashig rings, or a grid can be found as well as glass balls. Among the latter (the natural materials) diverse porous minerals and stones may be used, such as volcanic stone. Due to the nature of the support, a non-desired phenomenon can occur during the early cycles of operation: Adsorption (*Quezada et al., 2000*).

In the case of a SBBR, as the biomass is attached, the stages of a cycle defined in Figure 1.5-1 are a little bit different. In fact, some of the stages are not necessary. In this case, there is (a priori) no need of a settling stage. Moreover, instead of a mechanical mixing system, the fluid is recirculated from the top to the bottom of the reactor.

An initial solution of 200 $mg.L^{-1}$ of 4-CP is treated with a certain amount of $H_2O_2$ by Photo-Fenton, in order to obtain a product, which may be characterized as a function of this particular amount of $H_2O_2$ spent, as seen above (Section 3.2). Temperature is fixed at 27 ºC and $[Fe^{2+}]_0$ is 10 $mg.L^{-1}$. This product, after a preparation described in Section 2.1.3, is suitable to be fed into the biological reactor. Consequently, it is named ***Feed***. It is suggested that, depending on the characteristics of this Feed, the bioreactor might be able (or not) to treat efficiently the mixture. Thus, it may be possible to optimize the coupled system, spending enough amount of $H_2O_2$ in the Ph-F (but not in excess) to produce a readily biodegradable mixture, which may be treated fast and efficiently in the SBBR.

# 4.2.- Preliminary study

Different parts are carried out within this preliminary study. As the reactor is built up for the first time for this work, it must be learnt how to use properly the reactor. Thus, it might be possible to define the main characteristics of the reactor and to reveal problems of constructions, if they exist. It is important to elucidate the problems that could affect the appropriate operation. Among these problems, it may be pointed out mass transfer phenomena: stripping and adsorption.

The first attempt of operation is carried out by an aggressive mode; the 4-CP solution is not deeply treated. Only 120 $mg.L^{-1}$ of $H_2O_2$ are applied in the Ph-F treatment. Therefore, some amounts of early intermediates could remain in the solution. However, 4-CP is almost depleted. Moreover, TOC content is high, which is desirable, since it is expected to force mineralization to occur mostly by biological means. It is not rigorously a start-up, since it is not expected to execute more than a couple of cycles.

### 4.2.1.- Mass transfer phenomena

#### 4.2.1.1.- Stripping effect on the wastewater

The following step is to check the influence of the air stripping on the volatile compounds of the photo-Fenton products. To carry out this test, the same pre-treated solution that is going to be fed into the SBBR is used. 0.5 L of solution, with the corresponding amounts of micronutrients and trace elements, neutralized, and buffered is introduced in a 1.5 L vessel that has the same diameter of the biofilter. Then, air is supplied at a flow rate of 2 $L.min^{-1}$. For additional information about the device, refer to Section 2.1.5.

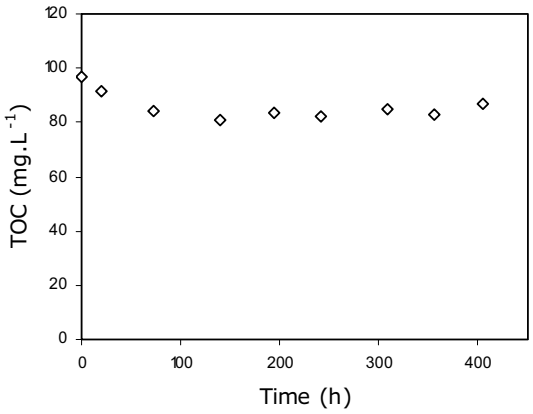


Figure 4.2-1: Stripping experiment of photo-Fenton products.

As it is shown in Figure 4.2-1, the stripping of photo-Fenton products, represent a loss of approximately 10 % of TOC due to dragging of volatile compounds. During the experiment, around 20 % of total volume is lost after 10 days. As the ratio between air and liquid is higher than in the reactor (the test is carried out with only 0.5 L) this loss is not worrying. Moreover, it is not expected to operate with cycles of 10 days.

However, in a further study, the flow of air is reduced in order to reduce the volume losses, and therefore to reduce the volatile products losses, but keeping in mind that enough oxygen concentration has to be maintained in the bioreactor for its good performance.

#### 4.2.1.2.- Adsorption effect

In parallel with the stripping experiment, an adsorption test is performed. The solution that is used is the same than in the previous case. Now, it is introduced in a 1.5 L vessel together with the necessary volume of stones to maintain the same ratio than in the biofilm (0.3 stones/liquid volume ratio) and stirred to avoid precipitation. The device is shown in Section 2.1.5.

The results of this experiment are depicted in Figure 4.2-2. After 250 hours, approximately 60 % of TOC is adsorbed by the porous stones. This percentage points out that any TOC removal obtained in the biofilm over this one is due to the biodegradation.

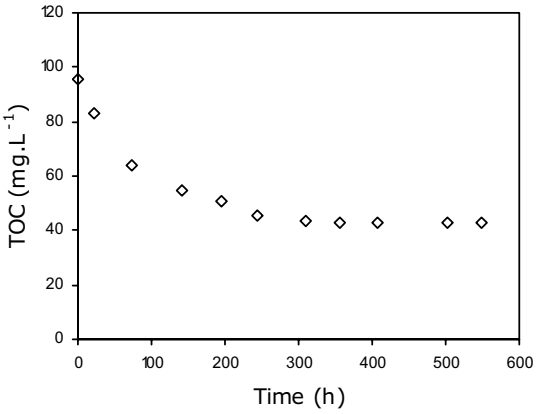


Figure 4.2-2: Adsorption experiment of photo-Fenton products.

As shown by Quezada et al (*Quezada et al., 2000*) in experiments carried out with colorants, sorption in this kind of material is significant and is the main phenomenon for the TOC removal during the first cycles. When the packing material becomes saturated, the removal rate can

decrease, but when bacteria become acclimatized the removal increases because of biodegradation.

Adsorption phenomenon seems to be quite important and in consequence, more experiments have to be done. In a further experiment, it is necessary to carry out an adsorption experiment in parallel with the biofilm with the same working conditions, such as temperature and cycle length, in order to study the material saturation.

**4.2.2.- Preliminary Study: assessing the process strategy**

Once the stripping and adsorption influences have been studied, a biodegradation test is performed. The biofilm is filled as said above, with a solution that has not been deeply treated, i.e. in the Ph-F, a low amount of $H_2O_2$ has been applied. Moreover, the same load is going to be maintained in the reactor even if there is no decrease in TOC. It is expected, by this procedure, to force the bacteria to consume all the organic species present in the mixture, and consequently, to become acclimatized faster and better.

In Figure 4.2-3 the TOC evolution is depicted, showing that the TOC level decreased until 30 $mg.L^{-1}$. Taking into account the percentage of TOC removal by adsorption, the amount of TOC removed by biodegradation seems to be 10 $mg.L^{-1}$ below the adsorption. The second cycle does not show any improvement.

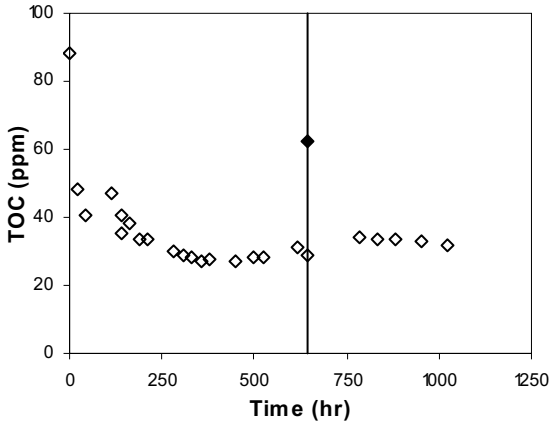


Figure 4.2-3: TOC evolution in 2 cycles.

Another parameter studied during this experiment is the evolution of TVSS (not shown). A decreasing trend it is clearly observed, from an initial value of 1140 $mg.L^{-1}$ to an approx. constant

value of 50 mg.$L^{-1}$. In fact, it is obvious, since the organic load supplied is low, and it is not enough to maintain this population. Other controls shows that pH remains constant at 7.1-7.2 and dissolved oxygen is constant at 7.7 mg $O_2$/L, which is the saturation concentration of oxygen in water at the working temperature (27 ºC).

#### 4.2.3.- Conclusions

It would be interesting to perform the start-up with a cycle length of max. 10-15 days, since the system shows no further improvement and repeating the cycles until an evolution is observed. Moreover, as adsorption phenomenon seems to be quite important, the test must be repeated, for example, in parallel with the SBBR stages.

## *4.3.- Coupling of the Biological process to the Photo-Fenton*

This section is in fact one of the main parts of the work. Both systems, Ph-F and the SBBR, have been already tested, and it is possible to characterize the products of Ph-F regarding the dose of $H_2O_2$. Now, both systems must be integrated. The objective is to reach the maximum mineralization (more than 90 % of TOC removal) by the coupled system, and spending the lowest possible amount of $H_2O_2$ in the Ph-F.

As seen in the previous Section (4.2), starting-up the reactor by the so-called "aggressive" strategy, does not produce the desired results. In the present Section, the pressure applied in the Ph-F is higher, i.e. more $H_2O_2$ is spent. Consequently, the product that is fed into the bioreactor is, according to the results of characterization (Section 3.2), more biodegradable than in the previous study, since biodegradability increases with the increase in $H_2O_2$.

It is important to point out that the period of acclimatization is essential for a good performance of the SBBR. It has been observed that acclimated activated sludge is more efficient than for example, isolated strains that are supposed to be the best in degrading a specific compound (*Buitron et al., 1998*).

During 8 months, the evolution of TOC content in the bioreactor has been checked, operating with different cycle times, and changing substrate (feed) conditions when it has been necessary. As seen in the previous chapter, the adsorption effect was significant enough to be considered. To this end, the adsorption test is repeated, in parallel with the biofilter operation.

### 4.3.1.- Start-up of the SBBR

First, it must be decided which Ph-F product is going to be fed into the SBBR for its Start-up. The solution treated with 300 mg.$L^{-1}$ of $[H_2O_2]_0$ is selected. If biodegradability ratio is observed, among products from 300 to 500 mg.$L^{-1}$ of $H_2O_2$, the differences do not seem to be high enough to decide which product is better. Other parameters have to be observed.

According to the characterization of products (Section 3.2), 300 mg.$L^{-1}$ plays a limit role. This product is the mixture that shows the highest $BOD_5$ value, i.e. a highest concentration of readily biodegradable matter. From that point on, as more $H_2O_2$ is consumed, $BOD_5$ decrease. Moreover, mineralization in this product is low. Thus, the organic content supplied to the reactor, i.e. Organic Loading Rate (OLR), is going to be high. Table 4.3-1 shows a review of results concerning the product of Ph-F at 300, 400 and 500 mg.$L^{-1}$ of $H_2O_2$.

Table 4.3-1: Removal and biodegradability enhancement results obtained by Ph-F with different reagent doses.

| Level | $[H_2O_2]_0$ (mg.$L^{-1}$) | $[Fe^{2+}]_0$ (mg.$L^{-1}$) | 4-CP removal | Ph-F TOC removal | $BOD_5$/COD ratio |
|---|---|---|---|---|---|
| A | 300 | 10 | 1.00 | 0.16 | 0.17 |
| B | 400 | 10 | 1.00 | 0.31 | 0.19 |
| C | 500 | 10 | 1.00 | 0.48 | 0.20 |

This level of pre-treatment is labelled as Level A. To start-up the reactor, the product of Ph-F is prepared (see Section 2.1.3 ) and is mixed with 200 mL of activated sludge collected at the sewage works of Gavà (Barcelona, Spain). The total volume is 1.6 L. The mixture is fed into the biological reactor, and the batch is maintained until no TOC decrease is observed. Then, a new cycle is started, achieving in each following cycle, better TOC removal results.

First cycles accumulate many errors. The carbon requirements for the initial biomass concentration are much higher than the OLR supplied. Furthermore, the bacterial culture is not acclimatized to the supplied feed. Another phenomenon that can occur is the endogenous respiration, in which the cells digest other cells, i.e. predation takes place.

In the net rate of bacterial growth, two terms are of importance; the cell growth and the endogenous decay (see Equation 4.3-1). The first term (growth) depends on the biomass concentration (X) and substrate concentration (S), and the death term, only depends on the biomass concentration. If the substrate is not tempting or available for the bacteria, (they are not

acclimated at the beginning), "S" in the equation is negligible and the second term is the most important. Moreover, during the first cycles, the biomass concentration is high.

$$r_g' = \frac{\mu_m X S}{K_s + S} - k_d X \qquad \text{Equation 4.3-1}$$

After 8 cycles, a steady state is observed. Visually, the reactor content has lost certain turbulence. As cycles go along, part of the biomass place on the volcanic stones, first only some flocks and with more time, a thin layer on the entire surface may be observed.

The lowest TOC value achieved is 30 $mg.L^{-1}$ and cycles last around 150 hours (6 days). The TOC evolution over a cycle in steady state at these operating conditions (Level A) is shown in Figure 4.3-1. Totally, 11 cycles were carried out under these conditions. Most of TOC abatement occurs within the early 48 hours of cycles, which means that it is possible to shorten the cycle. As the final TOC value does not fulfil the objective, an optimization of the integrated system must be carried out.

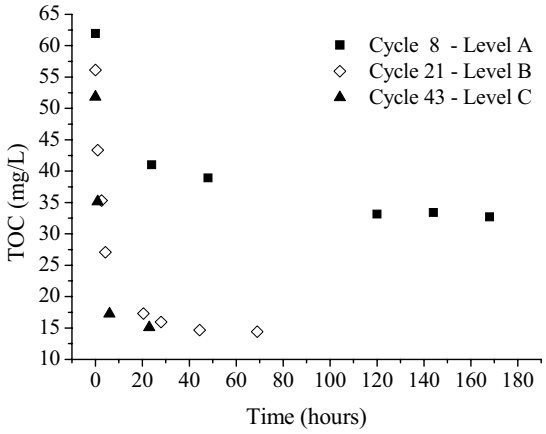


Figure 4.3-1: TOC evolution in the biological reactor through a cycle depending on the level of Ph-F treatment.

### 4.3.2.- Optimization of the coupled system

According to the results, an increase in the hydrogen peroxide dose in the Ph-F process is required due to the low TOC removal achieved at the end of the biological treatment (see Level A in Figure 4.3-1). A Ph-F treatment with 400 $mg.L^{-1}$ of $[H_2O_2]_0$ and 10 $mg.L^{-1}$ of $[Fe^{2+}]_0$ is carried out. This pre-treatment is named Level B. The removal ratio and biodegradability

enhancement results in the Ph-F are shown in Table 4.3-1. Figure 4.3-1 shows the TOC decrease over a steady-state cycle fed with Level B pre-treated product. 30 cycles are performed with these operating conditions. The steady-state cycles lasted 24 hours. Since under these operating conditions, the objective value is not reached, a third and harder level of Ph-F treatment, level C is required.

In this case, level C, the dose of $H_2O_2$ applied in the Ph-F is 500 $mg.L^{-1}$. The product characteristics are shown in Table 4.3-1. Figure 4.3-1 shows a cycle carried out with "Level C" feed. TOC removal rate in this case is in this case significant. Almost all the removal occurs during the early 8 hours. The final product in steady-state contains less than 10 $mg.L^{-1}$ of TOC, consequently, the objective is accomplished.

#### 4.3.2.1.- Comparison of the three operating conditions

Figure 4.3-2 summarizes the results that have been described. The figure shows the average cycle time at the steady-state (in triangles) and the best TOC value reached with each of the three levels previously described. The bottom part of each column depicts the mineralization achieved by Photo-Fenton and the rest, by SBBR.

The differences in time between the first level (300 $mg.L^{-1}$ of $[H_2O_2]_0$) and the rest are noteworthy. Concerning levels B and C, the differences are not high, but in level C the objective is accomplished faster, and the result is a little bit better. Maybe, the major drawback of level C is that more than half of mineralization occurs by Photo-Fenton. Interestingly, Microtox values of Photo-Fenton products (Section 3.2.2) seem to predict the results better than biodegradability ratio, since from the ratio results, the suitable conditions cannot be predicted.

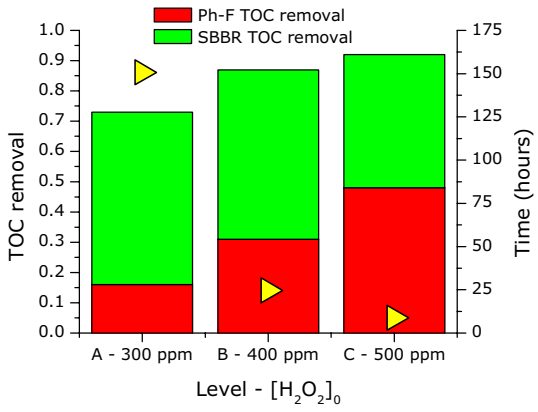


Figure 4.3-2: Comparison of results of the integrated system.

#### 4.3.2.2.- Evolution of Suspended Solids in the reactor

As said above, the biofilter is started-up with sludge coming from an urban wastewater treatment plant. In consequence, the concentration of solids at the beginning is high. TVSS content in the reactor decrease until a steady state is observed. This steady state might be related to the biomass generated due to the substrate and the biomass that is detached from the stones and the death microorganisms (Equation 4.3-1). Figure 4.3-3 shows the evolution of TVSS during 3000 hours of operation. The TVSS residue after 600 hr is due to the part of biomass that is not attached to the volcanic stones.

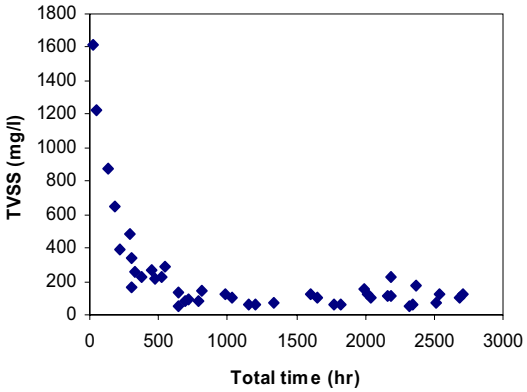


Figure 4.3-3: TVSS evolution until the 12th cycle.

### 4.3.3.- A simple characterization of the SBBR

The biofilter is under operation for eight months. During this period, Total Volatile Suspended Solids (TVSS) are also monitored. This parameter may be an estimation of the biomass not attached to the support. When the reactor operates in steady-state, the measure of TVSS at the end of a cycle might be related to the biomass generated per unit of carbon mineralized. The results are shown in Table 4.3-2. As it is expected, the value is low, meaning that the sludge growth is low and the SBBR is working properly. In a biofilter, the biomass is mostly fixed at the support and the sludge age is high compared to a conventional biological reactor (*Metcalf and Eddy, 1991*).

Table 4.3-2: Biomass generated per unit of carbon mineralized at steady-state

| TVSS average ($mg.L^{-1}$) | Withdrawn Volume (L) | Withdrawn biomass/cycle (mg biomass) | TOC mineralized/cycle (mg C) | TVSS/TOC (mg/mg C) |
|---|---|---|---|---|
| 50.2 ± 21 | 1.1 | 55.2 ± 23.8 | 40.5 ± 10.4 | 1.36 |

Normally, this parameter is usually called Yield or Heterotrophic Yield (Y or $Y_H$), and is estimated by monitoring oxygen decay in the reactor (dissolved oxygen and oxygen demand). Later, a characterization of the SBBR by means of this parameter is carried out.

### 4.3.4.- Adsorption effect

The adsorption effect test is repeated. In this case, the test was performed in parallel with the biofilter cycles, i.e. carrying out the empty and re-filling at the same time as in the biological reactor. To follow the effect that could entail the volcanic stones in the media, samples are withdrawn during each cycle and the TOC of the solution is measured. The device is described in chapter 2.1.5. The results of this monitoring are plotted in Figure 4.3-4.

Results are surprising and it is worth to comment them. Apparently, it occur adsorption from the beginning of the test. These results are in principle troubling, but it is not taken into account that the media is perfectly adapted for the growth of biomass –the content is the same than in the biofilter-. In consequence, from the 8th cycle on, pH is changed to produce the inhibition or death of the bacterial culture generated inside. The trend of apparent adsorption change and it is possible to say that at least after 8 cycles, there exist no adsorption and all the TOC removal in the biofilter is due to the bacterial activity.

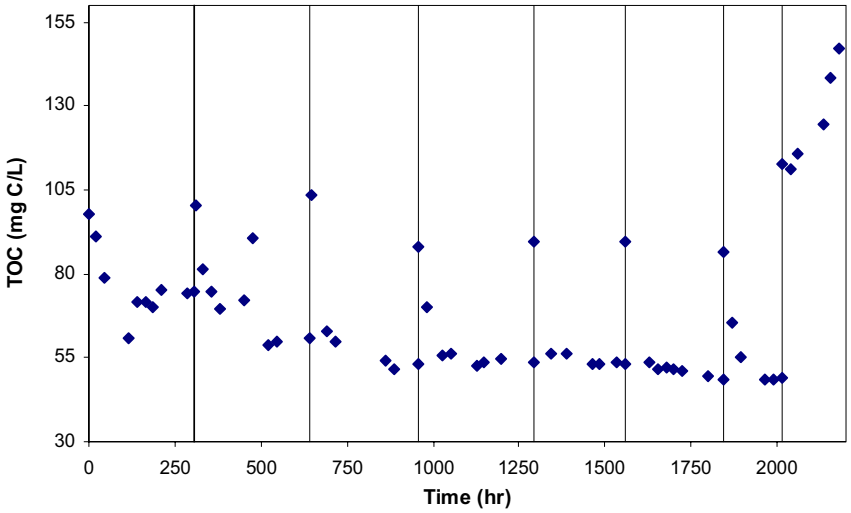


Figure 4.3-4: TOC evolution during the adsorption test. Vertical lines separate each cycle.

## 4.4.- Conclusions

The results achieved by the coupled system are satisfactory. The mineralization objective is accomplished when 500 $mg.L^{-1}$ of $H_2O_2$ are applied in the Photo-Fenton system. This result is accomplished within just 8 hours of SBBR cycle duration.

According to the results of Volatile Solids, biomass production is low, being this an advantage. One of the major problems of the conventional biological treatments is the large production of sludge, which then must be eliminated. In fact, conventional treatments are only partially degradation systems, since they transfer the problem to the sludge phase.

Concerning the objective of finding a parameter that predicts easily the integration possibilities, the suggested biodegradability ratio is not sensitive enough. The ratio values for the 3 substrates are no significantly different, and does not predict the SBBR results, since these Ph-F effluents, produce a very different result in the SBBR.

Probably, a combination of different parameters must be used. Among the parameters that have been monitored to characterize Photo-Fenton products, Microtox seems to produce a profile similar than the effects that have been observed in the SBBR (unfortunately, Microtox analyses were carried out after this experimental part, and their results could not be used to choose the appropriate conditions).

If Microtox analyses shown in Section 3.2.2 are observed, the product of 300 $mg.L^{-1}$ of $H_2O_2$ presents an effect concentration around 50 %, 400 $mg.L^{-1}$ around 90 % and 500 $mg.L^{-1}$ product does not produce effect (100 %). Actually, the SBBR results are similar (see Figure 4.3-2).

Another parameter that is likely to predict the SBBR results might be $BOD_{21}$, which is the BOD after 21 days. However, this parameter is not considered suitable, since it needs too long time.

# *Chapter 5: Characterization of the Sequencing Batch Biofilter Reactor (SBBR)*

In the previous chapter, it has been described how a combined Photo-Fenton/Biological system is able to treat a non-readily biodegradable solution. In summary, the best pollution remediation is reached when the solution is treated with 500 $mg.L^{-1}$ of $H_2O_2$, since shows a better biodegradability in the biological reactor. Apparently, the biological reactor does not show problems of inhibition in all the tested operating conditions.

In this chapter, the Sequencing Batch Biofilter Reactor (SBBR) is started-up with a solution treated in the Photo-Fenton reactor with $[H_2O_2]_0 = 500$ $mg.L^{-1}$. In this case, the aim of the study is the ***characterization*** of the SBBR. To this end, different parameters are estimated, such as the ***Oxygen Uptake Rate*** (OUR), which is an estimation of the oxygen consumption, or the biomass generation per unit of Chemical Oxygen Demand (COD) degraded, which is usually called ***Heterotrophic Yield*** ($Y_H$). By means of this study, an improvement of the ***description*** of the coupled system is obtained. By extrapolation, it might be possible to model the behaviour and needs of a scaled-up reactor.

Later, the properties of the feed are changed in order to verify the preconceived ***resistance*** of an attached biomass reactor. In consecutive stages, the solution fed into the SBBR is less biodegradable, since is treated in the Photo-Fenton with less amount of $H_2O_2$. This increase of exigencies goes so far as to feed a solution without treatment, i.e. a solution of 200 $mg.L^{-1}$ of 4-CP. Finally, the characterization of the microbial diversity of the SBBR in a certain moment is carried out. This means that the main bacterial strains and families present in the SBBR are identified.

# *5.1.- Introduction*

A high biomass concentration; achieved i.e. by means of a biofilm, improves the bioreactor activity (*Grady, 1990; Puhakka and Jarvinen, 1992*). In this type of reactor, because of substrate concentration variations in each cycle (decreasing in time), the growth rate of microorganisms changes from high to low. Furthermore, there is a selection of microbial community with a vast metabolic range, in which microbial species can differ greatly in growth rate and yield (*Moreno-Andrade et al., 2006*).

Biofilms can also have very long biomass residence times, which make them particularly suitable when treatment requires slow growing organisms with poor biomass yield or when the wastewater concentration is too low to support growth of activated sludge flocks (*Wilderer, 1992; Wilderer et al., 2001*).

The mathematical description and modelling of this kind of reactors is much more complicated than in the suspended biomass reactors. Both the organic and biomass content has to be measured in two phases: the liquid and the solid one (Figure 5.1-1). In the calculation of production and accumulation of biomass, the death term is accompanied by the detached biomass term. In addition, during the feed and empty processes, substrate and biomass are accumulated or lost (*Devinny and Ramesh, 2005; Metcalf and Eddy, 1991; Spigno et al., 2004; Zarook and Shaikh, 1997*).

Modelling of the whole biofilm performance is not attempted in this work. However, some aspects of the bioreactor are going to be characterized, since they can be used for control purposes. Recent studies (*Moreno-Andrade et al., 2006*) have shown that by measuring only the dissolved oxygen concentration and the volume of the reactor, it is possible to estimate the Oxygen Uptake Rate (OUR), which is linearly related to the Substrate Uptake Rate (SUR). Using this estimation, the optimal strategy sets the influent flow rate such that the substrate degradation

rate is maintained around its maximal value as long as possible, thus, minimizing the reaction time.

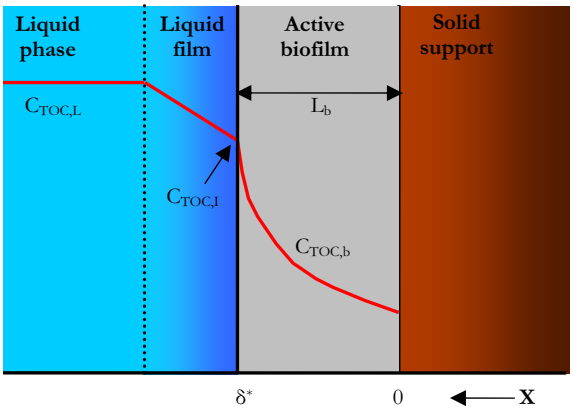


Figure 5.1-1: Conceptual biofilm model: concentration profile in a biofilm

When using biofilm processes, the inner layer of microorganisms is protected, tolerating changes in pH and temperature (*Wingender et al., 1999*), and even concentration of toxic substances or toxic shock loading (*Gantzer, 1989; Wingender et al., 1999*). This feature, entails a significant advantage over other reactor configurations, and places it as an important technology for the treatment of toxic and biorecalcitrant organic pollutants. In biofilm reactor systems, non-readily biodegradable matter can be sorbed onto and transferred into the biofilm and periodically removed by desorption and subsequent biodegradation (*Wilderer and McSwain, 2004*).

It is possible that due to a mistake in the control of the chemical step, a non-biodegradable and even toxic wastewater is fed into the biological reactor. If it is fed into a conventional biological reactor (suspended-growth), the toxic shock could cause an irreversible situation and consequently the death of the biomass. The fixed bed biomass is expected to overcome the problematic situation, and regain the steady-state operation in a short time.

### 5.1.1.- Oxygen Uptake Rate (OUR) and Yield ($Y_H$)

Oxygen Uptake Rate (OUR) is the comsume of oxygen due to bacterial requirements. If in a certain moment, there is no oxygen supply, OUR can be estimated by the oxygen concentration decay (Equation 5.1-1). As the experimentation deals with a biofilter, the estimation of OUR must be carried out in-situ, which has assessed to be an effective tool (*Yoong et al., 2000*).

$$OUR = -\frac{dS_O}{dt}$$ Equation 5.1-1

Heterotrophic Yield ($Y_H$) can be defined as the relation between the amount of new biomass generated per amount of substrate consumed. Measuring the generation of biomass, especially when is low, is difficult. However, it can be measured by difference and taking some assumptions.

The biodegradable substrate may be consumed for obtaining energy or for the generation of new biomass (Figure 5.1-2). Both mechanisms consume oxygen, but it can be considered that the oxygen requirements for new biomass generation are negligible in front of energy generation.

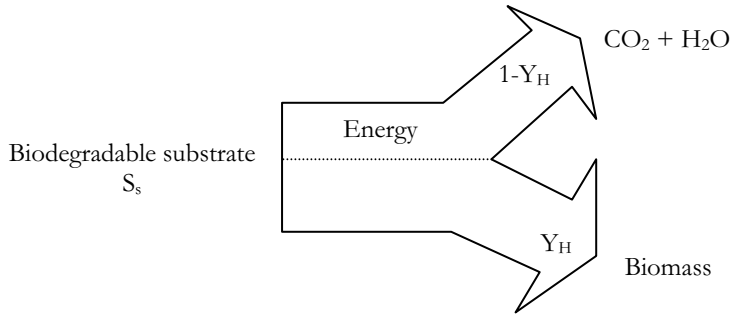


Figure 5.1-2: Schematic representation of aerobic heterotrophic metabolism and Yield ($Y_H$).

Abatements of oxygen (Equation 5.1-2) and substrate (Equation 5.1-3) can be described by the IWA's Activated Sludge Model 1 (ASM1) equations.

$$-\frac{dS_O}{dt} = \frac{1-Y_H}{Y_H}\mu_{mH}\left(\frac{S_S}{K_S+S_S}\right)\left(\frac{S_O}{K_{OH}+S_O}\right)X_{BH} \qquad \text{Equation 5.1-2}$$

$$-\frac{dS_S}{dt} = \frac{1}{Y_H}\mu_{mH}\left(\frac{S_S}{K_S+S_S}\right)\left(\frac{S_O}{K_{OH}+S_O}\right)X_{BH} \qquad \text{Equation 5.1-3}$$

By combination of these equations, Equation 5.1-4 is obtained. The integration of substrate and oxygen differential equations, leads to total oxygen consumed (Equation 5.1-5), which can be estimated by integration of OUR values, and total substrate consumed (Equation 5.1-6), which is the abatement of COD throughout a cycle. Thus, by integration, a simple expression that connects oxygen and substrate consumed is obtained (Equation 5.1-7). Heterotrophic Yield ($Y_H$) can be then estimated.

$$\frac{dS_O}{dt} = (1 - Y_H) \cdot \frac{dS_S}{dt}$$ Equation 5.1-4

$$\int_t \frac{dS_O}{dt} = OC$$ Equation 5.1-5

$$\int_t \frac{dS_S}{dt} = COD_{consumed}$$ Equation 5.1-6

$$OC = (1 - Y_H) \cdot S_S$$ Equation 5.1-7

## *5.2.- Start-up*

In this start-up of the SBBR, the best-known operating conditions, mainly regarding the feed preparation, are used. These are the operating conditions labelled "Level C" in a previous Chapter (Section 4.3.2, specifically). Consequently, in order to feed the biological reactor, a solution of 200 mg.L$^{-1}$ of 4-chlorophenol is treated in the Photo-Fenton reactor with 500 mg.L$^{-1}$ of $[H_2O_2]_0$ and 10 mg.L$^{-1}$ of $[Fe^{2+}]_0$ as a catalyst. Additional procedures are described elsewhere (Section 2.1.3.- Preparation of the feed for the biological reactor).

During the start-up and following cycles, the feed is let to react in the biological reactor for 168 hours (one week). To be precise, the Hydraulic Retention Time (HRT) is 168 hour. By this stage, different characteristics of the reactor and feed may be known, such as the maximum biodegradability, or the endogenous respiration. A summary of results of the start-up and following cycles is shown in Figure 5.2-1.

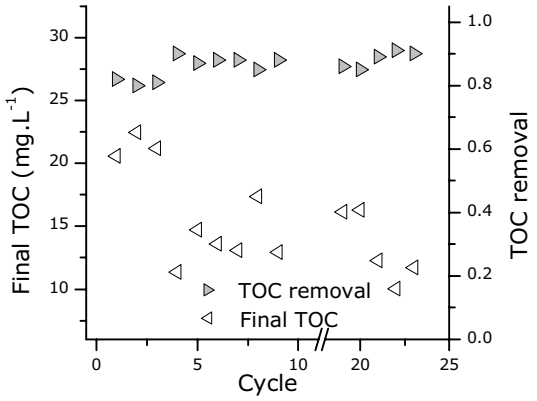


Figure 5.2-1: Summary of results. Start-up stage. HRT = 168 hour (1 week). In Ph-F process, $[H_2O_2]_0$=500 mg.L$^{-1}$

As shown in the figure, a steady state is rapidly reached, apparently after 4 cycles. The values of TOC achieved at the end of the cycle, which are named Final TOC in the graph, (white triangles), round 10 $mg.L^{-1}$, which is a value reasonably attributable to biomass lysis products (*Sahinkaya and Dilek, 2006*). Therefore, TOC removal values, considering both the Ph-F and the SBBR (grey triangles) are about 0.9 (90 %) which is the same level of mineralization achieved before (Section 4.3.2.1).

After the steady-state is reached, some cycles are observed in depth. For this purpose, samples are withdrawn throughout a cycle and TOC and COD is measured. Cycles 21 and 22 are taken as examples. The TOC and COD evolutions throughout cycles 21 and 22 are shown in Figure 5.2-2 and Figure 5.2-3 respectively. As shown in the figures, results of both cycles present slight differences. Interestingly, mineralization mostly occurs in the first hours of cycle, whereas some oxidation, i.e. COD decrease, also takes place in the rest of cycle time. This behaviour in the TOC degradation rate is also observed in the previous SBBR test period (Section 4.3). Cycle 22 is the last one carried out with the HRT of 168 hour, since in the following cycle HRT is reduced to 120 hour (5 days).

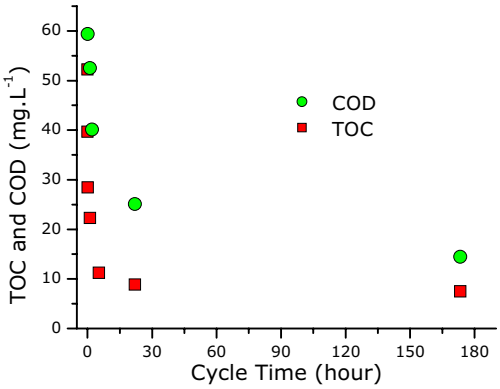


Figure 5.2-2: TOC and COD results. Cycle 21

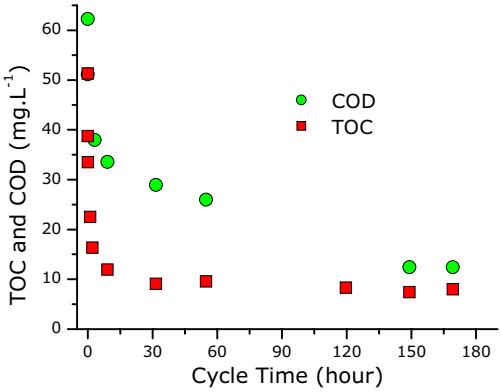


Figure 5.2-3: TOC and COD results. Cycle 22

As the results of cycle 22 are more complete, this cycle will be used as example to show how the various characterization parameters are calculated.

### 5.2.1.- Example of Oxygen Uptake Rate estimation

As stated in the introduction (Section 5.1.1), OUR is an important parameter in order to control the operation and performance of an aerobic biological reactor.

To carry out this test, air supply is sequentially stopped and switched on. This procedure is carried out by means of a programmable logical timer (see Chapter 2.1.4) and the air cut is kept enough time to measure the oxygen fall but maintaining the oxygen concentration always above 2 $mg.L^{-1}$.

During the stop, oxygen concentration in the reactor falls due to bacterial consumption, and if maintained above 2 $mg.L^{-1}$ the abatement rate follows a zero-kinetics order regarding the oxygen concentration. Therefore, if the dissolved oxygen (DO) concentration decrease is monitored, straight lines are obtained. A profile of DO of the first 5 hours during a respirometric test in the reactor is shown in Figure 5.2-4. Oxygen is measured every 20 seconds and its representation generates a graph with multiple straight lines. The slope of each line is calculated, and results in one point of the Oxygen Uptake Rate (OUR) plot (Figure 5.2-5). The area under the points is the total Oxygen Consumed ($OC_{total}$) per litre of reactor in this given period, which includes the Endogenous Respiration (ER).

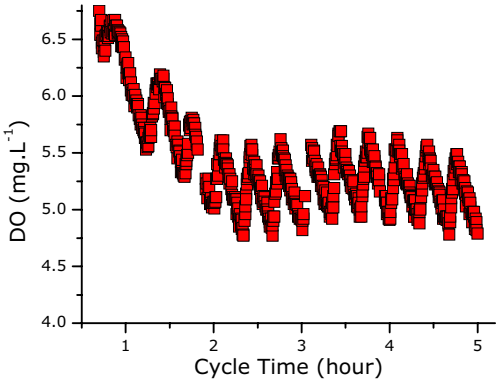


Figure 5.2-4: Example of DO (DO) profile during an OUR test. First 5 hours of cycle 22

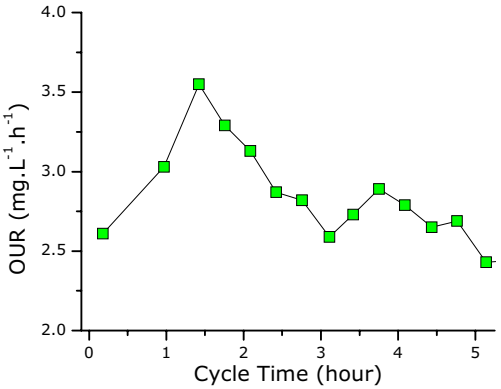


Figure 5.2-5: Oxygen Uptake Rate (OUR). First 5 hours of cycle 22.

After a first hour of acclimatization to the new load, oxygen consumption rises up to a maximum value of 3.5 and slowly decreases through the cycle. The small increases and decreases are not only a result of the accumulated error but the fluctuations of bacterial consumption, which is logical if it is taken into account that bacteria are living beings.

If OUR and COD are compared some considerations can be given. Figure 5.2-6 is a comparison of these parameters in the first 10 hours of cycle 22.

The first decrease of COD, which occurs during the first minutes of the cycle, corresponds to different phenomena that may occur in the reactor, such as anabolism, in which bacteria use organic matter for cellular synthesis. It is generally accepted that the oxygen consumption during this phenomenon is negligible, although probably occurs consumption during the oxidation-reduction reactions that bacteria promote to fix organic matter in their cellular structure.

Back to the figure, the degradation that occurs during the first 3 hours is under observation. This decrease of COD, which is important in the overall result, occurs when the OUR monitored is the highest. Thus, an important part of organic matter removed is by catabolism, in which bacteria consume organic carbon and oxygen to release energy. It is generally accepted that all the oxygen that is consumed by heterotrophic bacterial cultures is due to organic matter removal.

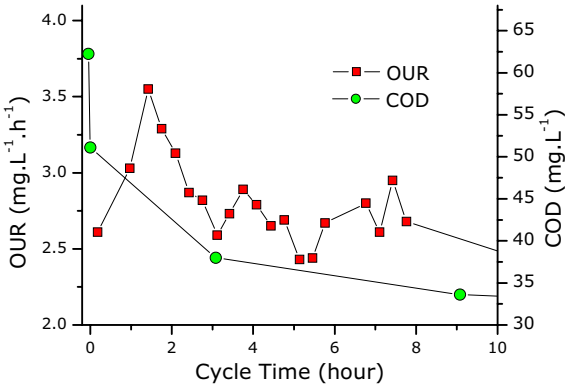


Figure 5.2-6: OUR and COD. First 10 hours of Cycle 22.

The degradation that COD suffers after the 3rd hour is in slower rate, what agrees to OUR profile, which is also lower in this period of the cycle.

With these considerations, the parameter named Yield ($Y_H$) can be calculated.

### 5.2.2.- Example of Heterotrophic Yield ($Y_H$) estimation

Heterotrophic Yield is a ratio between the new biomass generated and the milligrams of organic matter degraded. See Section 5.1.1 for extended information about Yield.

As stated in this chapter's introduction, organic matter removed can be divided into two groups. In the first group, organic matter is used for cellular synthesis (anabolism), and in the second, organic matter is used to meet bacteria's energy needs (catabolism). It is considered that all the

oxygen consumption during a biochemical treatment takes place in this second group. Thus, if the values of OC (subtracting the ER effect) and COD consumed in a given period are divided, the fraction of organic matter degraded by catabolism is known. Then, by difference to 1, the fraction of organic matter degraded by anabolism is estimated (Equation 5.1-7).

On aspect of importance to calculate with certain accuracy the OC, is the estimation of the endogenous respiration. This consume of oxygen is not linked to COD degradation, and if it is not considered and subtracted from the global OC entails an important error.

For the estimation of endogenous respiration, the final part of a cycle is observed, since in this part, the COD is constant, i.e. there is no more degradation. In Figure 5.2-7 and Figure 5.2-8 illustrations of COD and OUR through cycles 21 and 22 respectively are shown. The dashed lines in the lower part of the chart point out the contribution of endogenous respiration, which can be identified as Endogenous Oxygen Uptake Rate ($OUR_{end}$). The $OUR_{end}$ can be estimated as the average value of OUR when there is no more consumption of COD ($OUR_{final}$)

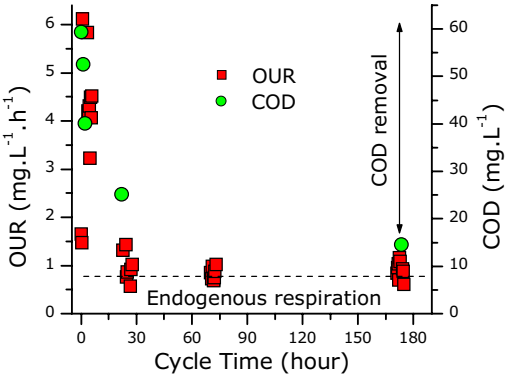


Figure 5.2-7: OUR and COD. Cycle 21

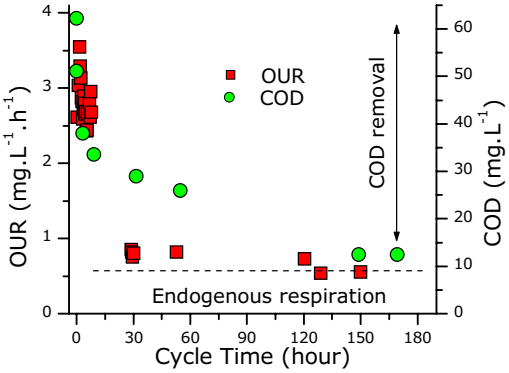


Figure 5.2-8: OUR and COD. Cycle 22

To calculate the area under the OUR points, i.e. the oxygen consumption, the trapezium numerical integration is done. In Figure 5.2-9 an example of trapezium numerical integration and the mathematical equation are shown.

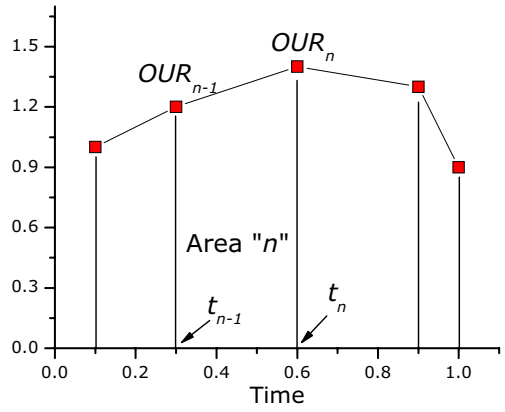


$$Area\ under\ points = \sum_{n} \frac{OUR_n + OUR_{n-1}}{2} \cdot (t_n - t_{n-1})$$

Figure 5.2-9: Example of trapezium numerical integration

Once all data is collected, Yield ($Y_H$) can be finally calculated. For this purpose, some parameters must be connected; $COD_{removed}$, which is the difference between the initial and final values of COD of a cycle; $OC_{total}$, which is the total Oxygen Consumed; ER, which is the Endogenous Respiration and $OC_{COD}$, which is the Consumed Oxygen due to COD digestion. These parameters are calculated by the following equations and the results are summarized in Table 5.2-1.

$$COD_{removed} = COD_0 - COD_{final} \quad \text{Equation 5.2-1}$$

$$OC_{total} = \sum_{n} \frac{OUR_n + OUR_{n-1}}{2} \cdot (t_n - t_{n-1}) \quad \text{Equation 5.2-2}$$

$$OUR_{end} = Average(OUR_{final}) \quad \text{Equation 5.2-3}$$

$$ER = OUR_{end} \cdot HRT \quad \text{Equation 5.2-4}$$

$$OC_{COD} = OC_{total} - ER \quad \text{Equation 5.2-5}$$

$$Y_H = 1 - \frac{OC_{COD}}{COD_{removed}} \quad \text{Equation 5.2-6}$$

Table 5.2-1: Summary of results of cycles with HRT = 168 h. Estimations of COD removed, OC, Endogenous respiration (ER), OC due to catabolism and Yield

| Cycle | COD removed ($mg.L^{-1}$) | $OC_{total}$ ($mg.L^{-1}$) | ER ($mg.L^{-1}$) | $OC_{COD}$ ($mg.L^{-1}$) | Yield ($Y_H$) (mg/mg) |
|---|---|---|---|---|---|
| 21 | 44.6 | 198.66 | 158.21 | 40.42 | 0.09 |
| 22 | 40.4 | 141.31 | 96.84 | 44.47 | -0.10 |

Interestingly, the amount of oxygen consumed per litre of solution seems higher in cycle 21, but the contribution of endogenous respiration is, as estimated, also higher in this cycle. After all, the amount of oxygen consumed for COD digestion ($OC_{COD}$) is similar in both cycles.

The lack of OUR estimations between the initial group (up to 5 hours of cycle time) and the group around 30 hours probably produces a significant error. In fact, this error might be the cause of obtaining a negative value of Yield (which is impossible). In order to correct this error and improve the results, from this point on OUR estimations are carried out more often during cycles.

A first conclusion that can be obtained is that the values of yield are low, that means that a low amount of new biomass is produced in each cycle, and the sludge age is high. As stated above in this Chapter's introduction (Section 5.1) low production of sludge is a typical characteristic of a biofilm reactor, such as a SBBR.

### 5.2.3.- Total and Volatile Suspended Solids

It is assumed (and expected) that in a steady-state fixed bed biological reactor, as a SBBR, active biomass is mostly attached to a support and concentration of suspended solids is low. Therefore, an increase of suspended solids may indicate a malfunctioning of the reactor, since it indicates detachment from the support and death of microorganisms.

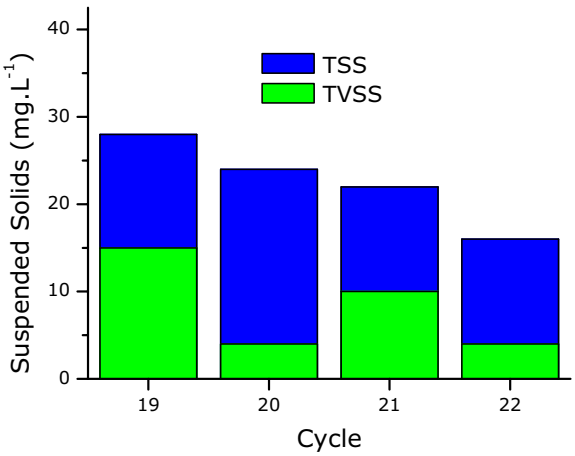


Figure 5.2-10: Total Suspended Solids (TSS) and Total Volatile Suspended Solids (TVSS). HRT = 168 h.

During the SBBR operation, suspended solids are monitored in order to control the reactor performance. Procedure of analysis is detailed in sections 2.3.8 and 2.3.9. Values of Total Suspended Solids (TSS) and Total Volatile Suspended Solids (TVSS) in the end of some cycles are shown in Figure 5.2-10. As it is expected, suspended solids concentrations are low, and their

values are similar. For example, TVSS in a suspended-growth activated-sludge process may be higher than 1000 $mg.L^{-1}$.

If a significant increase were detected, it would indicate a problem in the reactor, caused by a different operating condition or an unexpected situation. Suspended solids concentrations (total and volatile) will be measured in the end of every cycle and in some cycles, in different moments through the cycle.

## *5.3.- Leading the reactor to a minimum HRT*

As seen in Section 4.3, it is possible to treat efficiently a highly biodegradable feed with an HRT of 8 h. The aim of this chapter is to lead the reactor from the present HRT (168 h) to the objective of 8 hours. This reduction is carried out gradually, in order to observe the effects, if exist, that might have the increase of exigencies on the reactor performance.

After the start-up with cycles of 168 hours, the reduction of HRT starts with a 5 days cycle (HRT = 120 h). Follows a group of cycles at 48 h (2 days), then some cycles of 24 hours and ends a collection of cycles that HRT is 8 hours.

### 5.3.1.- Mineralization and COD abatement

Figure 5.3-1 to Figure 5.3-8 show the results of TOC and COD and the corresponding OUR profiles of the different HRT.

As shown in the figures, there exist no differences of TOC and COD achievements. Only in the last cycle (Cycle 49 - 8 hours), a slight difference can be observed, since TOC and COD values at the end of the cycle are a little bit higher. However, the overall efficiencies are similar, because specifically in that cycle the initials COD and TOC are also higher.

Concerning the degradation rate, it can be point out that as HRT is lower the processes follow faster kinetics, since the abatement in the first step occurs in the first 20 hours (Cycle 23), then in 10 hours (Cycle 28), later 5 hours (Cycle 33) and finally 2 hours (Cycle 49).

In so far as the supply of carbon (organic matter) per unit of time increases, which is the Organic Loading Rate (OLR), the population become accustomed to digest faster the matter, probably because there is a significant population growth. As explained, an important feature of bacterial

Sequencing Batch Reactors (SBR) is the ability to change its populations in order to become acclimatized to new situations.

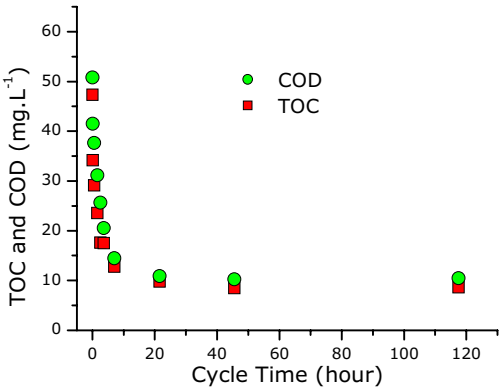


Figure 5.3-1: Cycle 23 – HRT = 120 h.

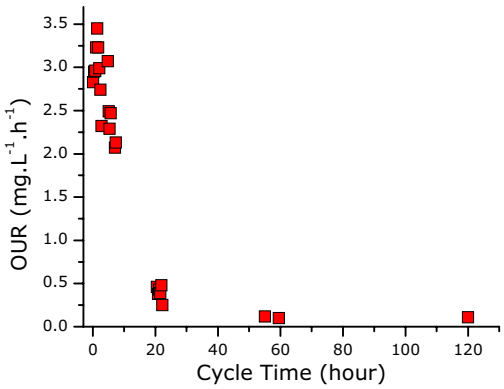


Figure 5.3-2: OUR Cycle 23 – HRT = 120 h.

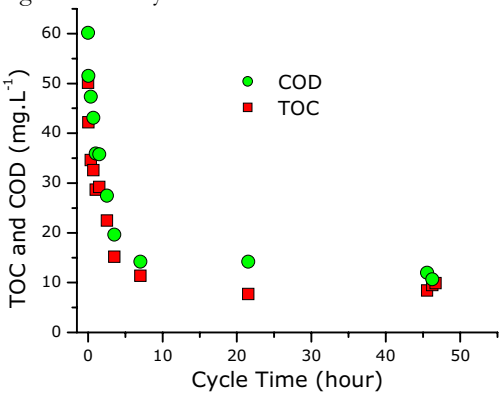


Figure 5.3-3: Cycle 28 – HRT = 48 h.

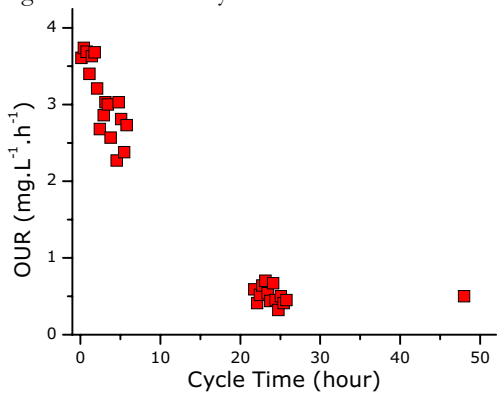


Figure 5.3-4: OUR Cycle 28 – HRT = 48 h.

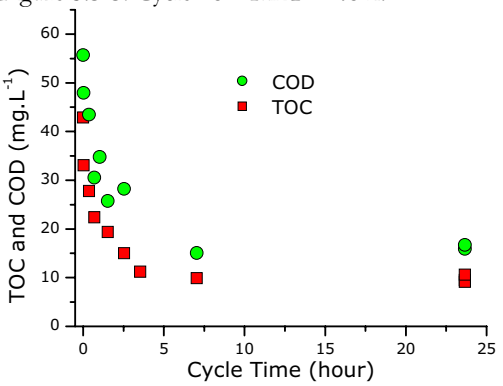


Figure 5.3-5: Cycle 33 – HRT = 24 h.

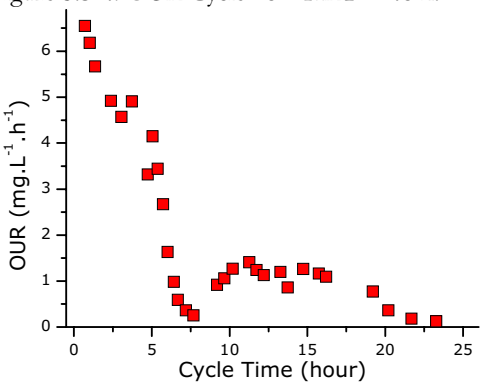


Figure 5.3-6: OUR Cycle 33 – HRT = 24 h.

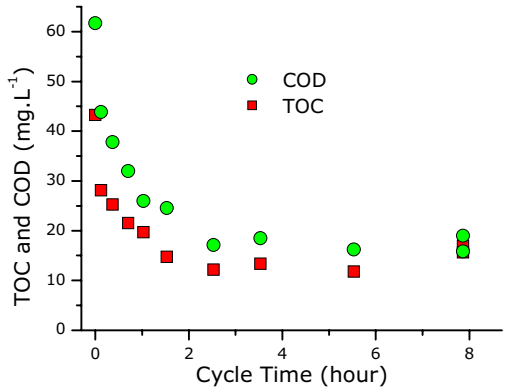


Figure 5.3-7: Cycle 49 – HRT = 8 h.

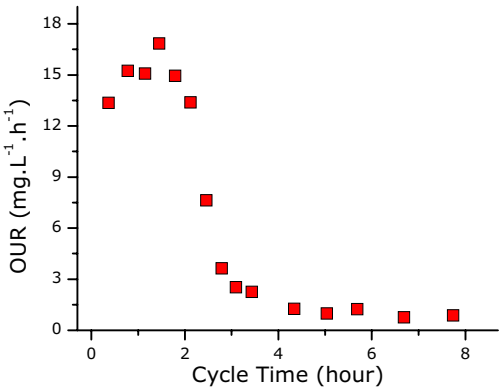


Figure 5.3-8: OUR Cycle 49 –HRT = 8 h.

### 5.3.2.- Oxygen Uptake Rate and Yield

Concerning the OUR profiles, more significant differences can be observed. It is remarkable, that as HRT decrease, OUR values at the first part of the cycle are higher. That means that the oxygen consumption in this certain moment of cycle is higher. In fact, these results are clearly linked to those of TOC and COD degradation rates explained above.

Also according to the OUR profiles in the cycles longer than 8 hours, the reactor remains in endogenous respiration during a significant part of the cycle. This might be affecting negatively the population, since during an endogenous period, due to the lack of food, microorganisms are forced to use the nutrients remaining in dead cells and also their own substances to carry out the metabolism. Thus, the reactor might be damaged, and this harm is noticed at the beginning of the next cycle, as a lower reaction rate.

As in an 8 hours cycle the endogenous phase is shorter, there remain in the SBBR a stronger and active bacterial population, which is able to treat the load of the following cycle faster.

In order to compare the reactor's operation, degradation achievements and oxygen consumptions are estimated and summarized in Table 5.3-1 as it is done in the previous section for the example of Yield estimation.

Table 5.3-1: Summary of results of cycles fed with Ph-F effluent treated with $[H_2O_2]_0$ = 500 mg.L$^{-1}$.

| Cycle | HRT (hour) | $COD_{removed}$ (mg.L$^{-1}$) | $OC_{total}$ (mg.L$^{-1}$) | ER (mg.L$^{-1}$) | $OC_{COD}$ (mg.L$^{-1}$) | Yield (Y) (mg/mg) |
|---|---|---|---|---|---|---|
| 21 | 168 | 44.6 | 198.66 | 158.21 | 40.42 | 0.09 |
| 22 | 168 | 40.4 | 141.31 | 96.84 | 44.47 | -0.10 |
| 23 | 120 | 39.54 | 50.21 | 12.96 | 37.25 | 0.06 |
| 28 | 48 | 37.31 | 56.59 | 24.22 | 32.37 | 0.13 |
| 33 | 24 | 35.75 | 40.77 | 8.55 | 32.22 | 0.10 |
| 49 | 8 | 42.73 | 41.12 | 7.70 | 33.42 | 0.2 |

With the exception of the last cycle (Cycle 49 – HRT =8 hours), Yield values are around 0.1, and in the last cycle 0.2, which means that only 10 % and 20 % respectively of COD degradation is used for synthesizing new cells. These results, as said above, are in accordance to the characteristics of a biofilm reactor, which generates much less sludge than a suspended biomass reactor. A typical Yield for a suspended biomass reactor is 0.6 (*Metcalf and Eddy, 1991*).

This soft trend of Yield to increase with decreasing HRT is also described by *Klimiuk and Kulikowska* (*2006*).

### 5.3.3.- Control of suspended solids

Any malfunctioning that might cause an increase of microorganisms' death or detachment rates can be detected by suspended solids analyses. A monitoring of TSS and TVSS measured in the end of several cycle is shown in Figure 5.3-9.

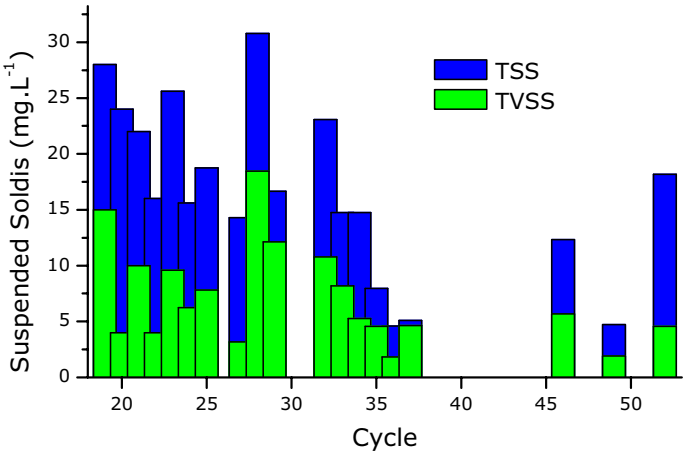


Figure 5.3-9: Total Suspended Solids (TSS) and Total Volatile Suspended Solids (TVSS) in the end of cycles fed with solution prepared in the Ph-F with 500 mg.L$^{-1}$ of $[H_2O_2]_0$.

As cycles go forward and HRT is reduced, values of suspended solids are in average lower. The gap between cycles 37 and 46 belongs to a weekend.

The measurement of TSS and TVSS is somehow connected to the estimated Yield. In suspended-growth bioreactors, which $Y_H$ are high, high amounts of sludge, i.e. suspended solids, are produced per unit of carbon degraded. As explained above, in the case of a SBBR, Yield values are usually low, and production of new bacteria is low. However, in the case that a SBBR shows higher $Y_H$, suspended solids in the reactor (total and volatile) would increase, since there would be an excess of population. This excess of population is detached from the support and becomes suspended biomass.

### 5.3.4.- Evaluation of Average Oxidation State

Another method to assess the process performance is by means of Average Oxidation State (AOS). AOS is a comparison of COD and TOC values (in molar concentrations) and is an indicator of how oxidized is in average the organic matter in a certain moment of the process. This parameter is calculated according to Equation 5.3-1. The equation is normalized to values from -4, which corresponds to the less oxidized species (methane), to +4, which is the value of $CO_2$.

$$AOS = 4 \cdot \frac{TOC - COD}{TOC} \qquad \text{Equation 5.3-1}$$

where TOC and COD are in molar units.

According to the results, AOS throughout the process increases, which means that end-products are more oxidized (more similar than $CO_2$) than initial substances. In Figure 5.3-10 an evolution of AOS throughout the coupled process is shown. The initial value, corresponds to a solution of 200 $mg.L^{-1}$ of 4-chlorophenol; the second value is the AOS after photo-Fenton treatment with 500 $mg.L^{-1}$ of $[H_2O_2]_0$; finally the last value is the average AOS after 8 hours of biological treatment. As shown in this figure, the main oxidation occurs in the Photo-Fenton treatment, and the oxidation change during the biological process is significantly lower, or even insignificant if the error is taken into consideration. The higher efficiency of Photo-Fenton (concerning the AOS) is understandable, if it is taken into account that this process is based on the generation of severe oxidizing agents.

Interestingly, in the course of different cycle, AOS do not follow the same profile in each other. AOS may accumulate a notable error, since is a calculation produced by two analytical

measurements, which, at the same time, can accumulate error, mainly the analysis of COD. Nevertheless, biochemical reaction pathways are not as fixed as chemical patterns, and can occur that the oxidation stages change depending on the bacterial culture in a certain cycle or a certain moment of the cycle. In some cases, the AOS attained in the middle of the process is lower than the estimated AOS at first, or in other situations, the AOS in the middle is even higher than in the end of the process.

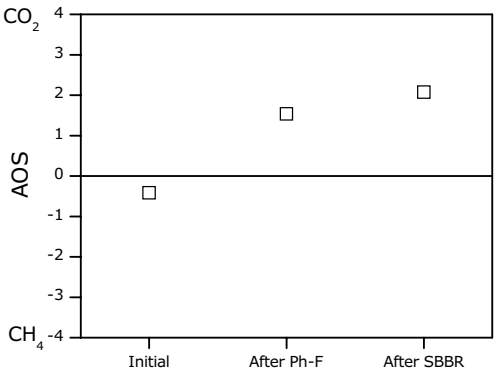


Figure 5.3-10: Average Oxidation State (AOS) of the Coupled Process. In Photo-Fenton: $[H_2O_2]_0$ = 500 mg.L$^{-1}$; In SBBR: HRT = 8 h.

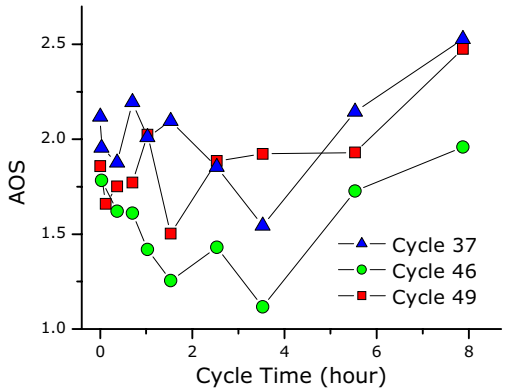


Figure 5.3-11: Average Oxidation State (AOS) during SBBR treatment.

### 5.3.5.- Global results

As a global result, it can be pointed out that the SBBR in the present operating conditions is able to treat efficiently and fast a solution that has been previously treated in the Photo-Fenton reactor with 500 mg.L$^{-1}$ of $[H_2O_2]_0$. An Hydraulic Retention Time of 8 hours is enough to allow the bacterial population degrade the organic matter, and according to the results the HRT could be reduced more, at for example 4 hours, or even less if necessary.

A summary of overall TOC and COD results is shown in Figure 5.3-12. TOC removal is calculated considering both the Photo-Fenton and the SBBR. As shown in the figure, after a start-up period, TOC removal achievements are similar with all HRT tested, and round 90 % of total mineralization. No differences of final degradation can be seen from the different operating conditions. Thus, it can be stated that the influent can be considered readily biodegradable.

Concerning COD removal, analyses were done from cycle 19 on. Remediation efficiencies in this case, are slightly higher, since values of 0.95 (95 %) are regularly achieved.

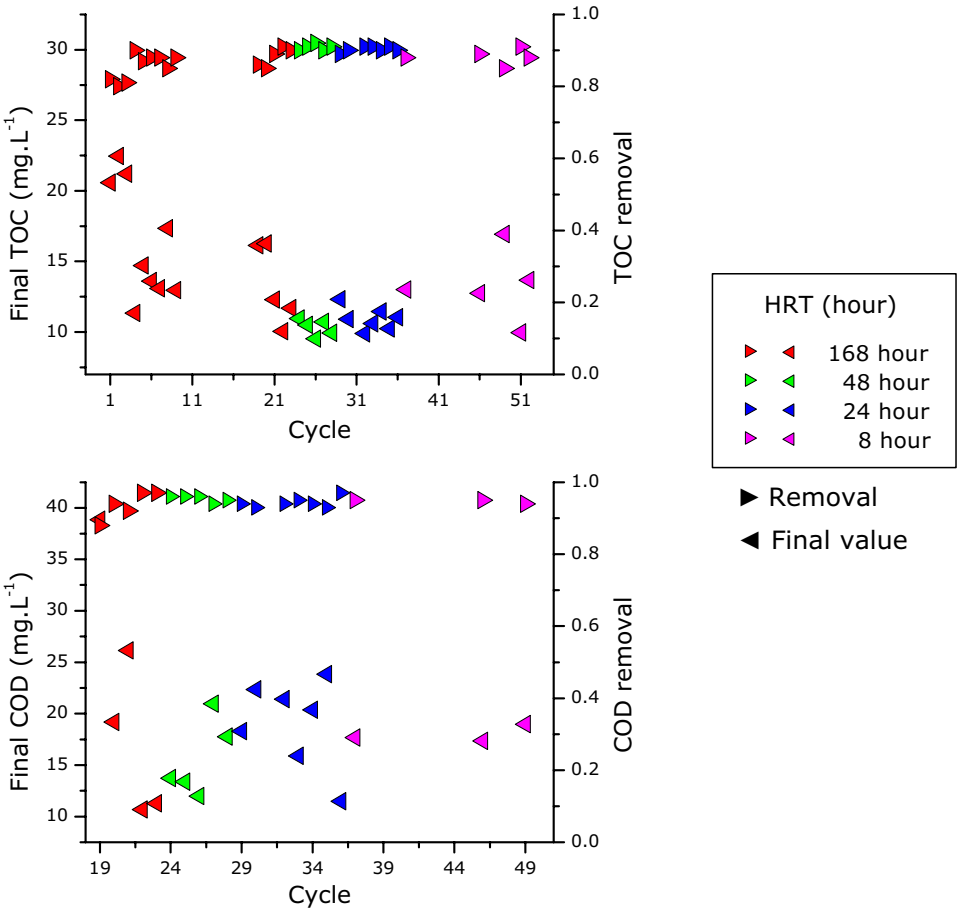


Figure 5.3-12: Summary of results. Final concentrations and removal for all the cycles carried out with Feed prepared with 500 mg.L$^{-1}$ of $[H_2O_2]_0$. On the top: TOC summary. Below: COD results.

# *5.4.- Testing the SBBR with less biodegradable feed*

The aim of this section is the characterization of the reactor and biomass with a partially biodegradable feed. In this case, the solution to be treated in the SBBR is the product obtained by Photo-Fenton treatment of 200 mg.$L^{-1}$ of 4-CP with 300 mg.$L^{-1}$ of $[H_2O_2]_0$ and 10 mg.$L^{-1}$ of $[Fe^{2+}]_0$. More information about the characteristics of this feed can be found in Section 3.2 (page 60).

As seen above, in Section 4.3.2.1, it is possible to abate more than 70 % of TOC by combination of Photo-Fenton -with the listed operating conditions- and Biological treatments. This results, does not accomplish the pre-established objective (more than 90 %), which is quite ambitious. Nevertheless, this combination conditions are really interesting, since a large part of total TOC abatement occurs in the biological treatment, and consequently the process might be more inexpensive.

Anyway, the most attractive characteristic is that it is possible to feed the biological reactor with more organic matter, which involve higher COD, and that it might be possible to distinguish between readily and slowly biodegradable substrate. Therefore, it is expectable to found and describe wider variety of behaviours and phenomena.

### 5.4.1.- Acclimation to the new feed: First cycles

The operation with the current conditions follows immediately the previous experimentation. Just after the last cycle with feed prepared with 500 mg.$L^{-1}$ of $H_2O_2$ and 8 h of HRT (Cycle 52), the SBBR is fed with the new feed, which is prepared with 300 mg.$L^{-1}$ of $H_2O_2$. That means that in the early cycles the bioreactor is influenced by the previous conditions, which drive to maintain a large population, since the reactor is brought to degrade more organic matter per time (the Organic Loading Rate (OLR) is high).

In order to study different characteristics of the reactor performance, as it is done before, HRT in the early cycles is fixed to 168 h, and cycles are repeated until a steady-state is observed.

Figure 5.4-1 and Figure 5.4-2 show OUR profiles in the early hours of cycles 53 and 54 respectively. As it is expectable, and in fact desirable, at the beginning of the earliest cycles OUR values are high and similar than in cycle 49 (Figure 5.3-8). It is desirable, because although the new feed might be more difficult to be degraded, do not produce a significant inhibition in the current bacterial population.

However, after few cycles, OUR values tend to be lower, since the SBBR gets acclimatized to the new situation. Figure 5.4-3 to Figure 5.4-6 show OUR profiles in cycles 55 and 57, accompanied by the corresponding TOC and COD values over time. A difference can be clearly discerned when comparing the OUR profiles. From a highest value of almost 18 $mg.L^{-1}.h^{-1}$ in cycle 53 (Figure 5.4-1), it falls up to 5 $mg.L^{-1}.h^{-1}$ in cycle 57 (Figure 5.4-6). As it happens with the experiments with highly biodegradable feed, long cycles force the reactor to spend most of the time in endogenous respiration. This imposes on the SBBR a selective pressure to adapt its population to the new situation and in consequence, it occurs a loss of activity.

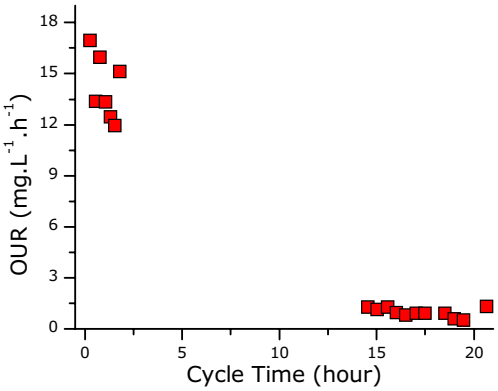


Figure 5.4-1: OUR – Cycle 53. HRT = 168 h.

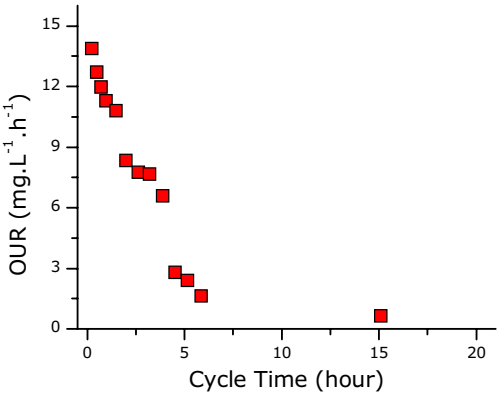


Figure 5.4-2: OUR – Cycle 54. HRT = 168 h.

Concerning the degradation levels (Table 5.4-1), a tendency can be described. As cycles follow one another, the abated amounts decrease in not only for TOC but also for COD. According to these results, it can be stated that a highly active population (like in cycle 53) is able to degrade more organic matter, but as soon as the bacterial culture lose activity, diminish the abated amount.

Table 5.4-1: Summary of results of cycles fed with Ph-F effluent treated with $[H_2O_2]_0$ = 300 $mg.L^{-1}$. HRT = 168 h.

| Cycle | Final TOC ($mg.L^{-1}$) | Final COD ($mg.L^{-1}$) | Overall Results[1] | |
|---|---|---|---|---|
| | | | TOC removal | COD removal |
| 53 | 16.19 | 25.06 | 0.86 | 0.92 |
| 54 | 21.28 | 30.84 | 0.81 | 0.91 |
| 55 | 20.16 | 34.25 | 0.82 | 0.90 |
| 56 | 23.60 | 39.19 | 0.79 | 0.88 |
| 57 | 25.12 | 47.66 | 0.78 | 0.86 |

[1]Considering Photo-Fenton and Biological treatments

It is remarkable that TOC removal achieved in this last cycle (cycle 57), is in the same range that the removal achieved in the previous experimental part with the SBBR (refer to the review of results in Section 4.3.2.1).

Consequently, it has been possible to start-up and acclimatize at least two times the SBBR by common bacterial cultures from a sewage plant, and to reach similar degradation levels.

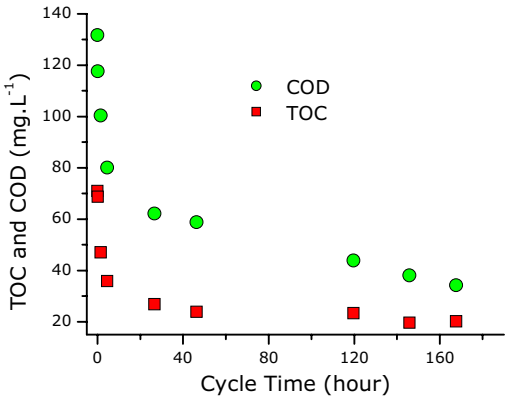


Figure 5.4-3: Cycle 55. HRT = 168 h.

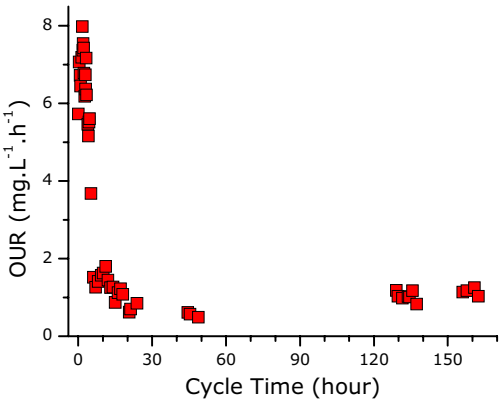


Figure 5.4-4: OUR - Cycle 55. HRT = 168 h.

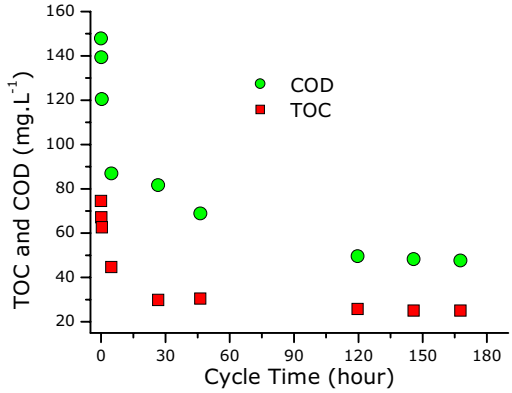


Figure 5.4-5: Cycle 57. HRT = 168 h.

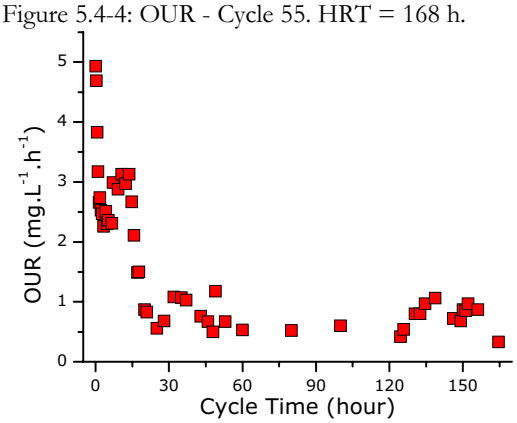


Figure 5.4-6: OUR - Cycle 57. HRT = 168 h.

Another situation that appears to be of importance is the difference of OUR profile. In cycle 57, OUR draws undulations, like a wave. This behaviour is probably due to the feed characteristics. As now, the feed suffers less pre-treatment in Photo-Fenton (with less $H_2O_2$ dose), there is a wider variety of compounds, more complex, and probably some of these compounds might imply more difficulties in order to be digested by bacterial activity. If this higher complexity is the cause of the undulations, it might be possible to ratify it with further experimentation.

Although it might be possible to see more differences with more repetitions of cycles with an HRT of 168 h, it is more useful to reduce HRT to obtain more information.

### 5.4.2.- Reducing Hydraulic Retention Time

The same procedure than the carried out in Section 5.3 is followed. HRT is reduced systematically up to 8 hours. Figure 5.4-7 to Figure 5.4-14 show TOC and COD results and the corresponding OUR profiles for cycles with different HRT.

In this case, unlike in the experimentation with highly biodegradable feed, it is possible to observe a significant difference among cycles, mainly with final degradation. As HRT is shorter, the bacterial culture tends to consume less organic matter. Furthermore, the difference between COD and TOC increase, which means that it might be also an important difference among the estimations of Average Oxidation State (AOS), which is commented later.

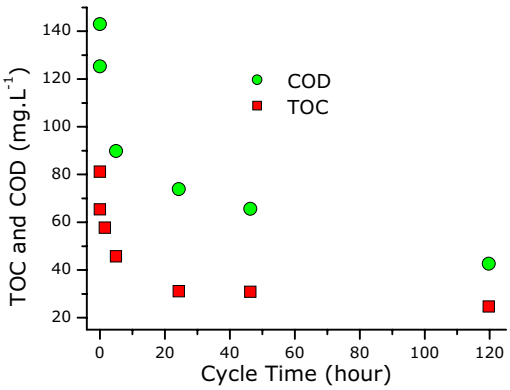


Figure 5.4-7: Cycle 58. HRT = 120 h.

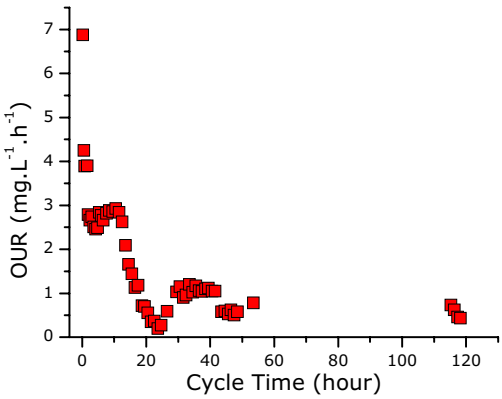


Figure 5.4-8: OUR - Cycle 58. HRT = 120 h.

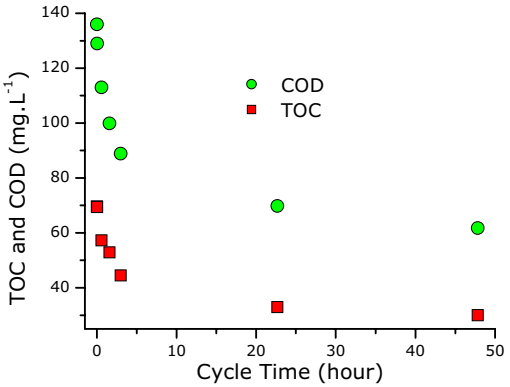


Figure 5.4-9: Cycle 63. HRT = 48 h.

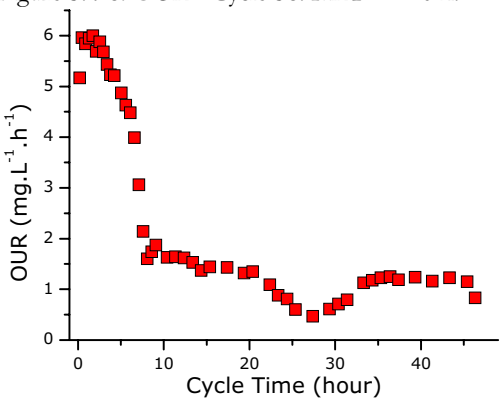


Figure 5.4-10: OUR – Cycle 63. HRT = 48 h.

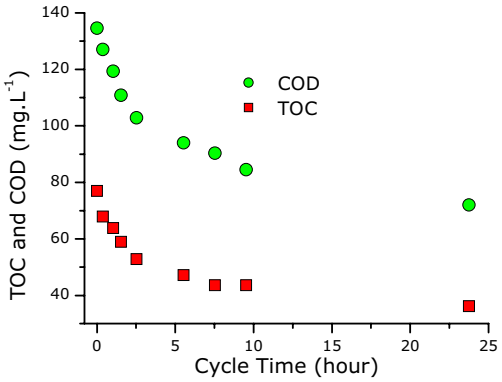


Figure 5.4-11: Cycle 71. HRT = 24 h.

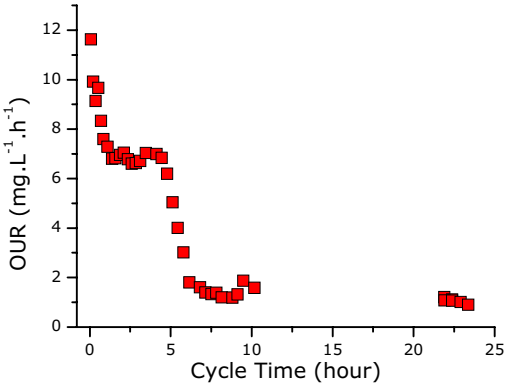


Figure 5.4-12: Cycle 71. HRT = 24 h.

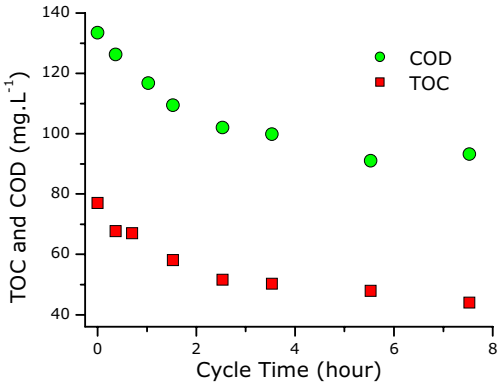


Figure 5.4-13: Cycle 87. HRT = 8 h.

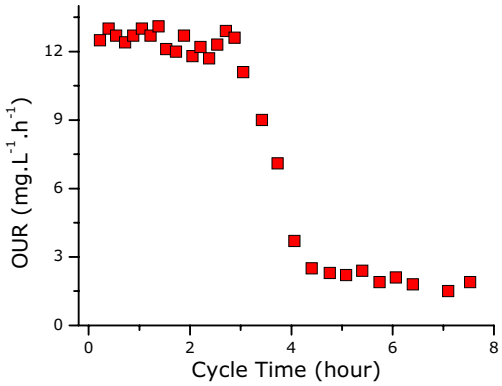


Figure 5.4-14: Cycle 87. HRT = 8 h.

On the other hand, OUR profiles seem to follow the same pattern that the observed with the highly biodegradable feed. As soon as the reactor is fed more often, i.e. the Organic Loading Rate (OLR) is higher the microorganisms get used to degrade faster at the beginning of each cycle.

Comparing COD and TOC analysis with OUR profiles, it is observable that the highest degradation rate in each cycle occurs at the same time that the highest OUR values are assessed, meaning that the reactor get used to consume faster as soon as is forced to do it.

Regarding the undulations in OUR profiles that are observed in the early cycles with the present feed, they are recurred in some cycles (like cycle 58 or 71). However, more experimentation and extensive information is needed in order to explain this behaviour.

### 5.4.3.- Oxygen Uptake Rate and Yield

With the appropriate mathematical treatment of all these data (as explained in Section 5.2.1), Yield estimations are obtained. A summary of these results is shown in Table 5.4-2.

Table 5.4-2: Summary of results of cycles fed with Ph-F effluent prepared with $[H_2O_2]_0$ = 300 mg.L$^{-1}$.

| Cycle | HRT (hour) | $COD_{removed}$ (mg.L$^{-1}$) | $OC_{total}$ (mg.L$^{-1}$) | ER (mg.L$^{-1}$) | $OC_{COD}$ (mg.L$^{-1}$) | Yield (Y) (mg/mg) |
|---|---|---|---|---|---|---|
| 55 | 168 | 97.45 | 179.75 | 146.16 | 33.59 | 0.66 |
| 57 | 168 | 100.21 | 153.41 | 121.20 | 32.21 | 0.68 |
| 58 | 120 | 100.41 | 122.00 | 67.15 | 54.85 | 0.45 |
| 63 | 48 | 67.45 | 84.61 | 54.45 | 30.16 | 0.55 |
| 71 | 24 | 62.59 | 64.57 | 25.50 | 39.07 | 0.38 |
| 87 | 8 | 40.25 | 52.73 | 14.62 | 38.11 | 0.05 |

Interestingly, Yield does not follow the same trend that describes with the previous feed. Instead of increasing with shorter HRT, in this occasion it decrease severely. Furthermore, Yield values for the longest cycles are significantly higher than the ones assessed in the previous part. As it is commented in the introduction of the current section (Section 5.4), it is presumed that due to the more complex characteristics of the present feed, it might be possible to observe different effects. However, this behaviour was not expected.

Nevertheless, an explanation is likely to be obtained if other studies are observed. For example, *Sahinkaya and Dilek* (*2006*) observed that as soon as increases the concentration of a readily biodegradable substrate in a slowly biodegradable feed, the estimated Yield is lower. By extrapolating this case to the present study, it could be said that in shorter cycles, biomass only consume highly biodegradable substrate, unlike in longer cycles, where consumes both kind of substrate.

*Moreno-Andrade et al.* (*2006*) state that in Sequencing Batch Reactors, there is a selection of microbial community with a vast metabolic range in which microbial species can differ greatly in growth rate and yield. If it is taken into account that the substrate "soup" is now more varied contrasting with the previous feed, the SBBR is forced to maintain a more diverse population, with their corresponding metabolic mechanisms. Furthermore, the same authors affirm that the growth rate of micro-organisms may change clearly during a cycle, since in a SBR (and a SBBR) substrate concentration decrease in time in each cycle.

### 5.4.4.- Control of Suspended Solids

As it is explained above (Section 5.2.3) there is a relation between Yield and Suspended Solids. If Yield in this stage follows the trend as it has been estimated (Table 5.4-2), there might be also an observable difference in Suspended and Volatile Solids.

The values of TSS and TVSS measured in the end of several cycles are shown in Figure 5.3-9. At the top of the plot, HRT is detailed.

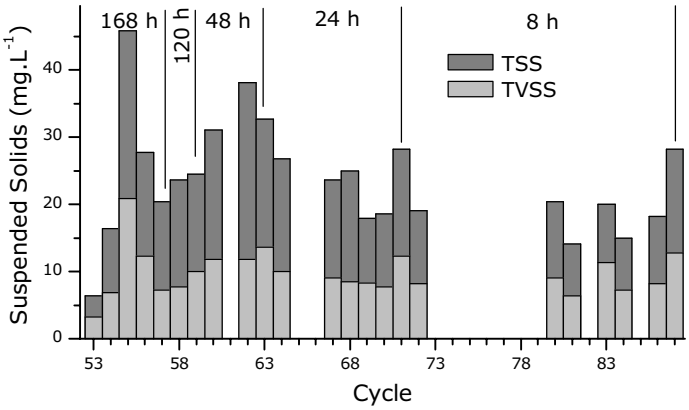


Figure 5.4-15: Total Suspended Solids (TSS) and Total Volatile Suspended Solids (TVSS) in the end of cycles fed with solution prepared by Ph-F with 300 $mg.L^{-1}$ of $[H_2O_2]_0$.

It seems that a trend can be described, in which the shorter the cycles, the lower the suspended solids concentration, following the same tendency as observed with Yield estimations.

### 5.4.5.- Evaluation of Average Oxidation State

Figure 5.4-16 and Figure 5.4-17 show different representations of AOS. The first one is an evolution of AOS of the coupled process. The last is a graph that shows the evolution of AOS during different cycles.

As it is expected with the already observed results, there are now significant differences depending on HRT. According to the results, as short is a cycle, the lower the AOS value in the end of the process.

If the AOS profiles in Figure 5.4-17 are observed, more information is likely to be obtained. Comparing the AOS profile of 168 hours cycle with the values of shorter cycles, seems that the SBBR becomes "lazy". AOS is a sum parameter; if AOS decreases, it means that in average, remaining products are less oxidized. This might point out that the readily biodegradable by-products, which are consumed firstly, are more oxidized than the slowly biodegradable species, which are digested later. Thus, in the 168 hour cycle, AOS firstly decrease, and after approximately 30 hours increase again.

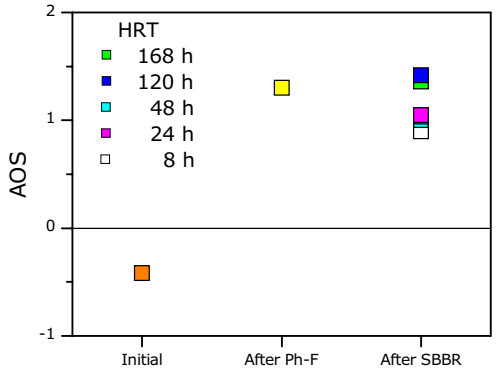


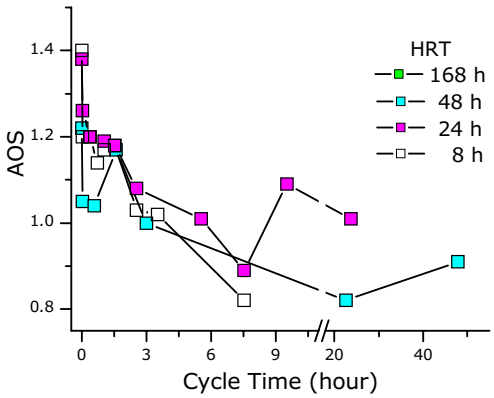


Figure 5.4-16: (top) Average Oxidation State (AOS) of the Coupled Process. In Photo-Fenton: $[H_2O_2]_0$ = 300 mg.L$^{-1}$; In SBBR, different HRT.

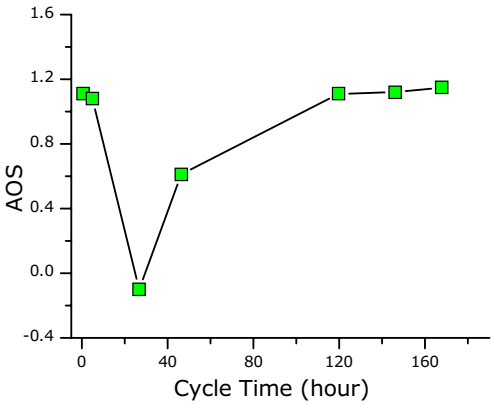


Figure 5.4-17: (right and top-right) Average Oxidation State (AOS) during different SBBR cycles.

### 5.4.6.- Global Results

As an overall result, it can be pointed out that the coupled system is able to mineralize between 60 and 80 % of initial TOC when the solution is pre-treated in the Photo-Fenton reactor with 300 mg.L$^{-1}$ of $[H_2O_2]_0$.

A summary of overall TOC and COD results is shown in Figure 5.4-18. TOC removal is calculated considering both the Photo-Fenton and the SBBR. As shown in the figure, TOC removal achievements change severely with HRT tested. Thus, it can be stated that the influent in this case is more complex and contains readily and slowly biodegradable substances, which follow different metabolic ways.

A combined process in which in the SBBR operates with an HRT of 8 hours is able to degrade only 60 % of initial TOC, which compared to the objective is a poor result.

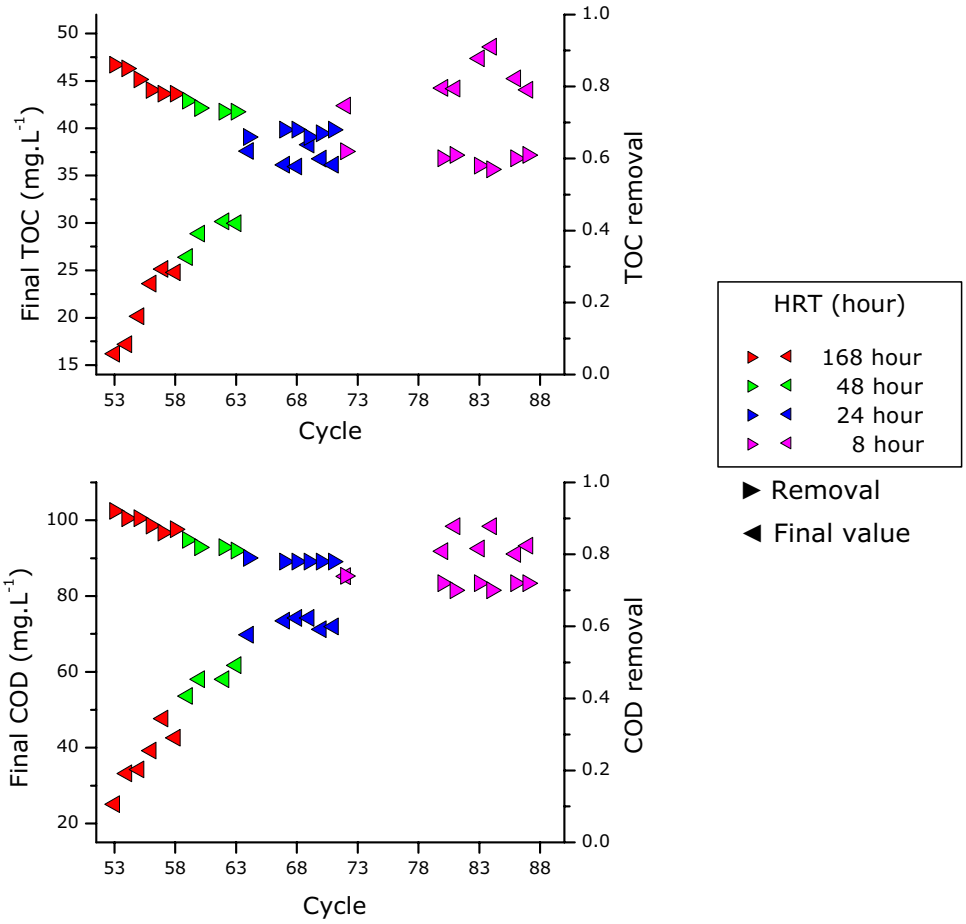


Figure 5.4-18: Summary of results. Final concentrations and removal for all the cycles carried out with Feed prepared with 300 mg.L$^{-1}$ of $[H_2O_2]_0$. On the top: TOC summary. Below: COD results.

As it is expected, due to the higher complexity of the current feed, a wider variety of behaviours and effects has been observed and described.

## *5.5.- Operation of the SBBR exposed to shock loads*

The aim of this Section is the study of the operation of the SBBR exposed to no-readily biodegradable substrate and likely to be inhibitory and toxic for the bacterial population, i.e. what can be defined as a shock load. As stated above, an SBBR is meant to be more resistant to theses situations.

These circumstances might occur in the case of a control failure in Photo-Fenton process, and the treatment by this failure becomes shorter or poorer than it should be.

In a first step, the experimental part consists of repeating cycles with a non-readily biodegradable feed that still contains little amounts of 4-chlorophenol, and 4-chlorocatechol, which is one of the earliest by-products, and really similar to 4-CP in structure. Different HRT are tested, and diverse parameters are observed as it has been done with the other feeds.

Later, the test consists of feeding the reactor with toxic solutions, maintaining the mixture for 8 hours, and after this time, observing the recuperation with a readily biodegradable feed. This stage is repeated three times with different solutions.

Figure 5.5-1 shows a diagram, which represents the experimental design that is carried out in this section.

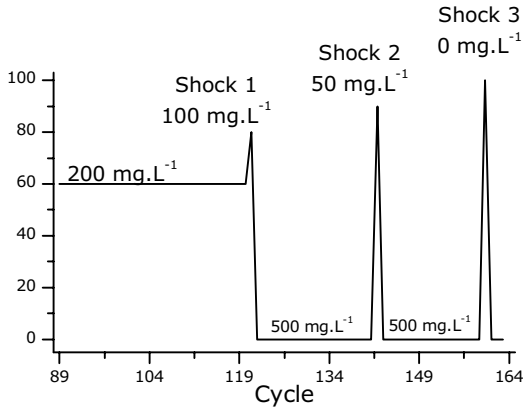


Figure 5.5-1: Qualitative representation of the experimental design. These concentrations are the amounts of $H_2O_2$ used in Photo-Fenton.

### 5.5.1.- Operation of the SBBR exposed to toxic substances

As it has been announced, the SBBR is now fed with a solution that still contains 4-CP and one of the early by-products, 4-CC. In this case, 200 $mg.L^{-1}$ of 4-CP are treated by Photo-Fenton with 200 $mg.L^{-1}$ of $H_2O_2$.

In a first cycle, HRT is maintained at 120 hours (5 days), and subsequently reduced to 8 hours. In Figure 5.5-2, an overview of results is shown. As it happens with the feed prepared with 300

mg.L$^{-1}$, which is a non-readily biodegradable feed, in so far as HRT is reduced the SBBR is able to degrade less COD and mineralize less TOC. With an HRT of 8 hours, only 40 % of TOC and around 60 % of COD is degraded considering the combination of Photo-Fenton and Biological treatments.

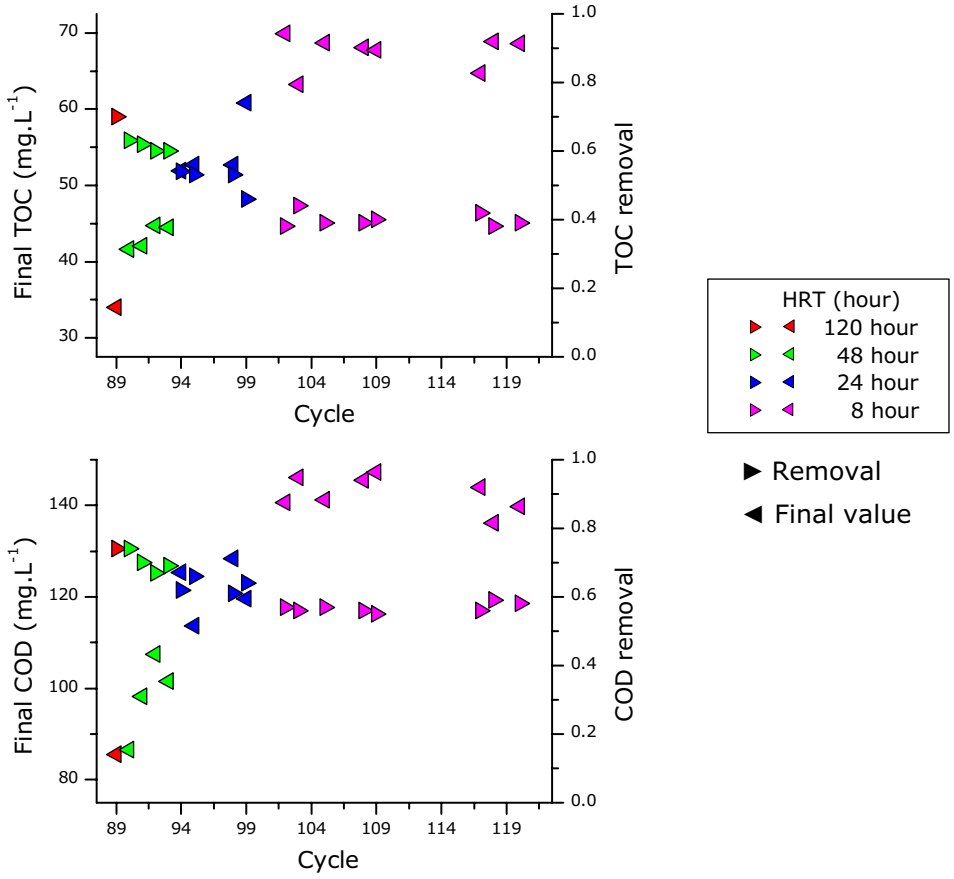


Figure 5.5-2: Summary of results. Final concentrations and removal for all the cycles carried out with Feed prepared with 200 mg.L$^{-1}$ of $[H_2O_2]_0$. On the top: Summary of TOC results. Below: COD results.

If values of COD and TOC over an 8 hours cycle are evaluated (Figure 5.5-4), it is clearly observed that in this case the degradation does not follow a similar tendency than before. With a readily biodegradable feed, degradation use to be high at the beginning of the cycle, and abatement rate decrease as the cycle progresses. In the present case, degradation occurs slowly during the cycle. This might be indicative of inhibition of bacterial activity due to the feed characteristics.

Fortunately, the detection of 4-chlorocatechol (4-CC) and 4-chlorophenol (4-CP) by means of HPLC is easy (refer to Section 2.3.1 for analytical procedures). Figure 5.5-3 is a waterfall representation of chromatograms obtained at 287 nm of wavelength by HPLC. By integration of these peaks, and a calibration, concentration of each compound in each sample is quantified. Figure 5.5-5 shows the concentration of 4-CC and 4-CP present in the SBBR during Cycle 118. Beyond 5.5 hours, none of them is detectable anymore.

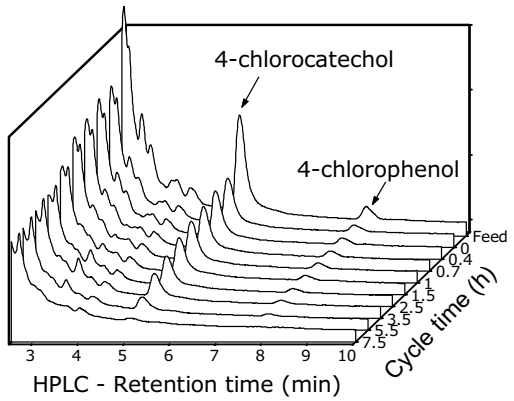


Figure 5.5-3: Superposition of HPLC chromatograms. Cycle 118 – HRT = 8h.

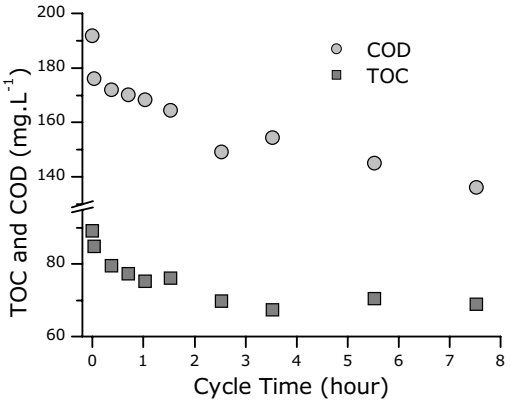


Figure 5.5-4: (top-right) TOC and COD values over time. Cycle 118 – HRT = 8 h. In Photo-Fenton $[H_2O_2]_0$ = 200 mg.L$^{-1}$.

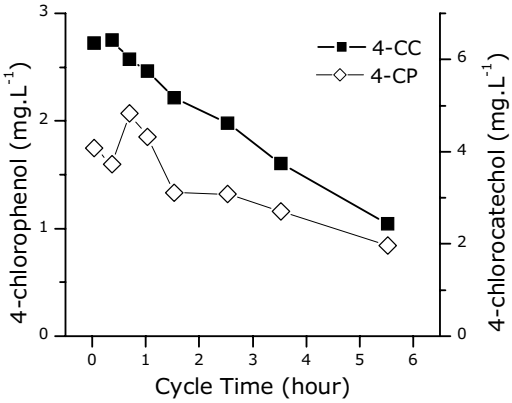


Figure 5.5-5: (right) 4-CP and 4-CC concentrations over time. Cycle 118 – HRT = 8 h. In Photo-Fenton $[H_2O_2]_0$ = 200 mg.L$^{-1}$.

### 5.5.2.- Operation of the SBBR exposed to shock loads

After an operation period in which the SBBR is fed with a product that contains inhibitory species, the SBBR is exposed to shock loads.

The test consist of feeding the SBBR with different Ph-F products, which are more toxic between each other, and analyzing whether the reactor afterwards is able to recover or not with a readily biodegradable feed. HRT in all cycles during this part is fixed at 8 hours, since this time is meant to be a reasonable HRT. Information of characteristics of all the feeds used in the following steps is described above, in Section 3.2 (page 60).

The First shock consists of feeding the SBBR with Photo-Fenton product with 100 mg.$L^{-1}$ of $H_2O_2$ (Figure 5.5-6). Afterwards, the SBBR is fed with readily biodegradable substrate, which is prepared in Ph-F with 500 mg.$L^{-1}$ of $H_2O_2$. Also HRT in these cycles is fixed at 8 hours, and multiple cycles are repeated. During this period, different parameters are monitored in order to assess the reactor recuperation.

After a certain level of recuperation is achieved, a second shock is carried out, in which the reactor is fed with Ph-F product prepared with only 50 mg.$L^{-1}$ of $H_2O_2$. TOC and COD measurements over cycle time are shown in Figure 5.5-7. Next, the reactor is again fed with readily biodegradable Ph-F product ($H_2O_2$ = 500 mg.L-1).

Finally, the last shock consists of feeding the reactor with 200 mg.$L^{-1}$ of 4-CP with no previous treatment (Figure 5.5-8), just with the appropriate medium of micronutrients (see Section 2.1.3).

The Figures show values of different parameters that are analyzed over the shock time. The parameters that are mainly of importance are TOC and COD. It is remarkable that in all of the tests, there is an apparent consumption of organic matter, of around 60 to 80 mg.$L^{-1}$ of COD and 40 to 50 mg.$L^{-1}$ of TOC. Nevertheless, volatilization is likely to be of importance in this case, since there are probably more volatile compounds in the medium. In fact, it is perceptible that the odour in the laboratory during these tests is more intense.

TSS and TVSS are analyzed in order to detect an increase of microorganisms' death and detachment. Interestingly, during the observed cycles there is no significant increase of suspended solids, meaning that the reactor at least during the shock has a remarkable resistance to toxic species.

Furthermore, the concentration of some certain species can be assessed by HPLC analysis. According to the results, it seems that 4-CC is abated faster than 4-CP. In the last test, as it starts with a solution of 4-CP there is no 4-CC to be analyzed (Figure 5.5-8-right).

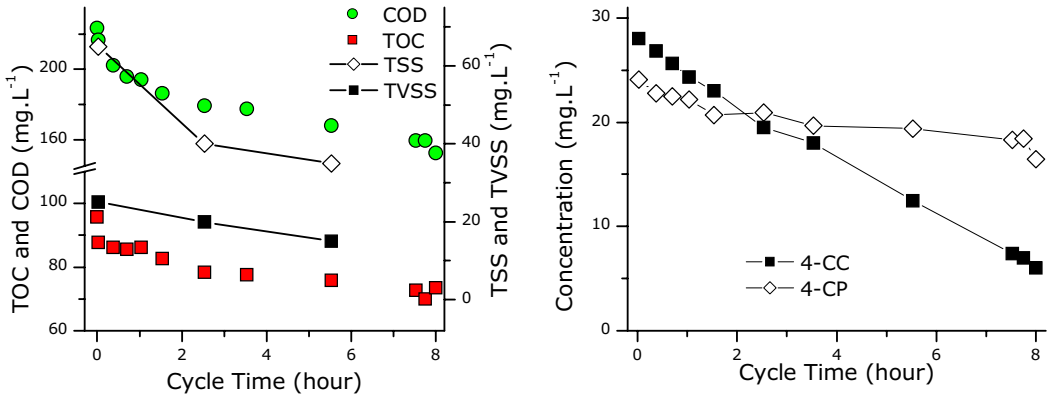


Figure 5.5-6: Shock 1. SBBR performance with feed prepared in the Ph-F with 100 mg.L$^{-1}$ of $H_2O_2$. On the left: TOC, COD, TSS and TVSS over cycle time. On the right, concentration of 4-CC and 4-CP during the cycle.

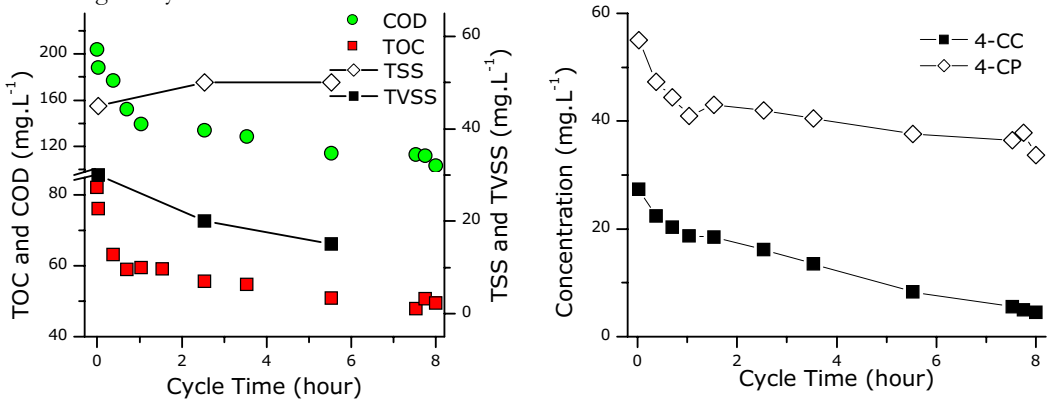


Figure 5.5-7: Shock 2. SBBR performance with feed prepared in the Ph-F with 50 mg.L$^{-1}$ of $H_2O_2$. On the left: TOC, COD, TSS and TVSS over cycle time. On the right, concentration of 4-CC and 4-CP during the cycle.

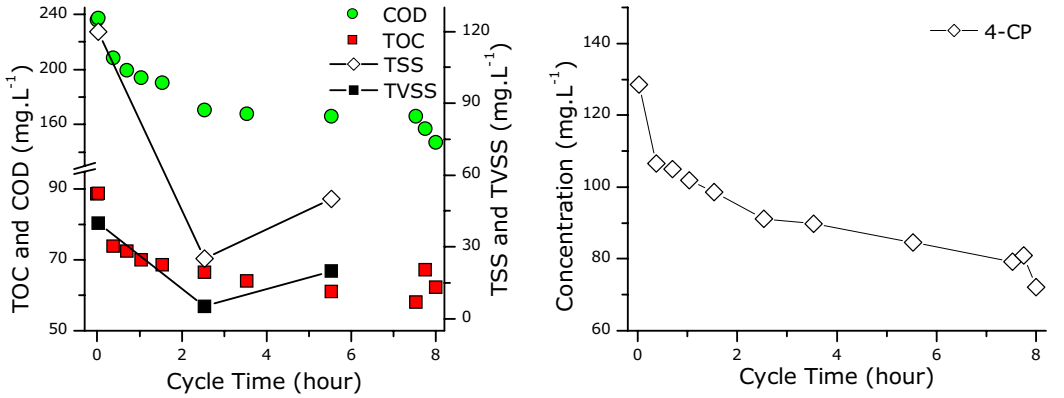


Figure 5.5-8: Shock 3. SBBR performance with feed with no-pretreatment. On the left: TOC, COD, TSS and TVSS over cycle time. On the right, concentration of 4-CP during the cycle.

As well as controlling the operation over the impact tests, the recovery process is also analyzed. In Figure 5.5-9 a review of results during the operation of the SBBR exposed to shock loads and its recovery is shown. Furthermore, this Figure allows comparing better each shock.

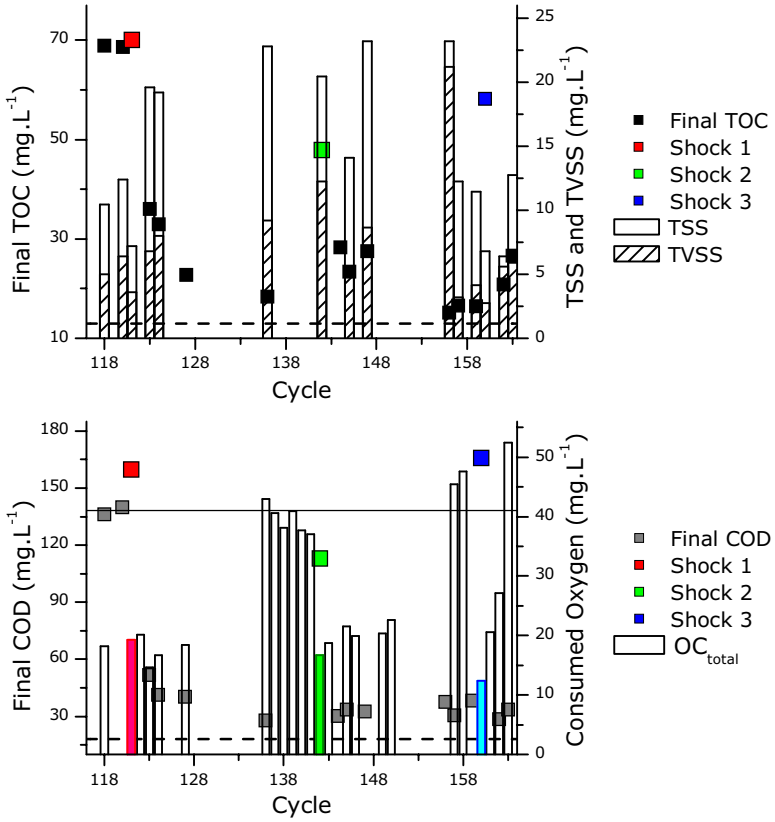


Figure 5.5-9: Consequences produced by Shock loads (in colour) and recovery process.

The consequences produced by each shock load are clearly observed. When the shock is carried out, final values of COD and TOC are significantly higher than with the readily biodegradable substrate, which means that the abatement is low. Furthermore, the amount of oxygen consumed by the SBBR is noticeably low.

After shocks 1 and 2, it is necessary to repeat more than 10 cycles in order to reach similar levels of Consumed Oxygen ($OC_{total}$) than in Cycle 49, which is fixed as a standard cycle with the readily biodegradable feed. The lines in Figure 5.5-9 indicate the Final TOC and COD values (dashed line) and $OC_{total}$ (solid line) reached in Cycle 49.

Interestingly, with the last shock load (Shock 3), which is carried out with 200 $mg.L^{-1}$ of 4-CP with no previous treatment, the SBBR apparently recovers faster than with the previous shock (Shock 2). Probably, some of the early intermediates of 4-CP degradation, which are present mainly in Shock 2, are even more toxic.

Moreover, the operation before Shock 1, with a feed prepared with 200 $mg.L^{-1}$ of $H_2O_2$, seems to affect significantly the SBBR. It might be possible that in the case of preparing the reactor prior to Shock 1, with the readily biodegradable feed, the recovery process would be shorter.

Concerning the final values of TOC and COD, the SBBR seems to achieve with a few cycles after each Shock high levels of degradation. Only after Shock 1, the SBBR needs more than a couple of cycle to achieve high levels of abatement. However, strictly speaking, the values are slightly higher than in Cycle 49. COD final values are around 10 $mg.L^{-1}$ higher.

The $OC_{total}$ measure appears to be a good parameter to control the SBBR performance. As shown in Figure 5.5-9 when a shock occurs, this parameter is significantly low, and as long as the reactor recovers the normal operation, $OC_{total}$ reach similar values than seen above in Section 5.3.2, and indicated in the Figure with a solid line.

In conclusion, the SBBR seems to overcome shock loads easily in most of the cases. Even with the most toxic conditions, the SBBR is able to reach similar values of treatment than the observed in Section 5.3. Furthermore if $OC_{total}$ can be automatically monitored, it can provide a method to control malfunctioning of the reactor and its (desired) recuperation.

## *5.6.- SEM imaging of biofilm samples*

Scanning Electron Microscope (SEM) is a powerful tool for imaging. The first set of images (Figure 5.6-1 and Figure 5.6-2) represents a new stone, without biofilm. In both the Secondary and Backscattered Electron images, the stone is very clean. No suspicious structures are present.

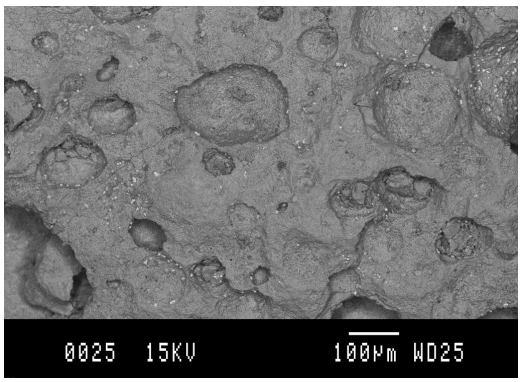


Figure 5.6-1: SEI image. New stone

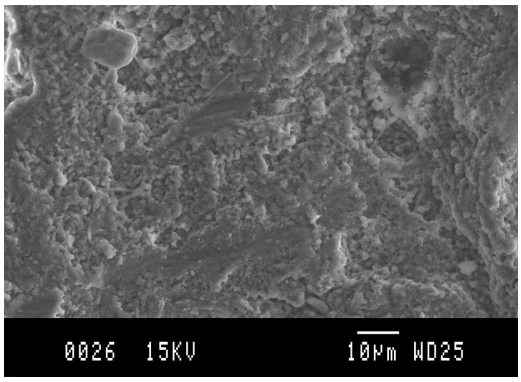


Figure 5.6-2: BEI image. New stone

A sample prepared as explained in the Methods Section, is observed.

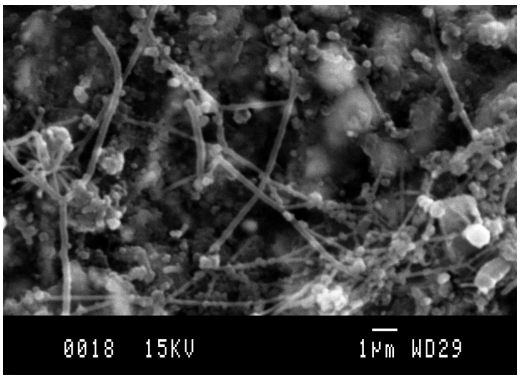


Figure 5.6-3: SEI image. Sample of biofilm

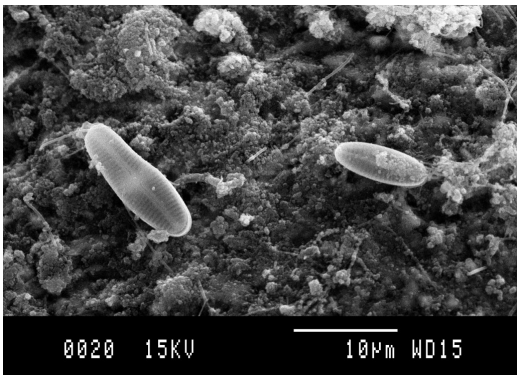


Figure 5.6-4: SEI image. Sample of biofilm

On the left (Figure 5.6-3), the image depicts filamentous bacteria. The structures can be observed clearly. Many images as the shown figure could be taken. If the sample is prepared well, it is possible to see the bacterial structures very clearly by SEM.

More clear is the image on the right. Two diatomea lay on a film of diverse nature. Diatomea are algae. In some periods of operation by the bioreactor, green aggregates have settled on the sides of the recirculation tubes. These tubes are transparent, and received the diffuse light of the laboratory. It should be pointed out that an irradiated and humid area consists of a propitious environment for the presence of algae. Later, these tubes have been replaced with black tubes and the green particles could no more be seen with the naked eye.

# 5.7.- Characterization of the microbial diversity

By the procedure explained in Section 2.3.12, 96 clones are generated. Among them, 89 can be analyzed for their identification. Figure 5.7-1 and Figure 5.7-2 are two different classifications of bacteria present in the SBBR identified by the RIBOSOMAL method. One is classified by Phylum, which is more general, and the later by Genus, which is more specific.

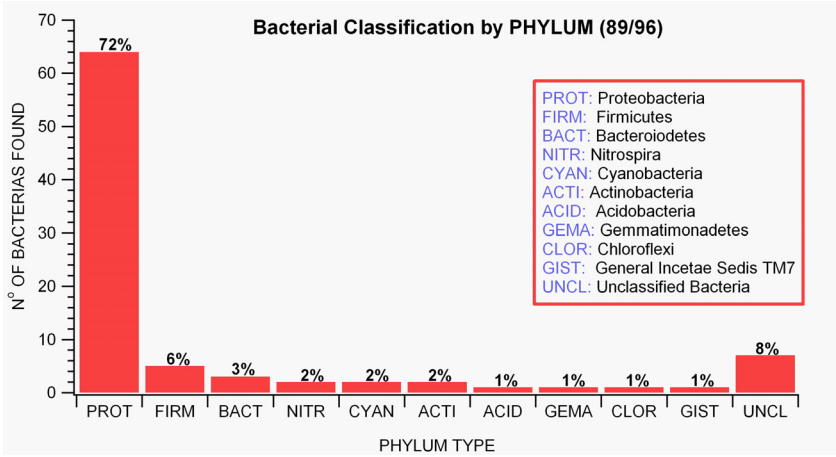


Figure 5.7-1: Bacterium classification by Phylum

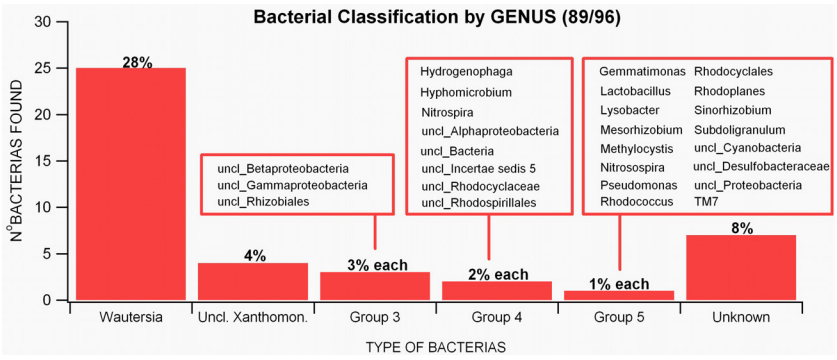


Figure 5.7-2: Bacterial Classification by Genus

A very interesting work would be to identify the changes that the bacterial population undergoes when there are significant changes of the operating conditions. This is usually called population dynamics, and is useful for determining which individual strains are more acclimatized to certain operating conditions or substrate characteristics.

# *5.8.- Conclusions*

The characterization of the SBBR has been carried out under different substrate conditions and different Hydraulic Retention Time.

According to the results, different substrates produce different responses of the SBBR, very interesting to be studied.

When the SBBR is fed with a readily biodegradable mixture, prepared with 500 $mg.L^{-1}$ of $H_2O_2$ by Ph-F, the reactor acclimatizes fast and is able to treat efficiently a high Organic Loading Rate (OLR), with even less than 8 hours of treatment.

When the substrate has been prepared with less $H_2O_2$ by Ph-F (300 $mg.L^{-1}$), its effect on the SBBR are more complex. Below a certain cycle time, the SBBR is not able to treat the same organic matter than the longest cycles. When the OLR is high, the reactor gets used to consume fast the (supposed to be) most biodegradable fraction, and avoid to degrade the difficult fraction.

The supposed resistance of the SBBR has been also proved. The SBBR is able to tolerate toxic shock loads, and is able to recover fairly well.

A simple measure of the dissolved oxygen (DO) during short cuts of air supply is a good control parameter of the reactor's performance. With an easy treatment of the DO data, Oxygen Uptake Rate (OUR) is measured. As it has been observed, OUR values have a direct relation with the Substrate Uptake Rate (SUR), which is the COD degradation rate. By means of the OUR monitor, it would be possible to maintain a high SUR, which means that the reactor may be directed to degrade the highest organic matter amount by the lowest reaction time. This is in fact an optimization of the process.

By means of Scanning Electron Microscopy (SEM) and microbial diversity description, it has been possible to see bacterial structures and identify bacterial strains.

# *Chapter 6: Conclusions and Recommendations*

A coupled photochemical-biological system to treat biorecalcitrant wastewater has been tested, studied and described. Conclusions in relation to the individual processes and their integration have been stated in each Chapter. The most relevant ones are now summarized, enclosed to a list of recommendations for future studies.

Concerning the coupled process:
- The coupled Photo-Fenton process-SBBR system is able to treat efficiently within 8 hours more than 90 % of the organic load of a 200 $mg.L^{-1}$ 4-CP solution, which is used as a model compound of biorecalcitrant pollutants.

*It is recommended to carry out the same study with model compounds that present other features, such as nitrogen containing species, non-aromatics or even mixtures of them.*

- The so-called biodegradability ratio ($BOD_5/COD$) as an indicator of coupling possibilities, presents unsatisfactory results. On one hand, it presents positive results since it partially indicates biodegradation possibilities, but, on the other hand, it is not sensitive enough to clearly distinguish whether a certain Ph-F effluent is readily biodegradable or not. Other parameters, such as acute toxicity by Microtox, seem to be more sensitive.

Regarding the Photo-Fenton process:
- A Response Surface Methodology (RSM) has been a useful tool to identify and mathematically describe influencing parameters. It is a powerful tool in order to diminish long experimental phases, since it works with a set of well-designed experiments, which can be planned with for example a Central Composite Design.

- The degradation possibilities of Photo-Fenton process can be described as a function of the dose of $H_2O_2$. According to the results, the products of Photo-Fenton under different temperature conditions, with different doses of $Fe^{2+}$, and even with other radiation sources and sizes are practically the same. Thus, iron and temperature affect neither the degradation efficiencies nor the biodegradability increases, but they affect the kinetics and they could be studied for process's optimization.

- Photo-Fenton control and modelling possibilities have been evaluated and described, all of them in relation to $H_2O_2$ dosage, which can be easily analyzed or even automatically monitored. For control purposes, $H_2O_2$ and Chemical Oxygen Demand (COD) of a Ph-F product appear to

be directly linked each other. The evolution of COD and $BOD_5$ over an experiment or depending on the dose of $H_2O_2$ has been modelled by mechanistic models. The results are satisfactory.

*Concerning the control possibilities, it is suspected that the found dependency that shows COD in front of $H_2O_2$ can be only stated for aromatic compounds, since the nature of them and their early intermediates is active in this type of photochemical processes.*

*Some effects that the statistical tools assessed to be not significant are quite interesting. Probably, they are assessed to be not significant because they are caused by conditions at the limit of the experimental design (the lowest or highest value). For example, the lowest iron dose seems to produce the most efficient degradation. Probably, a study around this effect can help in the modelling of the process, since the effect of iron could not be properly modelled.*

*Modelling seems an attractive field of study, and a pathway of importance for the process's industrialization.*

On the subject of SBBR:
- The SBBR response can differ significantly depending on the substrate conditions and HRT. When the SBBR is fed with a readily biodegradable mixture, the reactor acclimatizes faster and is able to treat efficiently a high Organic Loading Rate (OLR), within 8 hours of treatment. On the other hand, a slow biodegradable substrate produces effects that are more complex. The SBBR is not able to treat the same organic matter with short cycles than with the longest cycles. When the OLR is high, the reactor gets used to consume fast the (supposed to be) most biodegradable fraction, and avoid to degrade the difficult fraction.

*There are many works concerning the modelling of biological reactors, and some contributions concerning biofilter particularities. It would be very interesting to see if the models fit the COD degradation and parameters of the SBBR that treats an effluent of Photo-Fenton products. The concentration of active biomass, as it is attached, has not been calculated. By modelling, it could be estimated, and then it would be possible to predict its evolution depending on diverse operating conditions. Moreover, it is possible that the presence of iron salts (due to Ph-F), can produce inhibition effects. Thus, iron could be optimize not only taking into account Ph-F needs, but also the biological process.*

- The presumed resistance of the SBBR has been also proved. The SBBR is able to tolerate toxic shock loads, and is able to recover fairly well.

- The monitoring of OUR, appears to be a simple and efficient control parameter, since it is linked to the Substrate Uptake Rate (SUR). By means of a good control, it would be possible to maintain a high degradation rate, which means that the reactor may be directed to degrade the highest organic matter amount by the lowest reaction time. This is in fact an optimization of the process.

*Probably, it would be possible to improve the automation of the SBBR. Thus, it would be possible to study the optimal Organic Loading Rate (OLR), which is directly connected with the SUR that the reactor is able to treat efficiently.*

*The population dynamics is also a subject of possible study, since it would be possible to identify the individual microorganisms that are responsible of degradation of certain compounds or present a good synergy in combined processes.*